EFFECT OF NANOSTRUCTURED SILICA FILLER MATERIAL ON IONIC LIQUID-BASED LITHIUM ELECTROLYTES

SYSTEMATIC CHARACTERIZATION OF LIQUID AND GELLIFIED ELECTROLYTES

Effekt von nanostrukturierten Silica als Füllmaterial auf Lithiumelektrolyte basierend auf ionischen Flüssigkeiten

Systematische Charakterisierung von flüssigen und gelierten Elektrolyten

DISSERTATION

von

Nastaran Krawczyk

zur Erlangung des Grades

Doktor der Naturwissenschaften

– Dr. rer. nat. –

vorgelegt dem

Fachbereich 08 Biologie und Chemie

der Justus-Liebig-Universität Gießen

Gießen, 2014

Dekan / Dean:	Prof. Dr. Holger Zorn
1. Gutachter / 1st Reviewer:	Prof. Dr. Jürgen Janek
2. Gutachter / 2nd Reviewer:	Prof. Dr. Michael Fröba
eingereicht am / submitted on:	30.10.2014

Jeder Schritt ist der erste in den blauen Dunst.
Weiß nicht, was die Zukunft bringt,
weiß nur gestern überdauert uns.
Und wünsch mir mehr zu sagen an mei'm jüngsten Tag
als vom Mutterleib ins Grab 'ne gute Zeit gehabt.

„Erste Schritte / Retrospektive“ von Freundeskreis (Esperanto, 1999)

DANKSAGUNG

Mein herzlicher Dank geht an Herrn PROF. DR. JÜRGEN JANEK für die Ermöglichung der Promotion, die Betreuung und die bequemen Rahmenbedingungen, die er für die Arbeit zur Verfügung stellte.

Ein besonderer Dank geht auch an DR. BJOERN LUERßEN für die Betreuung, die fachliche und moralische Unterstützung während der Promotion wie auch während des Studiums, für die vielen hilfreichen Diskussionen, die zahlreichen Korrekturen in den letzten Jahren sowie die offene Tür und das offene Ohr.

Ich danke Herrn PROF. DR. MICHAEL FRÖBA für die anregenden Diskussionen und die netten Projekttreffen. Dank geht auch an SEINE ARBEITSGRUPPE, besonders an Jan Vogel, Sebastian Kraas und Annalena Vijn, für die Synthese der Silica, die Anregungen und Diskussionen sowie die angenehme Atmosphäre bei unseren Projekttreffen.

Des Weiteren danke ich KERSTIN SANN für die Betreuung während der Master-Arbeit, für die vielen anregenden Diskussionen und die nette Zusammenarbeit.

Ein besonderer Dank geht an meine KOLLEGEN AUS DEM LITHIUM-LABOR für die schöne gemeinsame Zeit. Besonders hervorheben möchte ich hier Benjamin Bergner, Martin Busche, Mareike Falk, Pascal Hartmann und Jochen Reinacher für die Unterstützung auf unterschiedlichste Art. Des Weiteren danke ich der FEINMECHANIK- UND ELEKTRONIKWERKSTATT für die vielen Reparaturen und hergestellten Apparaturen sowie DR. BORIS MOGWITZ für die Simulation der Leitfähigkeit von dispersen Elektrolyten.

Ein großes Dankeschön geht an die gesamte ARBEITSGRUPPE JANEK und besonders an meine ehemaligen und aktuellen BÜROKOLLEGEN für die schöne Atmosphäre und die angenehme Zeit.

Ein besonderer Dank gilt meiner FAMILIE für das Ermöglichen des Studiums, die Unterstützung und das Verständnis. Meinen FREUNDEN danke ich herzlich für das Verständnis für meine mangelnde Zeit, die Unterstützung und die Ablenkung in der Freizeit. Ein besonders herzlicher Dank geht an meinen MANN für seine Geduld, die große Unterstützung und sein großes Verständnis in den letzten Jahren sowie die Ablenkung, wenn die Arbeit nicht so verlief wie erhofft.

Die vorliegende Arbeit wurde am Physikalisch-Chemischen Institut der Justus-Liebig-Universität Gießen unter der Betreuung von Prof. Dr. Jürgen Janek und Dr. Bjoern Luerßen im Zeitraum von April 2011 bis 2014 angefertigt.

Ich erkläre:

Ich habe die vorgelegte Dissertation selbständig und ohne unerlaubte fremde Hilfe und nur mit den Hilfen angefertigt, die ich in der Dissertation angegeben habe oder aus Ratschlägen im Rahmen der Betreuung erhalten habe. Alle Textstellen, die wörtlich oder sinngemäß aus veröffentlichten Schriften entnommen sind, und alle Angaben, die auf mündlichen Auskünften beruhen, sind als solche kenntlich gemacht. Bei den von mir durchgeführten und in der Dissertation erwähnten Untersuchungen habe ich die Grundsätze guter wissenschaftlicher Praxis, wie sie in der „Satzung der Justus-Liebig-Universität Gießen zur Sicherung guter wissenschaftlicher Praxis“ niedergelegt sind, eingehalten.

Gießen, 30.10.2014

Nastaran Krawczyk

ABSTRACT

Ionic liquid-based electrolytes (IL electrolytes) are known to have advantageous properties to be applied in lithium (ion) batteries but show poor lithium ion conductivity. In the present work IL electrolyte properties were influenced by adding an isolating second phase. Systematical measurements of the obtained dispersed electrolytes are presented. As standard IL electrolyte 15 wt% lithium bis(trifluoromethylsulfon)imide (LiTFSI) as conducting salt in N-butyl-N-methylpyrrolidinium TFSI (BMP-TFSI) was used. Silica particles with varying morphologies and surfaces acted as filler materials. The total conductivity of the neat IL electrolyte decreased by max. 54 % for mass fractions of silica up to 10 wt%. At the same time viscosities and shear moduli increased partially by several orders of magnitude. Moreover, the electrochemical response in half cells with lithium iron phosphate hardly changed with respect to the neat IL electrolyte. Since the electrical properties hardly changed despite a severe viscosity increase, an increased lithium ion mobility is assumed in the composite electrolytes. No obvious correlation of electrolyte properties with chemical composition of silica surfaces was observed. Hence, it is concluded that the morphology of the filler material is crucial for the observed effect. As a model for enhanced lithium ion mobility in the composite electrolytes it is proposed that silica particles form interphases with the IL electrolyte containing ordered arrangement of the IL ions. This interphase seems to be relatively long-ranged influencing the bulk electrolyte. The lithium ion conductivity may be increased in the interphase due to altered conduction paths with respect to the bulk IL electrolyte. Moreover, lithium ion concentration in the bulk electrolyte may be changed resulting in higher lithium ion conductivity.

ZUSAMMENFASSUNG

Auf ionischen Flüssigkeiten basierende Elektrolyte (IL-Elektrolyte) sind dafür bekannt, vorteilhafte Eigenschaften für Lithium(-Ionen)-Batterien aufzuweisen, werden aber auf Grund ihrer schlechten Lithium-Ionenleitfähigkeit nicht eingesetzt. In der vorliegenden Arbeit wurden die Eigenschaften eines IL-Elektrolyten durch Zugabe einer isolierenden zweiten Phase beeinflusst, und es werden systematische Messungen der entstandenen dispersen Elektrolyte präsentiert. Als Standard-Elektrolyt wurde N-Butyl-N-methylpyrrolidinium-bis(trifluoromethylsulfon)imid (BMP-TFSI) mit 15 Gew.-% Lithium-TFSI (LiTFSI) als Leitsalz verwendet. Silica-Partikel mit unterschiedlichen Morphologien und Oberflächen dienten als Füllstoffe. Für Silica-Massenanteile von bis zu 10 Gew.-% verringerte sich die Gesamtleitfähigkeit des IL-Elektrolyten um max. 54 %. Gleichzeitig erhöhten sich die Viskositäten und Schubmoduli teilweise um mehrere Größenordnungen. Das elektrochemische Verhalten in Halbzellen mit Lithiumeisenphosphat änderte sich kaum im Vergleich zum reinen IL-Elektrolyten. Da sich die elektrischen Eigenschaften trotz der deutlich erhöhten Viskositäten kaum änderten, wird in den Komposit-Elektrolyten eine erhöhte Lithium-Ionenmobilität angenommen. Eine Korrelation der chemischen Natur der Silica-Oberflächen mit den Elektrolyteigenschaften war nicht zu beobachten. Daher lässt sich schließen, dass die Morphologie der Füllmaterialien für die Beobachtungen entscheidend ist. Als Modell für die verbesserte Lithium-Ionenleitfähigkeit in den Komposit-Elektrolyten wird vorgeschlagen, dass die Silica-Partikel eine Grenzphase mit dem Elektrolyten ausbilden, in der die IL-Ionen in geordneter Form vorliegen. Diese Grenzphase scheint relativ weitreichend zu sein, sodass die Volumeneigenschaften des IL-Elektrolyten beeinflusst werden. Die Lithium-Ionen könnten auf Grund von veränderten Leitfähigkeitspfaden eine erhöhte Leitfähigkeit in dieser Grenzphase aufweisen. Außerdem könnte die Konzentration der Lithium-Ionen in der flüssigen Phase verändert sein, sodass eine höhere Lithium-Ionenleitfähigkeit resultiert.

TABLE OF CONTENTS

1 INTRODUCTION

Lithium ion batteries (LIB) and so-called next generation batteries (e.g. Li-S_8 or Li-O_2 cells) gained a lot of interest in recent years. Usually, liquid electrolytes with organic solvents are used, which often cause safety issues due to a high vapor pressure going along with high flammability. Hence, liquid electrolytes with higher safety are an important technological target. As ionic liquids show a diminishingly small vapor pressure they are considered to be promising for application as lithium electrolytes.

Pure salts in the liquid state are well known since long time in the form of molten salts at high temperatures. To obtain the liquid state at ambient temperatures the melting point has to be decreased considerably. This is achieved for ionic liquids (ILs) which are defined as molten salts with melting temperatures below 100 °C [1, 2]. A subcategory of ionic liquids was established for molten salts with melting temperatures below room temperature called room temperature ionic liquids (RTILs). Due to their liquid phase but ionic nature they show properties lying between the ones of common solvents and solids. To achieve the low melting points cations and anions with clearly different symmetries are combined. Thus, a lot of ion combinations are possible which strongly influence chemical and physical properties of the material. Conversely, the properties can be tuned on demand by adequate choice of cation and anion. Usually ionic liquids have high conductivities being comparable to common liquid electrolytes. Moreover, they exhibit mostly high chemical, thermal and electrochemical stability with a diminishing small vapor pressure. Due to their high variety of properties which can be adjusted and their advantageous properties ionic liquids are potential solvents in a lot of different areas like synthesis, catalysis, process technology or energy devices [1, 3].

In recent years much effort was spent on research for lithium ion batteries and next generation batteries. Electrode materials were clearly improved and numerous studies were published providing a better understanding of the electrolyte properties [4–7].

Mostly, commercially available organic solvent-based lithium electrolytes are used which usually do not show sufficient electrochemical stability. Therefore, decomposition products are formed during cell cycling resulting in a solid electrolyte interphase (SEI) at the anode [8] and a cathode electrolyte interphase (CEI) at the cathode [9]. These interphases usually decrease the cell capacity and performance. Moreover, the film formation is not sufficiently understood to be actively controlled for adjusting them in an advantageous way. Apart from that, common liquid lithium electrolytes have high vapor pressures and are flammable establishing a high safety risk. Solid and polymer electrolytes appear to be an appropriate alternative to these liquid electrolytes, but they bring some critical drawbacks since they provide a poor contact with the porous electrodes due to their rigidity. Thus, ionic liquid-based electrolytes might represent a good compromise for application in electrochemical cells.

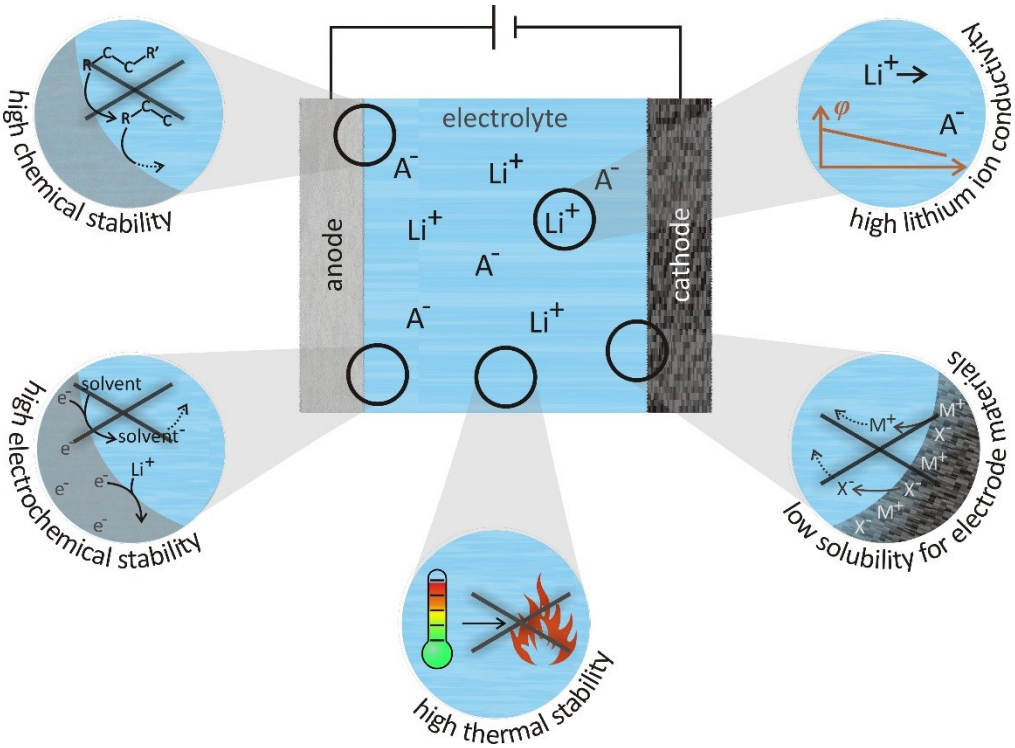

Figure 1.1: Summary of requirements for lithium electrolytes applied in lithium (ion) batteries.

The main demands for lithium electrolytes beneath sufficient lithium ion mobility are a high thermal, chemical and electrochemical stability to ensure cell safety. Moreover, it is required to minimize dissolution of electrode active material which decreases cell life time and performance. Figure 1.1 summarizes the requirements of a lithium electrolyte for lithium (ion) batteries. By adequate choice of cations and anions ionic liquids fulfill most of the requested demands, especially the aspect of safety which is crucial for battery applications.

Cell tests with ionic liquid-based electrolytes showed that sufficient cell capacity and life time can only be achieved at very small current densities which prohibit the achievement of high performance. The main reason for the poor performance of ionic liquid-based electrolytes is their low lithium ion mobility resulting from strong coordination of the lithium ions by the IL anions since no neutral solvent is present for the solvation of ions [10–13]. Thus, IL electrolytes can only be applied to electrochemical cells using additives which increase lithium ion mobility. One approach is to add common solvents to the electrolyte. However, this introduces again volatile compounds and reduces the advantages of ILs. Thus, the question arises whether the lithium ion mobility can be improved without changing the physical properties of the liquid phase. For solid, liquid and polymer electrolytes enhanced lithium ion mobility was achieved by introducing a solid second phase being itself electrically insulating [14–18]. If the surface of this second phase attracts anions and forms a negative surface charge, a positive space charge may form. For solid and liquid electrolytes it was reported that this space charge region at the isolating surface establishes enhanced cation conductivity. If percolation of the space charge regions is achieved the cation conductivity of the electrolyte can be improved remarkably. For polymer electrolytes a different mechanism is identified. It was shown that the second phase reduces the crystallinity of the polymer and therefore enhances the ion mobility. Since the properties of ionic liquids are not quite comparable with these systems it is interesting whether the lithium ion mobility can also be enhanced by introducing an inert second phase. This approach was already reported in literature [11, 19–29] but the results are not consistent, yet. So far, different materials were used as second phases and the ionic liquid was also varied. Hence, results from literature can hardly be compared. The missing systematics in the investigated systems do not allow an unambiguous conclusion on the effect of a second phase on the IL electrolyte properties.

Thus, in the present work exclusively one material was chosen as second phase, namely silica and its morphology and surfaces were varied systematically in one IL electrolyte, being N-butyl-N-methylpyrrolidinium bis(trifluoromethylsulfon)imide (BMP-TFSI) with lithium bis(trifluoromethylsulfon)imide (LiTFSI) as conducting salt. The effect of the second phase could be prevention or weakening of anion coordination on the lithium ions resulting in enhanced lithium ion mobility. By adequate choice of second phase, the anions could be bound to the interface region. Then, less solvating anions are available in the bulk electrolyte. Hence, less anions would be available to coordinate the lithium ions, increasing the concentration of free lithium ions and therewith the lithium ion conductivity (cf. Figure 1.2).

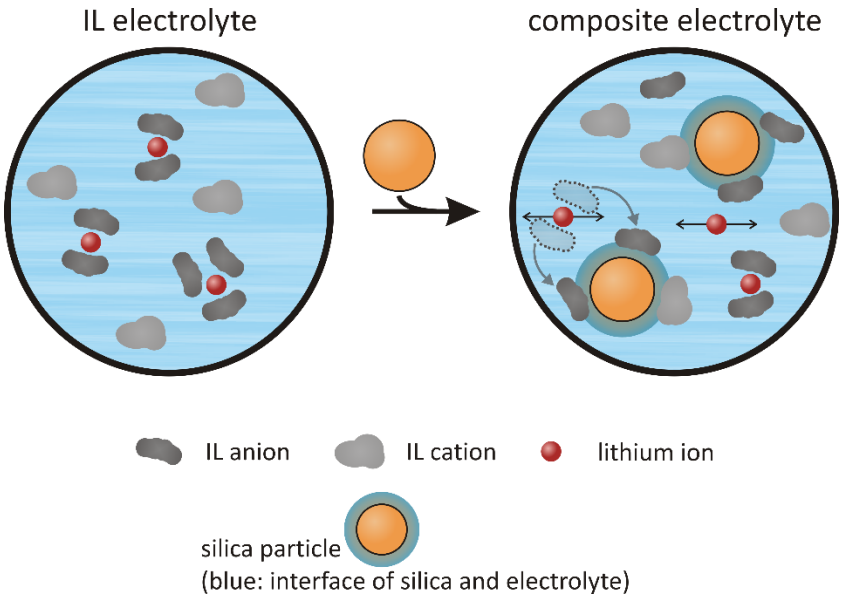

Figure 1.2: Schematic description of the effect of filler material (isolating second phase) in a lithium ionic liquid-based electrolyte to enhance lithium ion conductivity. The filler material may form an interface region with the IL electrolyte which immobilizes the anions. Hence, complexation of lithium ions may be decreased. Moreover an improved lithium ion mobility may be achieved in the interface region.

In the following detailed studies of the IL electrolyte 15 wt% LiTFSI in BMP-TFSI with silica which vary in morphology and surface functionalization are presented. Total conductivity of the composite electrolytes is presented as well as cyclic voltammograms of half cells with lithium iron phosphate and results on the electrochemical windows. The mechanical properties of the electrolytes were investigated by rheological rotation and oscillation experiments, providing the viscosities and viscoelastic properties. Finally, a model is proposed to describe the influence of silica filler on the coordination properties of the IL. Prior to the experiments the theoretical background is summarized for a better understanding of the results. Within this ionic liquid-based electrolytes are described and literature-known composite electrolytes are discussed. Then, the interface effect of ionic liquids in contact with solid surface is described prior to presenting IL electrolytes with silica. Finally, in the second chapter some basics on the conductivity as well as on the transference number are reviewed and rheology basics are presented. In the fourth chapter the results are summarized, and an outlook on further investigations for a deeper understanding of the presented system is given.

2 THEORETICAL BACKGROUND

The application of ionic liquids as electrolytes in lithium (ion) batteries is discussed and it is pointed out that it is crucial to enhance lithium ion mobility. In the second part conductivity enhancement by heterogeneous doping of solid, liquid and polymer electrolytes is introduced. Prior to present recent literature describing how this approach is applied to ionic liquid-based electrolytes, the interface of ionic liquids in contact with an inert surface is considered. Conductivity fundamentals are discussed briefly in the third part and some concepts on describing the conductivity of electrolytes containing an isolating phase are introduced. The significance of measuring the partial conductivities of electrolytes is outlined, and different methods to measure the partial lithium ion conductivity in liquid lithium electrolytes are reviewed briefly. For a better understanding of the mechanical properties and their measurements, some important fundamentals of rheology are presented in the last part.

2.1 IL electrolytes

In recent time a few reviews were published dealing with ionic liquid-based electrolytes (IL electrolytes) [4, 30–34]. Despite the advantageous properties of ionic liquids – high chemical and electrochemical stability, non-flammability, good wettability – IL electrolytes have some serious drawbacks. The discharge capacities with IL electrolytes are usually lower than discharge capacities obtained with common molecular solvent-based electrolytes [35–39]. Due to the high viscosity of ionic liquids the kinetics of electrode reactions is very slow. Thus, cycling can occur with IL electrolytes only at small current rates reversibly [40, 41]. Furthermore, the lithium ion conductivity in IL electrolytes is low since the lithium ions are coordinated by the IL anions forming negatively charged lithium complexes [42]. For TFSI-based ILs it

was shown by spectroscopic results and theoretical calculations that lithium ions are coordinated bidentately by two anions [10–13, 43–47]. Moreover, the results gave evidence on the *cis* conformer of TFSI anions being more stable in presence of lithium ions than in the neat IL electrolyte where the *trans* conformer is more favored [46]. Conductivity of IL electrolytes is mostly below 1 mS/cm and the reported transference numbers for lithium ions in the neat IL electrolytes do hardly exceed 0.1 [48]. Lassègues et al. showed that the lithium ions in different imidazolium-based ILs are coordinated by two anions at the usually used lithium salt concentrations [13]. This coordination is schematically shown in Figure 2.1. For higher mole fractions of lithium salt than 0.2 the authors reported nanostructering of the lithium and TFSI ions forming multinuclear complexes.

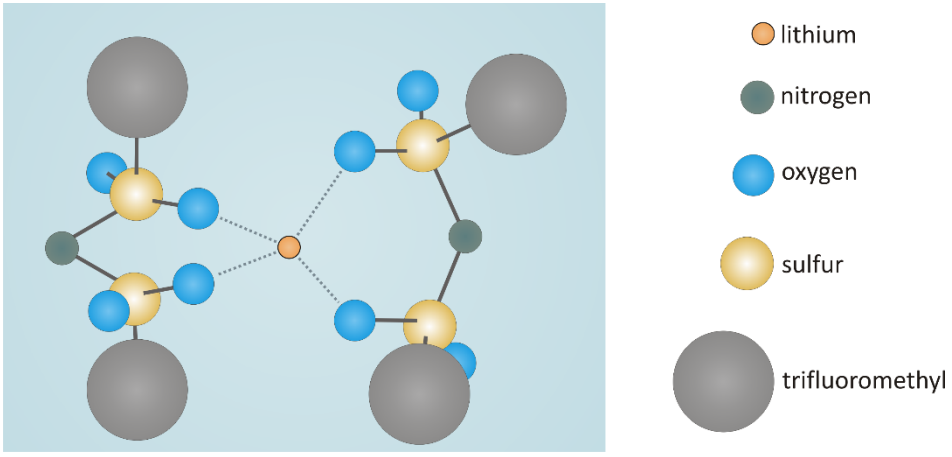

Figure 2.1: Lithium ions in IL electrolytes are strongly coordinated by the anions. This schematic view shows the tetrahedral coordination of lithium ions by TFSI anions (modified after [13]).

IL electrolytes are also discussed for lithium air batteries since these require chemically highly stable electrolytes which are inert to the aggressive oxygen radical anion formed during discharge. An informative review on lithium-air battery electrolytes was given by Balaish et al. [49]. For lithium-sulfur batteries IL electrolytes are also mentioned as they have a lower solubility for polysulfides formed during discharge. Recently Scheers et al. gave a review on electrolytes for lithium-sulfur batteries [40].

To understand IL properties it is important not to consider them as common liquids. Although they are in the liquid state, their mobility mechanism is different compared to neutral solvents. In a conventional electrolyte the lattice energy of the conducting salt is overcome by forming solvation shells whereas in the ionic liquid the lattice energy is small enough to be overcome by thermal energy. The reason for the low melting points being below room temperature is the very small lattice energy due to the mismatching symmetries of cations and anions [50, 51]. Using diffraction

experiments it was shown that ionic liquids show a short range order which appears similar as in an ionic crystal in the first coordination shells but is damped very fast [52, 53]. To describe the properties of ionic liquids the so-called hole model was established which predicts small empty volume elements with different sizes and shapes which fluctuate [54–57]. These holes in ILs are thermally generated for entropy reasons. Thus, these vacancies form continuously and show thermal motion leading to disappearance and reformation of larger and smaller holes. For ion diffusion a neighboring vacancy with adequate size is required. Since the probability for the formation of such a vacancy is not high in room temperature ionic liquids they show high viscosities and low conductivities compared to classical (high temperature) molten salts where the probability of vacancy formation is considerably higher. Hence, regarding ion mobility room temperature ionic liquids are not superior. To improve the properties of lithium IL electrolytes the ion mobility, especially the lithium ion mobility, has to be increased. One possible approach is to directly address the lithium ion mobility by weakening the interactions of lithium ions with the anions.

2.2 Composite electrolytes – Influence of interface

Solid electrolytes (SE). One approach to influence the ion conductivity of an electrolyte is to form interface regions with enhanced ion conductivity by introducing a second phase into the conducting matrix. For solid electrolytes it was already shown in the 1970s [58] that the presence of an isolating phase may induce space charge regions in the electrolyte with enhanced conductivity [14, 15, 59–62], which are formed due to the surface potential of the isolating phase. By adequate choice of second phase the counter ions are adsorbed at the insulator surface, resulting in an enrichment of mobile charge carriers in the space charge region. Thus, the conductivity in the interface region is enhanced compared to the bulk conductivity. This is only the case for intrinsic conductors where the concentration of mobile charge carriers is controlled by a defect formation equilibrium. Hence, this effect of heterogeneous doping is only significant for weak electrolytes where the adsorption/desorption equilibrium of charge carriers competes with the defect formation equilibrium resulting in an enhanced concentration of mobile charge carriers in the interface regions (cf. Figure 2.2).

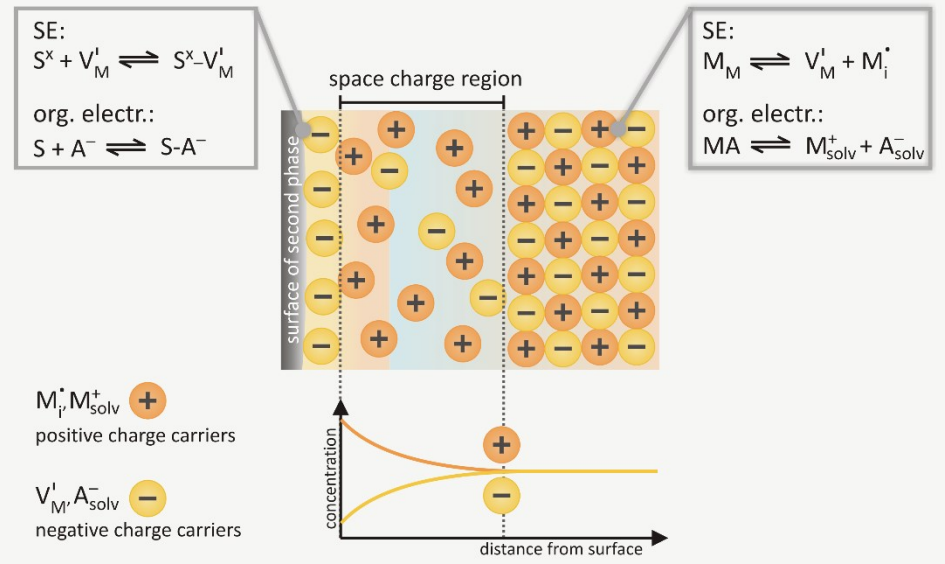

Figure 2.2: Schematic view of space charge regions formed by introducing an isolating phase with adsorption sites S into a cation conducting matrix. Adsorption/desorption equilibrium and charge carrier formation equilibria are shown in the reaction equations. Consuming of charge carrier by adsorption shifts bulk equilibrium towards formation of mobile charge carriers resulting in space charge regions with enhanced conductivities.

Percolation of these local space charge regions is required to cause a change of the mean conductivity [63]. Thus, conductivity enhancement occurs only if a minimum amount of second phase is present to form percolating space charge regions, called the percolation onset. For a volume fraction of second phase above the percolation onset the conductivity increases until a maximum is reached due to percolation paths which are shown schematically in Figure 2.3. Then the percolation threshold is reached and the conductivity starts to decrease with increasing amount of second phase. This decrease is due to sterically blocked percolation paths by second phase particles because of their too high volume fraction. Several authors presented experimental data approving this theory of percolating space charge regions. The investigations were mostly carried out with alumina or silica doped halides [58, 64–70].

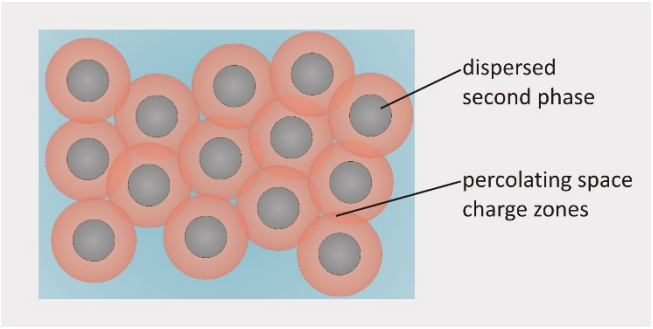

Figure 2.3: Conducting matrix (blue) with dispersed second phase (grey) is shown schematically. The space charge regions (red) with enhanced cation mobility overlap forming percolation paths with enhanced conductivity

Organic solvent-based electrolytes (org. electr.). This effect of enhanced conductivity due to percolating space charge regions in composite electrolytes was also reported for liquid lithium electrolytes based on neutral solvents. Bhattacharyya et al. showed for several lithium electrolytes a conductivity increase with rising amount of silica as filler material and called the electrolytes "soggy sands" [71–77]. He used mainly lithium perchlorate ($LiClO_4$) containing electrolytes with methanol, tetrahydrofuran (THF), ethylene glycol and low molecular polyethylene glycol [72–75], but also technical electrolytes as lithium hexafluorophosphate ($LiPF_6$) in carbonate-based solvents [71, 76, 77]. The reported conductivities pass through a maximum with varying amount of filler material as already shown for solid composite electrolytes [14]. Similar results were achieved in lithium electrolytes based on borate esters by Kaskhedikar et al. [78]. The conductivity enhancement increased with decreasing particle sizes of the filler materials, increasing Lewis acidities of the surfaces of filler materials and decreasing dielectric constants of the electrolyte solvents [73]. Beneath unmodified silica nanoparticles Bhattacharyya et al. also used methyl-, octyl- and aminopropyl-modified silica particles [71, 74–77]. Although both hydrophobic silica formed stable networks, resulting in viscoelastic electrolytes, a conductivity enhancement occurred only in the electrolytes with methyl-modified silica. The authors assume that the octyl groups hinder the lithium ion mobility sterically. The aminopropyl-modified silica formed only a sol indicating that no stable network with percolating space charge regions could be formed. The results were in good accordance with the zeta potentials of the silica which were all negative except in the case of the aminopropyl-modified silica.

Comparable conductivity measurements as carried out by Bhattacharyya et al. in carbonate-based lithium electrolytes [71, 76, 77] were carried out by Sann et al. [79], leading to contradictory results since a continuous decrease of conductivity with increasing amount of silica as filler material was reported. Even using the same electrolytes and particle sizes of silica led to different results compared to Bhattacharyya et al. Since the effect of heterogeneous doping occurs at the interface of filler material and electrolyte Sann et al. [80] also used carbonate-based lithium electrolytes with mesoporous silica which had high surface areas. By varying the volume fraction of mesoporous silica in the electrolytes the measured conductivities still decreased continuously. In this context Pfaffenhuber et al. presented an in-depth discussion of the so-called "soggy-sand" electrolytes [16]. The authors showed that ion pairs have to dominate in the neat electrolyte to achieve an improvement by the concept of heterogeneous doping [16, 81]. Using dye-sensitized silica they demonstrated by confocal fluorescence microscopy that the required network for space charge percolation forms slowly on the time scale of several days. This observation

was complimented by conductivity measurements, showing that the conductivity varied with time. Furthermore, the authors showed that ultrasonic treatment which was applied by Sann et al. to disperse the filler material interrupts this network formation of filler material. The authors emphasize that the network structure, which is essential for conductivity enhancement – since percolation paths are necessary – is kinetically controlled and hence, the reproducibility of the results is difficult to achieve even in computer simulations. These comments support the assumption that the continuous conductivity decrease with increasing amount of filler observed by Sann et al. [80, 82] might be explained by an incomplete formation of filler network. The conductivity measurements of Sann et al. were carried out at different temperatures. Hence, the measurement of one electrolyte took about two hours. If the network formation was time dependent, the conductivities would have been not consistent with varying temperature. Interestingly this effect was not observed in any experiment, indicating that conductivities of the investigated electrolytes were not time dependent.

Conductivity enhancement resulting from heterogeneous doping can only be observed if the conductivity of space charge regions is higher than the bulk conductivity. This is only the case for weak electrolytes in which ion pair formation dominates. In the bulk the solvated ions which contribute to electrolyte conductivity are in equilibrium with ion pairs. In weak electrolytes the equilibrium is shifted towards the formation of ion pairs. The adsorption of one ion species at the surface of the second phase shifts the equilibrium towards the formation of solvated ions (cf. Figure 2.2). In strong electrolytes ion pairs are hardly present. Thus, adsorption of ions reduces the concentration of mobile charge carriers and decreases the total conductivity. Since Sann et al. investigated lithium electrolytes with high bulk conductivity the effect of heterogeneous doping could not be observed. In the light of this, the conductivity enhancement observed by Bhattacharyya et al. in carbonate-based electrolytes with $LiPF_6$ is surprising.

Pfaffenhuber et al. reported for a 0.1M solution of lithium perchlorate in THF an increase of the lithium transference number from 0.13 to 0.41 upon dispersing 0.15 vol% silica [83]. Transference numbers were determined by potentiostatic polarization which is discussed below in Chapter 2.3.2. For the polyethylenglycol-based electrolytes containing silica an increase of lithium transference number was reported [84]. Moreover, a slight conductivity enhancement was observed for small volume fractions of about 0.01 of silica followed by a strong conductivity decrease considerably below the conductivity of the pristine electrolyte [16, 85, 86]. The authors assume an enhanced transference number even at decreased conductivities. Some other works dealing with silica filled liquid electrolytes were also presented but did not give further mechanistical explanations [87–94]. Composite electrolytes based on organic

solvents with silica as filler materials are discussed in-depth in the PhD thesis of Kerstin Sann [82].

Polymer electrolytes. Dispersing an isolating second phase in electrolytes to improve properties is a known strategy in polymer electrolytes, too. Hence, a selection of the numerous results on filled polymer electrolytes are presented in the following. It is shown that adding filler material to the polymer electrolyte enhances conductivity. This enhancement is not explained by space charge percolation solely but by decreased crystallinity of near-surface polymer caused by the filler material [17, 18, 95–105].

Ionic liquid-based electrolytes. In the context of heterogeneous doping IL electrolytes depict a difficult intermediate case since they consist solely of ions. It is clear, that space charge layer can be neglected in ionic liquids due to their high ionicity which leads to small Debye lengths. The question arises whether the effects on the surface of the second phase will be able to compete with the bulk properties and how the hole formation is influenced since ion mobility in ionic liquids occurs through vacancies, the so-called holes.

2.2.1 Interface effects in ionic liquids

As described above interface effects in electrolytes containing a second phase improved properties in some cases. From the theoretical point of view, significant effect is only expected once the concentration of mobile charge carriers is governed by a “buffer” equilibrium. Since ionic liquid properties are close to solid electrolytes, combining the advantageous properties of liquids with a high safety it is interesting to investigate the influence of interface effects on IL electrolytes. Space charge regions as described for solid and liquid composite electrolytes can be neglected in ionic liquids due to their high ionicity resulting in very short Debye lengths. Therefore, the interfaces of ionic liquids are described first to give a basis for the discussion of ionic liquid-based composite electrolytes.

It is well known from literature that ionic liquids interact with surfaces they are in contact with and that they form different structures on different surfaces. Su et al. [106], Steinrück et al. [107], Perkin [108], Drüschler et al. [109] and Fedorov et al. [110] give overviews on the studies presented so far concerning the interface of ionic liquids with different surfaces. A Helmholtz-like layer with a thickness of one ion layer [111, 112] as well as multiple ion layers [109, 113–116] are reported for ionic liquids in contact with solid surfaces. Since the Gouy-Chapman-Stern model and the Debye-Hückel theory describe dilute solutions they cannot be used to describe interfaces with ionic liquids [115]. The work of Carstens et al. [113] showed by in situ STM and AFM the preferential adsorption of anions on positively polarized gold

surfaces and adsorption of cations at negatively polarized and not polarized gold surfaces. This conclusion is not restricted to gold surfaces but is valid for metal surfaces in general. The investigations were carried out with gold surfaces since an ionic liquid in contact with a gold surface is the most frequently reported model system. Highly charged surfaces might cause an organization of the IL ions into multiple layers [114]. The higher the surface potential of the Au(111) surface the more ion layers are formed on the surface. Thus, the innermost layer has a templating effect [115]. At positively charged Au(111) surfaces a weaker near surface structure is developed than at negatively charged surfaces. Hayes et al. explained this by the less ability of adsorbed anions to template further ion layers [115, 117]. Perkin concluded that multiple layers are formed on charged surfaces because the innermost layer may contain more charge than necessary to screen the surface charge [108]. Hence, a second layer of ions is formed to screen the charge of the innermost layer and so on. On surfaces with less charge density only one ion layer is formed to neutralize. Similar results were obtained by Mezger et al. investigating ionic liquids with tris(pentafluoroethyl)trifluorophosphate (FAP) anions on charged sapphire surfaces [118]. There are several works reporting an orientation of the ions in the innermost layer on the surface [112, 114, 116, 119]. Baldelli showed that imidazolium ions align parallel to negatively charged surfaces and are repelled from positively charged surfaces [112]. Mao et al. described a micelle-like adsorption of imidazolium on the Au(100)(1x1) surface because of a crystallographic dependence of the molecule-surface interaction [120]. Smith et al. [121] reported that pyrrolidinium-based ILs with different alkyl chains and TFSI (bis(trifluoromethylsulfon)imide) anion forms different structures between two charged mica surfaces depending on the alkyl chain length. Up to chain lengths of $n = 8$ altering cation-anion monolayers are formed. Pyrrolidinium cations with chain lengths above $n = 10$ form bilayers with full interdigitation of the alkyl chains.

Although the results are not systematic yet, it is obvious that the formed interface depends strongly on polarization of the surface and the nature of ionic liquid. Drüschler et al. [109] and Baldelli [111] believe that impurities in the ionic liquids are the reason for the different results in different publications. By and large, it can be concluded that confined IL electrolytes will have different properties than bulk IL electrolytes due to the interface effect which cannot be predicted yet, as no clear model exists. Since the present work deals with IL electrolytes filled with silica, the confinement of neat ionic liquids by a silica matrix is highlighted before discussing IL electrolytes in contact with silica surfaces.

Atkin et al. [122] was the first to describe several ion layers on electrode surfaces in contact with ionic liquids. In his work he presented AFM measurements of different

ionic liquids in contact with mica, graphite and silica surfaces. Silica supported ionic liquids show liquid-like behavior with restricted mobility due to solid-like ordered structure under confinement (cf. Figure 2.4) [117, 123–129]. Several studies gave evidence on the interaction of IL ions with silica walls [123, 127, 130, 131] which decreases with rising temperature [132]. Conboy et al. [133, 134] reported a favored orientation of IL ions on silica surfaces. Amongst others they showed that imidazolium ions take a tilted orientation to the silica surface with the alkyl chain almost perpendicular to the surface. Orientation of the imidazolium on the surface mostly depends on the alkyl chain lengths and is also influenced by the surface charge density of the silica. Hayes et al. reported that substrate smoothness is crucial for interface organization since the forces promoting the formation of interface structures have only short range [115, 117].

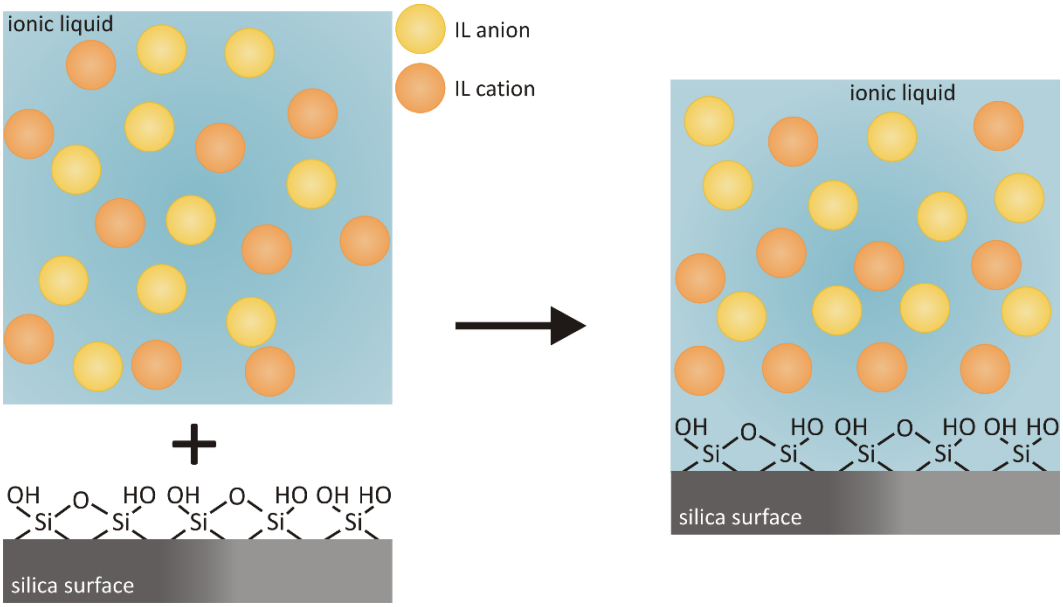

Figure 2.4: Reorganization of ions in ionic liquids in contact with a silica surface is shown schematically. The ions on the silica surface are ordered but still remain mobile.

Ueno et al. [127] showed that viscosities of ILs increase by a factor of 1 to 3 upon confinement but still keep liquid-like mobility. Iacob et al. [130] showed by NMR measurements that the diffusion coefficient of HMI-TFSI (1-hexyl-3-methylimidazolium TFSI) decreased by a factor of ten upon confinement in a silica monolith and was increased again upon using a silica monolith with silanized walls. Hence, the decreased ion mobility in ILs with contact to silanol groups was explained by hydrogen bonds between the IL ions and the silanol groups on the silica surface. Several works showed that confining ILs changes their phase behavior. Göbel et al. [128, 135] showed by DSC measurements that the phase behaviors of confined ILs depend on the silica surface. Singh et al. [131] reported decreasing melting points of

ILs upon confining in a silica matrix. A critical review on confined ionic liquids was given in 2011 by Le Bideau et al. [132]. Néouze et al. [136, 137] confined ILs in a silica matrix by a nonaqueous sol-gel process leading to transparent ionogels with high thermal stability. They showed by DSC and NMR measurements that the IL in the silica network exhibits an intermediate behavior between liquid and solid. The properties of the ionogels depend on the choice and amount of the IL and silica matrix.

2.2.2 IL-based electrolytes in contact with silica

There are also some reports on IL electrolytes confined in a mesoporous silica matrix which are schematically presented in Figure 2.5.

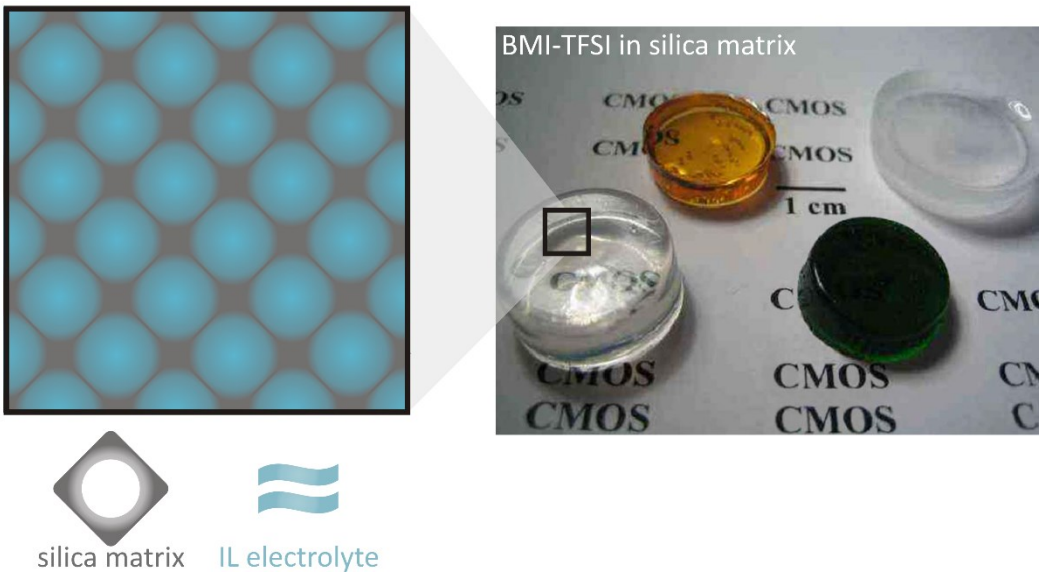

Figure 2.5: Ionogels describe confined ionic liquids or IL electrolytes in a silica matrix. On the right side ionogels consisting of BMI-TFSI in a silica matrix are shown from reference [136]. On the left side a schematic view of their structure is shown.

The so-called ionogels were published for the first time by Echelmeyer et al. [19]. A one-pot sol-gel synthesis of a silica glass network confining lithium triflate (LiTf) in BMI-BF_4 (1-butyl-3-methylimidazolium tetrafluoroborate) was presented where the BMI-BF_4/LiTf-ratio was varied between 1/1 and 4/1. A fully condensed silica matrix in form of a transparent, colorless glass monolith resulted. In analogy to already reported results on confined ILs the authors showed by NMR that the ion mobility of the IL electrolyte decreased in the ionogel but a liquid-like mobility still remained. The highest diffusion coefficients were obtained for the imidazolium cation and the lowest for the lithium ions. The authors concluded that the BMI ions exist as single ions and the lithium ions are coordinated by the anions as in a neat IL. Furthermore, the authors

reported an increasing mobility of lithium ions with rising IL/LiTf-ratio which is in good agreement with spectroscopic results mentioned above, expressing that lithium ion complexation is rising with increasing amount of lithium salt in the IL electrolyte.

Table 2.1: Summary of the main results achieved in investigations of lithium ionogel electrolytes so far.

Electrolyte in silica matrix	Experiments	Main results	Ref.
LiTf in BMI-BF_4	NMR PEIS	Decreased ion mobility compared to neat electrolyte $D(BMI^+) > D(BF_4^-) > D(Li^+)$ $D(Li^+)$ increases with decreasing LiTf concentration	[19]
LiTFSI in PMP-TFSI	Half cell tests with LFP and LNMCO SEM	Lower capacities compared to neat IL electrolyte: 110 mAh/g (C/20 rate, r.t.)	[20]
LiTf in BMP-TFSI	Half cell tests with LFP PEIS SEM, TEM	Good cycle stability and coulombic efficiency at 328 K and C/10 rate Discharge capacity 133 mAh/g at r.t. and 154 mAh/g at 328 K (C/10 rate)	[21]

Le Bideau et al. [20] also presented an ionogel consisting of 0.5M LiTFSI/PMP-TFSI (lithium bis(trifluoromethylsulfon)imide in N-propyl-N-methylpyrrolidinium TFSI) in a silica matrix which was used as electrolyte and separator simultaneously in half cells with LFP (lithium iron phosphate) and LNMCO (lithium nickel manganese cobalt oxide). The resulting ionogel contained 90 vol% IL electrolyte. During cell preparation the sol was applied on the cathodes prior to condensation. Since the sol was less viscous than the IL electrolyte a good contact with the electrodes was achieved which was supported by SEM and EDX measurements. In the half cells with LFP slightly lower capacities being 110 mAh/g were reached with the ionogel compared to the neat IL electrolyte. With the cell test with LNMCO also a capacity of 110 mAh/g was reached with the ionogel and 105 mAh with the neat IL electrolyte. All cell tests were carried out with a C/20 rate at room temperature, and no information was given on the used separator in the cells with the neat IL electrolytes. The results agreed well with literature data using a conventional organic electrolyte (lithium hexafluorophosphate in a mixture of ethylencarbonate and dimethylcarbonate).

Wu et al. [21] investigated a silica matrix filled with LiTf in BMP-TFSI (N-butyl-N-methylpyrrolidinium TFSI). Electrochemical characterization with LFP as cathode material showed a discharge capacity of 133 mAh/g in the 9th cycle at room temperature. At 313 K 149 mAh/g with 100 % efficiency was reached and 154 mAh/g at 328 K. The presented galvanostatic cycling experiments were carried out at C/10 rate. The scan rates were increased to 1C showing still a good cycle stability. Initial discharge capacities could be reached after decreasing the C rate to its initial value. Table 2.1 summarizes the results on ionogel electrolytes.

The IL electrolyte is completely confined in the ionogels and still shows liquid-like mobility. As no bulk electrolyte is present in ionogels the ion mobilities are very low. Due to resulting small conductivities stable cycling with adequate capacities is only possible with very low current densities. Thus, it is interesting whether a dispersed composite electrolyte consisting of IL electrolyte with isolating second phase shows an improvement of the ion mobility due to interfaces which influence bulk properties positively as already shown for heterogeneous doped solid and liquid electrolytes. A schematic picture of a dispersed composite electrolyte is given in Figure 2.6.

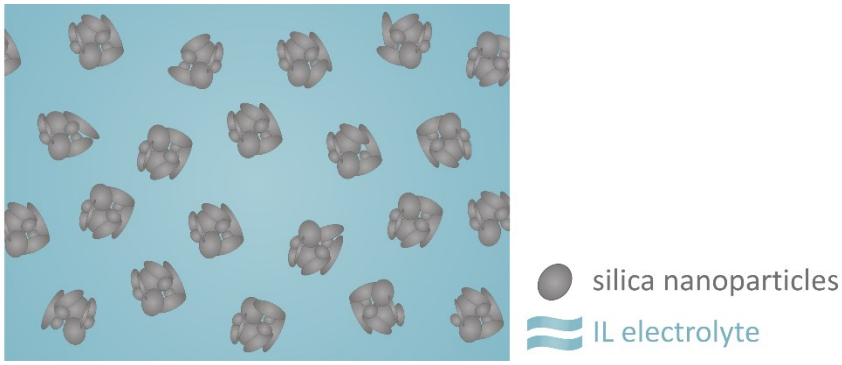

Figure 2.6: Schematic view of a composite electrolyte consisting of a dispersed isolating phase in a liquid electrolyte.

A commonly used filler material is silica since it is an isolating inert material and its surface can be modified easily. Several works were already reported dealing with silica filled IL electrolytes and are summarized in the following. In all cases conductivities of the composite electrolytes were decreased compared to the neat electrolyte. Honma et al. [22–24] used silica fractions higher than 25 vol% in 0.2M and 1M LiTFSI/EMI-TFSI (LiTFSI in 1-ethyl-3-methylimidazolium TFSI) and 1M LiFSI/EMI-FSI (lithium bis(fluorosulfon)imide in EMI-bis(fluorosulfon)imide). The high fractions of filler material led to solid-like electrolytes [22, 23]. The authors showed by NMR experiments that silica promotes the dissociation of EMI-TFSI and EMI-FSI and does not influence the lithium ions significantly. Only in 1M LiFSI/EMI-FSI the authors observed a decreased diffusion coefficient of the lithium ions and

lithium ion containing complexes. The conductivities of these quasi-solid electrolytes were considerably decreased compared to the neat electrolyte, values between 0.05 mS/cm at 283 K and 10 mS/cm at 523 K were reported. 25 vol% silica in 1M LiTFSI/EMI-TFSI was used as thick-film electrolyte in a half cell containing $LiCoO_2$ as cathode and the theoretical cell capacity was reached at 338 K (C/10 rate) [24].

Saito et al. [11] investigated 20 wt% polymer and silica as filler materials, respectively, in 3 wt% to 24 wt% LiTFSI in BMI-TFSI (1-butyl-3-methylimidazolium TFSI) and BDMI-TFSI (1-butyl-2,3-dimethylimidazolium TFSI), respectively. By comparison of the diffusion coefficients of the different ion species obtained by NMR measurements the authors concluded that silica promotes the release of the TFSI ions from the lithium complexes. Thus, the lithium transference number is enhanced by adding silica to the IL electrolyte. The polymer restricted the diffusion of the lithium ions since the oxygen atoms of the polymer interacted with the lithium species and solvated them. The authors also investigated 20 wt% LiTFSI/EMI-TFSI with 5 wt% and 10 wt% silica [25]. They determined diffusion coefficients by NMR and conductivities by impedance spectroscopy which both decreased with increasing content of filler material. At the same time strong increase in viscosity was observed. Applying the Stokes-Einstein relation showed that the hydrodynamic radius of the lithium ions decreased with higher silica content. The Stokes-Einstein relation is depicted in equation (2.1) where D describes the measured diffusion coefficient, k_B the Boltzmann constant, T the temperature, r the ion radius and η the viscosity of electrolyte.

$$D = \frac{k_B T}{6\pi \cdot r \cdot \eta} \tag{2.1}$$

The authors did not discuss the applicability of the Stokes relation to real systems, especially to ionic liquids, and no statement was given concerning the error. The only parameter which changes in the compared electrolytes is the amount of filler material and thus, the electrolyte volume fraction. As the chemical composition of the electrolyte remains the same it may be assumed that the error is high but systematic by applying the Stokes relation. Hence, the radii can be treated as relative values allowing the comparison between the electrolytes. The authors concluded that complexation of lithium ions is decreased by addition of silica. The comparably small diffusion coefficients of lithium were explained to arise from the strong increase in viscosity. Contradictory results were reported by Nordström et al. [26]. They investigated 4 wt% $LiBF_4$ (lithium tetrafluoroborate) in BMI-BF_4 (1-butyl-3-methylimidazolium BF_4) with 1 wt% and 5 wt% silica as filler materials by Raman spectroscopy and

impedance spectroscopy. Their conclusion was that lithium ions are immobilized on the silica surface.

Sun et al. [27] reported on PMP-TFSI (N-propyl-N-methylpyrrolidinium) with silica particles which were surface-modified with lithiumpropylsulfonate. The content of surface-modified silica was varied between 3 wt% and 15 wt% and it was shown that lithium ions dissociate from the silica surface. The dissociation could be enhanced by addition of the zwitterion 1-butylimidazolium-3-butansulfonate. However, the electrochemical response in the CV experiments with platinum or copper as working electrode and lithium as reference and counter electrode was very poor.

Honma et al. [28] presented a quasi-solid-state lithium-sulfur cell by using 0.64M LiTFSI in DEME-TFSI (N,N-diethyl-N-methyl-N-(2-methoxy-ethyl)ammonium TFSI) with 25 vol% silica. By adding 5 wt% PTFE (polytetrafluoroethylene) self-standing membranes were achieved and used as electrolyte. The so-called quasi-solid-state electrolyte was also used as additive in the cathode. Galvanostatic cycling tests showed an initial discharge capacity of 1370 mAh/g at 308 K (C/20 rate) which decreased to 600 mAh/g during 10 cycles. The authors also investigated 1M LiTFSI in different ionic liquids, namely EMI-TFSI, DEME-TFSI and PMPip-TFSI (N-propyl-N-methylpiperidinium TFSI) with 25 vol% silica [29]. Self-standing membranes were obtained by adding 5 wt% PTFE and characterized by impedance spectroscopy, NMR and cell test. They reported liquid-like high ion transport coefficients. Nevertheless, in cell tests with symmetric cells using lithium electrodes high rate performances were not achieved. Table 2.2 gives an overview of results on dispersed composite lithium electrolytes based on ionic liquids presented so far.

Table 2.2: Literature overview on ionic liquid-based composite electrolytes with silica as filler material.

Filler material	Electrolyte	Experiments	Main results (as given by authors)	Ref.
> 25 vol% SiO_2	0.2M/1M LiTFSI/EMI-TFSI 1M LiFSI/EMI-FSI	NMR, PEIS Cell test SEM, EDX	Dissociation of EMI from anions promoted Theoretical capacity reached at 338 K with $LiCoO_2$	[22–24]
< 10 wt% SiO_2	3 wt% - 24 wt% LiTFSI in BMI-TFSI and BDMI-TFSI	NMR, Rheology	Release of TFSI from Li complexes promoted	[11]
< 10 wt% SiO_2	20 wt% LiTFSI/EMI-TFSI	NMR, PEIS Viscosity	Complexation of Li ions decreased	[25]
< 5 wt% SiO_2	4 wt% $LiBF_4$/BMI-BF_4	PEIS Raman Viscosity, DLS	Lithium ions immobilized on silica surface	[26]
< 15 wt% SiO_2-$C_3H_6SO_3Li$	PMP-TFSI	NMR, PEIS, CV DSC DLS	Lithium ions dissociate from silica surface Poor electrochemical response in CV	[27]
25 vol% SiO_2	0.64M LiTFSI/DEME-TFSI + 5 wt% PTFE	Cell test N_2-physisorption SEM, EDX, XRD	Self-standing membranes with PTFE Discharge capacity with sulfur composite cathode was 1370 mAh/g (308 K, C/20 rate) at 1st cycle and 600 mAh/g at 10th cycle	[28]
25 vol% SiO_2	1M LiTFSI in EMI-TFSI, DEME-TFSI and PMPip-TFSI + 5 wt% PTFE	Cell test NMR, PEIS Viscosity SEM, EDX	Self-standing membranes with PTFE Liquid-like high ion transport	[29]

In summary, the ion mobility was positively influenced by filler materials in solid and polymer electrolytes. In commonly used liquid electrolytes, based on organic solvents, ion mobility also seems to be affected by silica as filler material, but a conductivity enhancement was only observed for electrolytes with high ion pair concentrations and therefore intrinsically low conductivities. For ionic liquids in contact with solids the formation of ordered structures was reported. The structures strongly depend on the nature, surface structure and surface dipole of the solid as well as on the nature of the ionic liquid. In interaction with silica ionic liquids show a solid-like structure with liquid-like mobility. However, no consistent model has been developed so far to explain the interaction microscopically. For IL electrolytes confined in a silica matrix the mobility was reported to decrease but the liquid-like mobility was still maintained. With composite electrolytes consisting of dispersed silica in IL electrolytes cell cycling was possible with low current density. Contradictory results were presented concerning the influence of silica on the lithium mobility. Saito et al. [11, 25] reported a decreased complexation of lithium ions and therefore an increased lithium ion mobility whereas Nordström et al. [26] reported an immobilization of lithium ions on the silica surface.

2.3 Conductivity

Ion transport occurs in electrolytes due to a non-equilibrium state and the attempt of the system to reach equilibrium. Thus, to describe transport properties the temporal change of the system has to be considered. The driving force for ion flux in an electrolyte is a gradient in free energy across the system. Considering the electrolyte between two planar electrodes as presented in Figure 2.7 the potential difference φ between these electrodes corresponds to an electric field E which is the sole driving force for the positively charged ions to move towards the negatively polarized electrode and vice versa, if no concentration gradient is present.

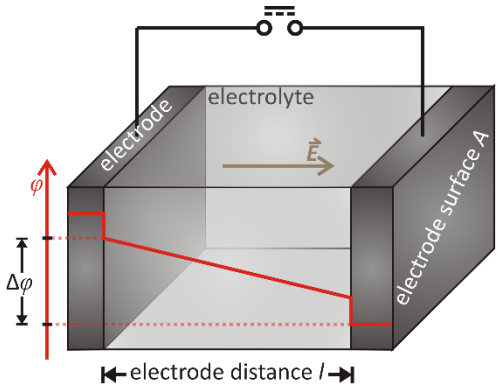

Figure 2.7: Electrolyte between two planar electrodes with the surface A and distance l. The potential difference φ between the electrodes is shown by the red line and the electric field E by the brown vector.

At steady state the ion flux J and therefore also the current density j are proportional to the driving force, which in this case is the electric field E, with the proportionality factor A and B, respectively (cf. equations (2.2) and (2.3))

$$J = A \cdot E \tag{2.2}$$

$$j = B \cdot E = B \cdot \frac{\Delta\varphi}{l} \tag{2.3}$$

$\Delta\varphi$ describes the potential difference and l the distance between the electrodes. Hence, the resulting current in an electrolyte between two polarized electrodes depends on the cell geometry. Equation (2.3) contains the distance l between the electrodes, and the area A of the electrodes is included in the current density j. Substituting the current density with the current I and identifying the proportionality factor B as the conductivity σ of the electrolyte, equation (2.4) results.

$$I = \sigma \cdot \Delta\varphi \cdot \frac{A}{l} \tag{2.4}$$

Comparison of equation (2.4) with Ohm's law shows that the resistance R of electrolyte depends on the cell geometry and electrolyte conductivity (equation (2.5)).

$$R = \frac{l}{A} \cdot \frac{1}{\sigma} = \frac{K_{\text{cell}}}{\sigma} \tag{2.5}$$

K_{cell} represents the cell constant. Thus, the smaller the distance between the electrodes and the higher their geometrical area the higher is the current of the electrochemical cell by polarizing the electrodes. The conductivity depends on the concentration of mobile charge carrier. Hence, differently concentrated electrolytes consisting of the same salt and solvent have different conductivities. Thus, to facilitate comparison of electrolytes a concentration normalized conductivity is used. The molar conductivity Λ_{m} (equation (2.6)) is normalized to concentration c of the conducting

salt but still depends on the ion charge since higher charged ions experience the electric field stronger than lower charged ions. Thus, the equivalent conductivity Λ which is normalized to the concentration and the charge number z (equation (2.7)) is more useful to compare different electrolytes.

$$\Lambda_m = \frac{\sigma}{c} \tag{2.6}$$

$$\Lambda = \frac{\Lambda_m}{z} = \frac{\sigma}{c \cdot z} \tag{2.7}$$

Conductivity of an electrolyte is dependent on the electric field as well as on the concentration and charge number of the mobile charge carriers. Moreover, the conductivity is influenced by the environment of the mobile charge carriers. Ions in liquid electrolytes are solvated with the solvation shell depending on different factors as charge density, ion size and nature of the solvent. The hydrodynamic ion size and ion dissociation depends on the conducting salt and the solvent. Thus, ion-ion and ion-solvent interactions are very dominant in liquid electrolytes and strongly influence ion transport.

2.3.1 Conductivity of composite electrolytes

Liquid electrolytes with a dispersed isolating second phase were already reported in the literature as discussed above. If no interface effect occurs between the dispersed material and the electrolyte the isolating material represents solely an exclusion volume. Hence, the total conductivity should decrease depending on the morphology and arrangement of the second phase. This scenario is schematically presented in Figure 2.8 assuming the second phase to be small particles.

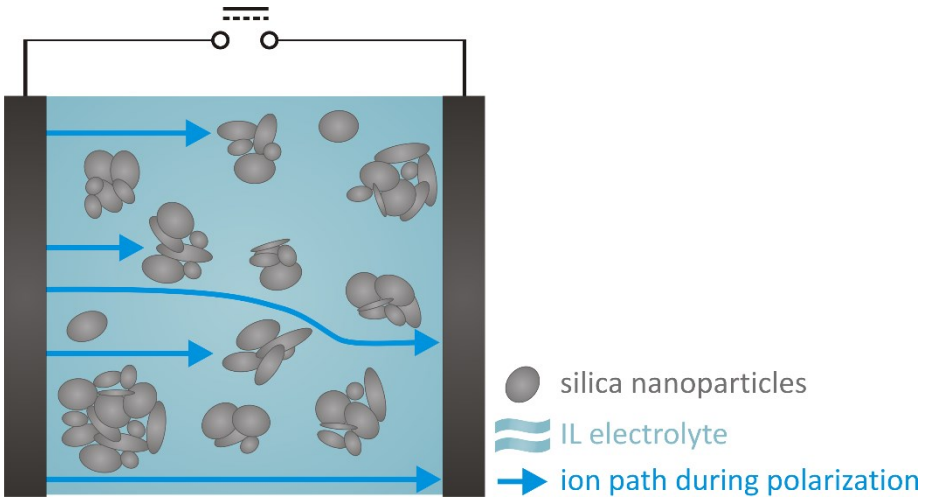

Figure 2.8: Dispersed isolating phase interrupts ion transport sterically. If no interface effect occurs the dispersed phase presents an exclusion volume solely.

Maxwell predicted the conductivity behavior of liquid composite electrolytes in their wet limit where the volume fraction of the electrolyte ε clearly dominates over the volume fraction of the isolating second phase φ [138]. The second phase was assumed to be spherical particles. Equation (2.8) describes the conductivity decrease σ' of the composite electrolyte with varying amount of spherical second phase if no interface effect is assumed. The conductivity decrease σ' is defined as the relative conductivity of the composite electrolyte with respect to the conductivity of the conducting matrix.

$$\sigma' = 1 - \frac{3}{2}\varphi \tag{2.8}$$

In the dry limit where the volume fraction of the second phase φ dominates the conductivity change was described by Lemlich [139]. Equation (2.9) treats the spherical second phase also as exclusion volume solely.

$$\sigma' = \frac{1}{3}\varepsilon \tag{2.9}$$

Feitosa et al. [140] presented equation (2.10) to predict the conductivity decrease for all volume fractions of the isolating phase.

$$\sigma' = \frac{2\varepsilon \cdot (1+12\varepsilon)}{6+29\varepsilon-9\varepsilon^2} \tag{2.10}$$

If the conductivity of a liquid composite electrolyte does not decrease in one of the predicted ways the spherical isolating phase does not act as exclusion volume solely. Hence, there should exist an interface effect which influences the ion mobilities in the electrolyte.

2.3.2 Partial conductivity

Regarding non-ideal electrolytes ion-ion and ion-solvation interactions cannot be neglected the way they are in ideal electrolytes or rather electrolytes at infinite dilution. Hence, ions interact and show different mobilities due to size, charge number, ion-ion and ion-solvent interactions. Thus, transference number t is introduced for the individual ions which describes the ratio of the conductivity of one individual ion species σ_i to the total conductivity σ (equation (2.11)).

$$t_i = \frac{\sigma_i}{\sum_i \sigma_i} \tag{2.11}$$

From equation (2.11) it is obvious that the sum of the transport numbers of all ion species has to be one. To characterize battery electrolytes the partial conductivity of

the lithium ion is crucial since a minimum partial conductivity of the ion involved in the redox reactions at the electrodes is required to avoid high concentration gradients which limit the cell performance [141, 142]. Solid lithium electrolytes have only one mobile ion species which has to be separated from the electronic conductivity to obtain the ionic transference number. The electronic conductivity can be measured by the Wagner-Hebb method using a non-symmetric cell with a blocking and a reversible electrode [143, 144]. In liquid electrolytes the situation is more complicated, since the cation and anion conductivities have to be separated. For aqueous electrolytes there exist established methods for determining the cation transference number [145–148]. For nonaqueous lithium electrolytes there is no established method so far since solvation of ions is weaker resulting in more complex ion pair formation. Therefore, properties of nonaqueous electrolytes depend stronger on the electrolyte concentration leading to clearly higher errors during measurements of transference number.

Zugmann et al. compared four different methods to determine lithium transference numbers of different carbonate-based electrolytes [142]. They used the two most frequently applied methods being potentiostatic polarization and PFG-NMR and faced them with the methods of galvanostatic polarization and electromotive force. The same electrolytes showed different transference numbers with the different methods. By PFG-NMR all lithium nuclei are detected independent of their coordination. Hence, lithium ions embedded in neutral or negatively charged complexes are also detected and considered for the transference number although they do not contribute to the lithium ion current in an electric field. Therefore, the transference number determined by PFG-NMR is considerably overestimated. The potentiostatic polarization method was introduced by Bruce and Vincent [149] and is only valid for ideal solid polymer electrolytes but can also be applied to dilute binary liquid electrolytes [150]. Therefore, reproducibility applying this method to liquid lithium electrolytes is very poor. For applying the method of electromotive force it has to be assumed that the transference number does not depend on ion concentration. Since this assumption is not correct, interpretation of the results becomes difficult. Hence, the method does not yield correct values and the results are hardly reproducible. The galvanostatic polarization method which is only valid for binary solutions is the most reliable method since it comprises only a few assumptions and is valid for electrolytes with ion-ion and ion-solvent interactions [151]. This approach combines three different methods. Thus, the resulting error is significant. Zugmann et al. applied the four methods to a set of electrolytes. The presented results matched more or less with each other. Unfortunately, there was no electrolyte presented which was investigated by all four methods to enable clear evaluation of the different methods. Nevertheless, potentiostatic polarization is applied often to determine transference numbers without

discussing the fact that the method is only valid for ideal electrolytes without any interactions of ions [29, 152–160]. For IL electrolytes mostly PFG-NMR is applied hardly respecting the fact of overestimated transference numbers [19, 22, 48, 161–166]. The resulting lithium transference numbers in ILs determined by PFG-NMR are very low, meaning that the real lithium ion transference numbers are probably even smaller. Duluard et al. assume that the transference number determined by NMR is dominated by the complexed lithium ions which exhibit a negative charge [12]. Since electrochemical cells using IL electrolytes are still able to run they conclude that the complexes are not stable. Thus, the anions in the coordination shell of lithium exchange so that the positively charged lithium ions still experience the applied electric field.

2.4 Rheology

The term rheology originates from the Greek and means the study of flow (ῥεῖν (rhein) = flow, λόγος (logos) = study). Hence, rheology deals with the deformation and flow of matter. Two different cases of rheological behaviors are distinguished: liquids with ideal viscous flow behavior and rigid solids with ideal elastic deformation. Mechanical properties of most materials lie between these two extreme cases and show viscoelastic behavior (cf. Figure 2.9). These materials can be liquids like glue or solids like eraser. A very good overview on rheology was given by Mezger in his "Rheology Handbook" [167].

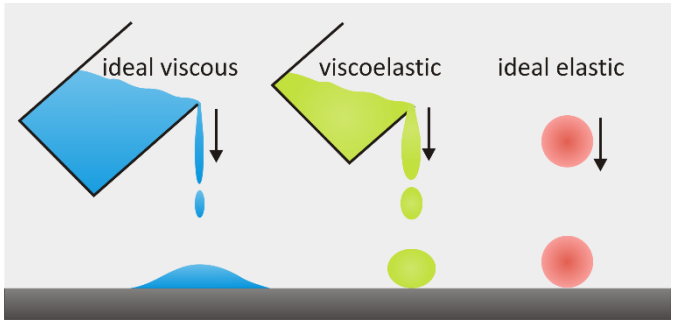

Figure 2.9: Different behaviors of ideal viscous, viscoelastic and ideal elastic materials by falling on a solid surface.

The principle of rheological measurements can be described by the parallel-plate model, which is demonstrated schematically in Figure 2.10.

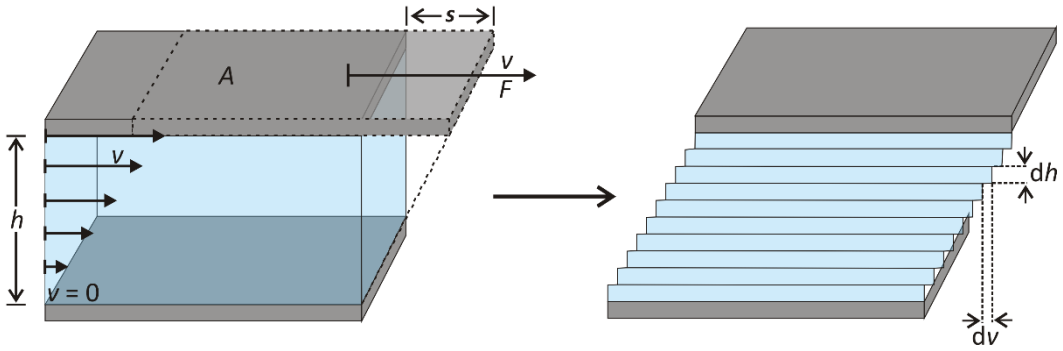

Figure 2.10: Parallel-plate model for the description of rheological measurements. The sample is confined in a small gap with the height h between two parallel plates with surface A. The upper plate is moved by the length s and the force F with velocity v.

Two plane plates with surface A are oriented parallel to each other resulting in a gap with the height h between them which contains the viscoelastic sample. The lower plate is fixed and the upper plate is moved by the length s in one direction by the shear force F. The velocity v of the resulting movement which depends on the rheological properties of the sample is measured. There are two conditions which need to be fulfilled for the measurements. The sample has to adhere on the plates and laminar flow has to be ensured. Turbulent flow would disturb the measurement and is avoided by using small gaps. The shear stress τ applied to the sample in the gap is defined as the ratio of the applied shear force F to the surface area of the plates A (equation (2.12)). The shear strain γ experienced by the sample is the ratio of the length s which the upper plate is moved to the height h of the gap (equation (2.13)).

$$\tau = \frac{F}{A} \tag{2.12}$$

$$\gamma = \frac{s}{h} \tag{2.13}$$

For a laminar ideal viscous flow the velocity decreases linearly in the gap. Since turbulent flow is excluded the gap can be assumed as sum of infinitely small layers with the height dh. As the velocity v decreases linear in the gap, dv/dh is a constant. Hence, for ideal viscous materials the shear rate $\dot{\gamma}$ can be described as ratio of velocity v to height h (equation (2.14)).

$$\dot{\gamma} = \frac{\partial \gamma}{\partial t} = \frac{v}{h} \tag{2.14}$$

In a flowing fluid the molecules are slipped against each other upon applying shear stress. Hence, frictional forces occur between the molecules resulting in frictional heat and flow resistance. The frictional heat is dissipated by the fluid as a result of deformation work. Although Newton was the first to describe the fluid motion Stokes was the one to establish the equations and to give a detailed explanation on viscosity

[168–172]. For ideal viscous materials the shear stress τ is proportional to shear rate with the viscosity η of the fluid as proportionality factor. This relation is described by Newton's law shown in equation (2.15).

$$\eta = \frac{\tau}{\dot{\gamma}} \tag{2.15}$$

Viscosities are usually measured in rotational experiments. Therefore, the upper plate is moved with varying shear stress or shear rate and the responding shear rate or shear stress is measured, respectively. Fluids with non- ideal viscous behavior usually exhibit a more or less rigid network or superlattice. These materials show no linear dependence between shear stress and rate. It can be distinguished between shear thinning and shear thickening materials. Shear thinning materials, also called pseudoplastic materials, show a viscosity decrease with increasing shear rates. The opposite case of shear thickening materials, also called dilatant materials, applies when the viscosity increases with rising shear rates. Figure 2.11 shows flow curves which describe the dependence of shear stress or viscosity on shear rate for the three different material classes of fluids.

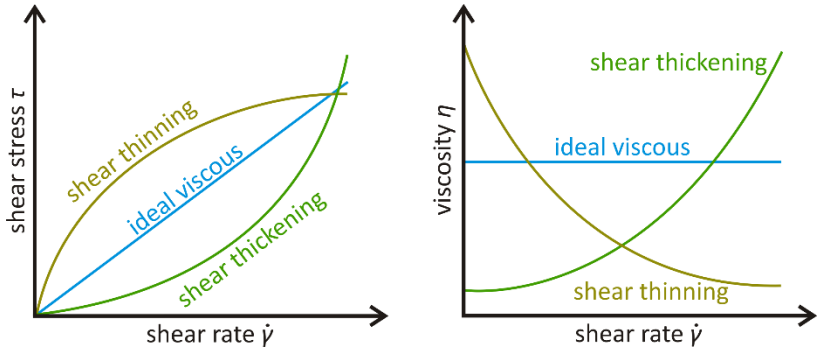

Figure 2.11: Schematic flow diagrams of three different materials, namely ideal viscous, shear thinning and shear thickening materials.

Dispersions show typically shear thinning behavior. The particles of dispersed phase are usually agglomerated in the continuous medium. Upon a certain shear stress the agglomerates are broken and the dispersion contains mostly primary particles as shown in Figure 2.12. Thereby the interaction in the dispersion is decreased resulting in a lower flow resistance and viscosity.

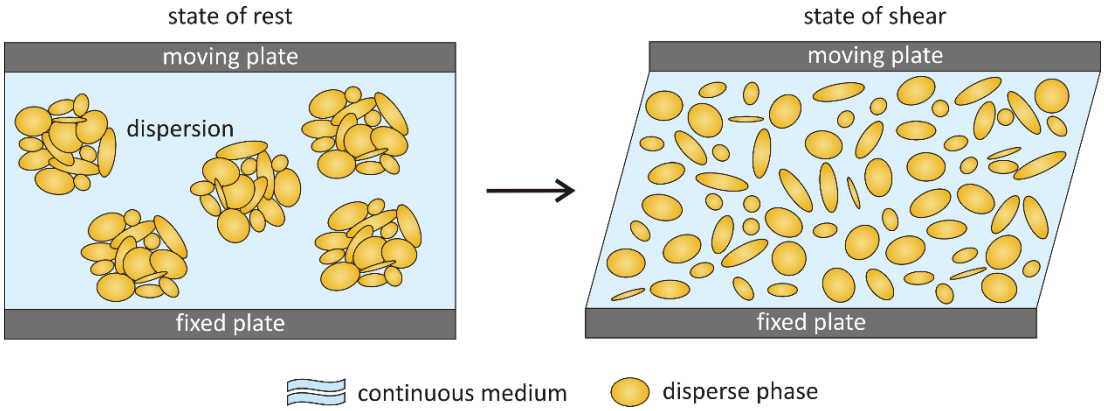

Figure 2.12: Shear behavior of dispersions in the parallel-plate model. Dispersed phase agglomerates in the dispersion in rested state. Upon shearing the dispersion in the gap, the agglomerates break until isolated primary particles remain.

The shear modulus G is a material constant for ideal elastic solids and describes the rigidity of the sample. The higher the intermolecular or cohesive forces the higher the rigidity and the shear modulus. The latter is defined by Hooke's law as the ratio of shear stress to shear strain (equation (2.16)) [173].

$$G = \frac{\tau}{\gamma} \tag{2.16}$$

Thus, the shear modulus of an ideal elastic solid material does not depend on the value and duration of shear stress in the linear regime. The applied deformation energy is stored completely in the material during deformation. Upon release this deformation energy can be regained without loss. Such ideal elastic deformation behavior can be observed in materials with strong interactions between the atoms or molecules e.g. rigid materials with crystalline structure. The rheological behavior of ideal viscous materials can be illustrated by a dashpot where the frictional heat produced by applied force is consumed and deformation occurs irreversibly analogous to Newtonian fluids. Mechanical properties of ideal elastic materials are visualized by a spring. Upon applying force, deformation energy is stored and deformation occurs completely reversible in analogy to ideal solids. Both models for ideal viscous and ideal elastic materials are demonstrated in Figure 2.13.

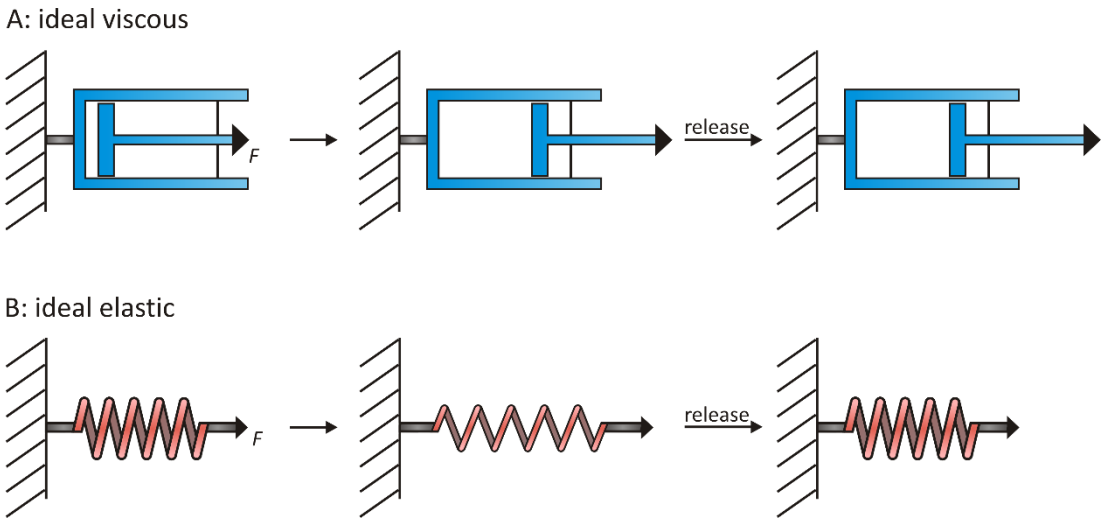

Figure 2.13: Dashpot (A) and spring (B) as models to describe mechanical properties of ideal viscous and ideal elastic materials, respectively.

For describing the rheological behavior of viscoelastic materials the two models have to be combined. Viscoelastic liquids are described by the Maxwell model where the dashpot and spring are connected in series as shown in Figure 2.14. Applying a force the reversible process takes place first where the deformation energy is stored in the material. By increasing the applied force an irreversible process follows where the deformation energy is consumed as deformation work.

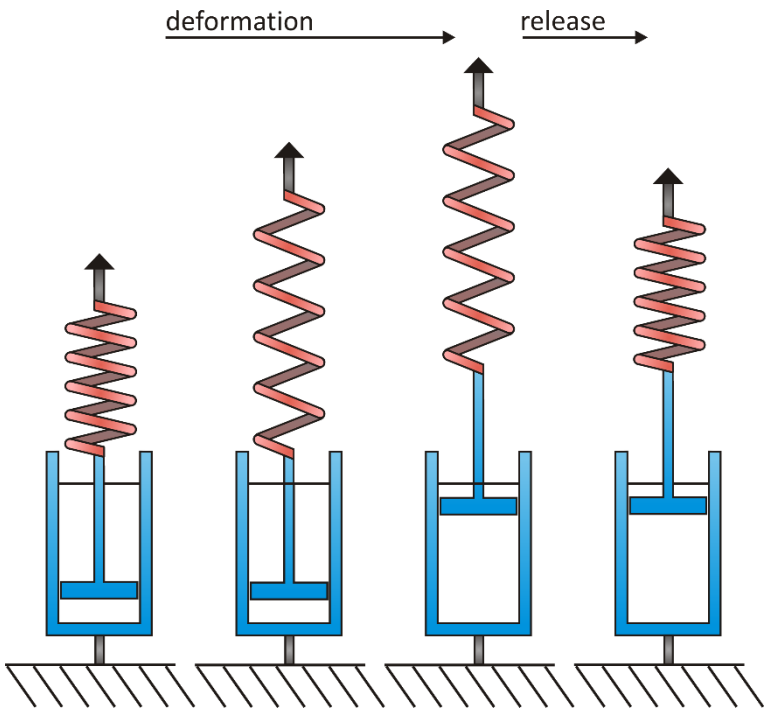

Figure 2.14: Maxwell model to describe mechanical properties of viscoelastic liquids. Dashpot and spring are connected in series. Hence, upon deformation the energy is stored in the spring first. With increasing force the dashpot starts to consume the energy resulting in irreversible deformation.

To illustrate mechanical properties of viscoelastic solids the dashpot and spring have to be connected parallel as described by the Kelvin-Voigt model (cf. Figure 2.15). After applying a force storage and consumption of deformation energy occur parallel to each other. The deformation energy is not stored completely since part of the energy is consumed by the dashpot or rather ideal viscous part of material. Upon release the deformation energy is regained with a delay since the spring/elastic part forces the dashpot/viscous part to reach its initial state. Thus, the Maxwell model and Kelvin-Voigt model can be regarded in analogy to electric networks. There, the dashpot represents the resistance which consumes the energy and the spring behaves analog to the capacitor which stores the energy.

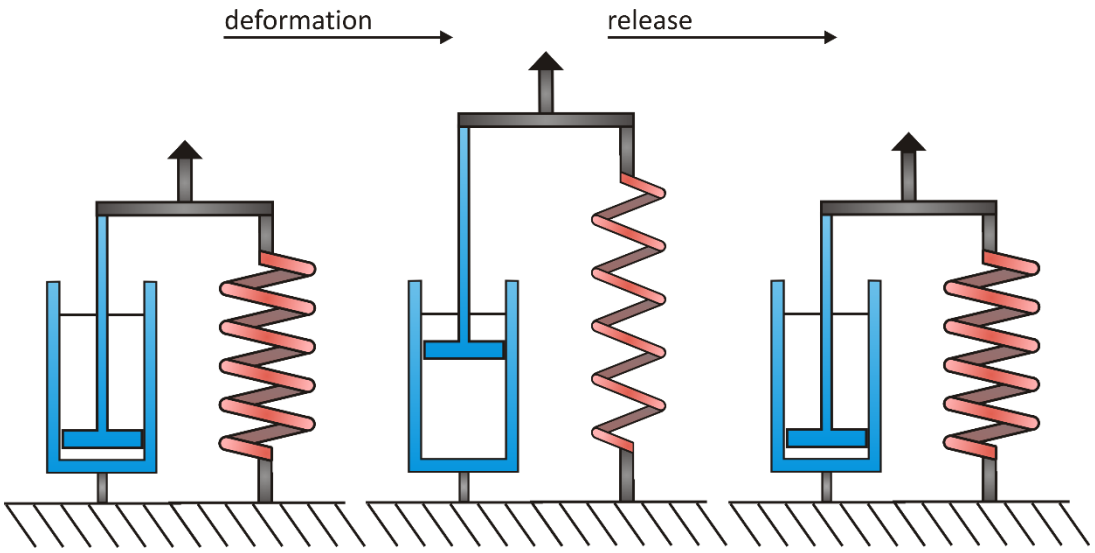

Figure 2.15: Kelvin-Voigt model to illustrate mechanical behavior of viscoelastic solids. The dashpot and spring are connected parallel to each other. Upon deformation storage and consumption of energy occurs simultaneously. After release the deformation energy is regained completely with a delay.

Rheological characterization of viscoelastic materials can be carried out well by oscillation experiments, which have a close analogy to the analysis of electric networks by impedance spectroscopy. Viscoelastic liquids are described equal to equivalent circuits consisting of a resistance and capacitor connected in series. Viscoelastic solids are treated analog to equivalent circuits comprising a parallel connection of a resistance and capacitor.

The above mentioned parallel-plate model can be used to describe the oscillation experiment. The lower part is fixed and the upper plate is moved bidirectional by a drive wheel with the force F resulting in the displacement $\pm s$ with an angle of $\pm\varphi$ (cf. Figure 2.16). Hence, in the oscillation test shear stress τ and deformation γ are sinusoidal functions of time t as shown in equations (2.17), (2.18) and (2.19).

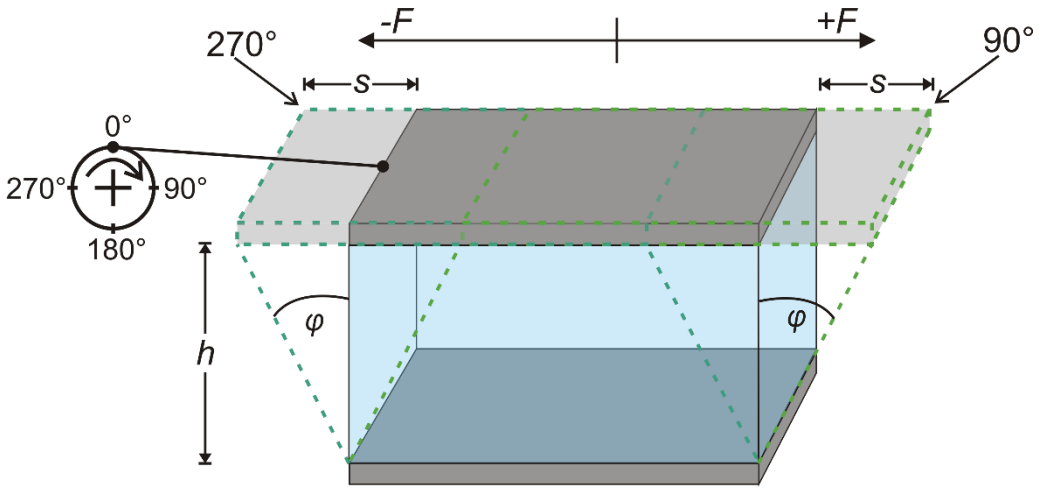

Figure 2.16: Parallel-plate model for oscillation experiment. The upper plate is not moved in one direction as described above for rotational experiments but it is moved bidirectional with the force *F* by the length *s* and the angle *φ*.

$$\tau(t) = \tau_A \cdot \sin(\omega t + \delta) \tag{2.17}$$

$$\gamma(t) = \gamma_A \cdot \sin(\omega t + \delta) \tag{2.18}$$

$$\dot{\gamma} \qquad \omega \cdot \cos(\omega t + \delta) \tag{2.19}$$

τ_A, γ_A describe the amplitudes of the shear stress and shear strain, respectively. The phase shift between shear stress and shear strain is described by δ. ω is the angular frequency which is applied to displace the upper plate. Thus, the shear modulus which gives evidence on the rigidity of the material becomes a complex quantity (cf. equation (2.20)) with an imaginary and a real part.

$$\tau(t) = G^* \cdot \gamma(t) \tag{2.20}$$

The relation of the complex shear modulus G^* to the real part which is the storage modulus G' and the imaginary part, the loss modulus G'', is shown in equation(2.21).

$$G^* = G' + iG'' \tag{2.21}$$

The storage modulus G' describes the stored deformation energy upon applying shear stress in analogy to the imaginary part of the impedance which describes charge storage in the capacitive part of the electric network. Though, it describes the elastic part of the material. The loss modulus G'' represents the lost deformation energy upon applying shear stress and describes the viscous part of the viscoelastic material. Hence, the loss modulus is analog to the real part of the impedance representing the resistive part of the electric network. As the complex shear modulus G^* is constant for ideal elastic materials the shear stress τ and deformation γ are in phase (cf. Figure 2.17). The

viscosity also becomes a complex value in oscillation experiments and describes the proportionality of shear stress τ and shear rate $\dot{\gamma}$ as mentioned above (equation (2.22)).

$$\tau(t) = \eta^* \cdot \dot{\gamma}\ t \tag{2.22}$$

Since for ideal viscous materials the shear stress τ and shear rate $\dot{\gamma}$ have to be in phase with each other a phase shift δ of 90° results for the shear stress and deformation (cf. Figure 2.17).

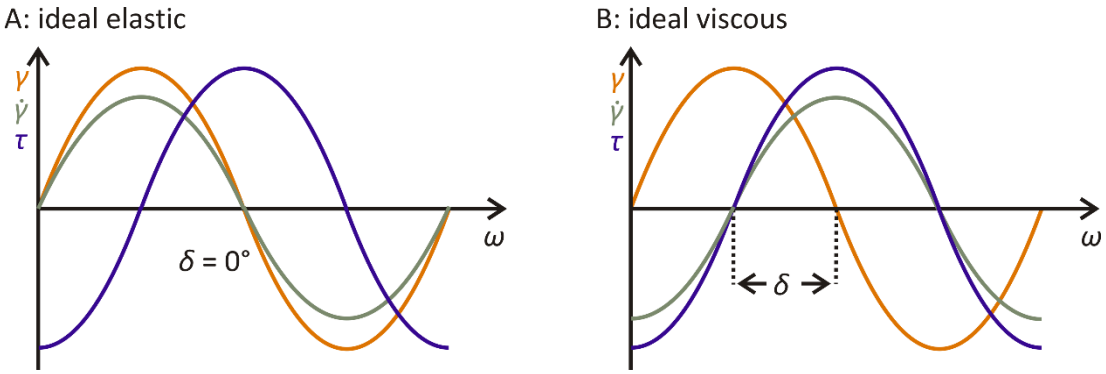

Figure 2.17: Shear strain, shear rate and shear stress in dependence on angular frequency for an oscillation experiment of an ideal elastic (A) and ideal viscous (B) material, respectively.

Considering the complex shear modulus in a vector diagram (cf. Figure 2.18) it becomes obvious that the phase shift can be described by the storage and loss modulus G' and G'', respectively.

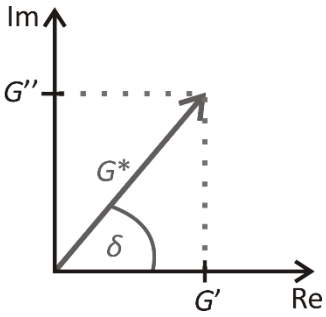

Figure 2.18: Complex shear modulus G^* in a vector diagram. The imaginary part, namely the loss modulus G'', of the complex shear modulus is plotted on the y-axis and the real part, the storage modulus G', on the x-axis. The angle of the complex shear modulus vector with the real axis describes the phase shift δ of shear stress and shear strain.

$$\tan\delta = \frac{G''}{G'} \tag{2.23}$$

The tangent of phase shift δ (equation (2.23)) is called damping factor as it describes the ratio of stored and lost deformation energy. As already depicted in the Maxwell and Kelvin-Voigt model viscoelastic materials combine viscous and elastic properties. In viscoelastic liquids the viscous part dominates resulting in a phase shift between

45° and 90°. Accordingly, in the case of viscoelastic solids the elastic part dominates with phase shifts between 0° and 45°. At a phase shift of 45° the system undergoes a sol-gel-transition. Phase shifts and damping factors of ideal viscous and ideal elastic as well as of viscoelastic liquids and solids are summarized in Table 2.3.

Table 2.3: Phase shifts and damping factors of ideal viscous, ideal elastic and viscoelastic materials.

Ideal viscous	**Viscoelastic liquid**	**Sol-gel-transition**	**Viscoelastic solid**	**Ideal solid**
$\delta = 90°$	$90° > \delta > 45°$	$\delta = 45°$	$45° > \delta > 0°$	$\delta = 0°$
$\tan \delta \rightarrow \infty$	$\tan \delta > 1$	$\tan \delta = 1$	$\tan \delta < 1$	$\tan \delta \rightarrow 0$
$G' \rightarrow 0$	$G' < G''$	$G' = G''$	$G' > G''$	$G'' \rightarrow 0$

Oscillation experiments can be carried out by applying a fixed amplitude of shear stress or shear strain and varying the angular frequency. The responding shear strain or shear stress is measured to obtain the required values. Another possibility is to keep the angular frequency fixed and vary the amplitude. Which measuring mode is applied depends on the required information. In the frequency sweep where the amplitude remains constant the time dependent mechanical properties are in focus. The amplitude sweep which is carried out with constant frequency gives evidence on the mechanical strength of the sample.

3 EXPERIMENTAL

Ionic liquid-based dispersed lithium electrolytes with different silica as filler material were prepared. The resulting electrolytes were characterized concerning their electrical, electrochemical and mechanical properties. Scanning electron microscopy images of selected silica were collected and surfaces of pure silica and electrolyte coated silica were investigated by IR spectroscopy. An attempt to determine the lithium transference number of a liquid electrolyte by a four-probe measurement is presented.

3.1 Electrolyte preparation

As IL electrolyte 15 wt% LiTFSI in BMP-TFSI was used (15 wt% LiTFSI/BMP-TFSI) which was achieved by stirring an appropriate amount of LiTFSI in BMP-TFSI for at least 12 h. For preparation of silica filled IL electrolyte the appropriate amount of silica was added to the electrolyte and stirred by magnetic stir bar. Composite electrolytes with a silica amount of 2.5 wt%, 5 wt%, 7.5 wt% and 10 wt% were prepared. For the composite electrolytes with fumed silica 5 wt% silica was the highest amount since its gel-like consistency did not allow handling of the electrolyte with higher silica fractions. The composite electrolytes containing 10 wt% SBA-15 and 5 wt% SiO_2-fumed were stirred by spatula due to their high viscosity.

Material storage and electrolyte preparation was carried out in a glovebox (MBraun LABmaster) under argon atmosphere with oxygen and water contents below 5 ppm. Argon was purchased from Praxair with a purity of 99.999 %.

3.1.1 Material preparation

The ionic liquid and the lithium salt were vacuum-dried for at least 48 h at 70 °C and 200 °C, respectively. The water content of both materials was determined by coulometric titration using a Karl-Fischer coulometer (Metrohm, 831 KF Coulometer). The surface-unmodified and surface-modified silica were vacuum-dried for at least 16 h at 300 °C and 80 °C, respectively.

3.1.2 Materials

N-Butyl-N-methylpyrrolidinium bis(trifluoromethylsulfon)imide (BMP-TFSI) in ultrapure quality (99.5 %) and lithium bis(trifluoromethylsulfon)imide (LiTFSI) in high purity (99 %) was purchased from IoLiTec GmbH. The fumed silica with a particle size of 7 nm was purchased from Sigma Aldrich.

Silica nanoparticles with a particle size of 80 nm were used as synthesized (SiO_2-NP80) and after ball-milling (SiO_2-NP80-milled). These ball-milled nanoparticles were surface modified with methyl-, aminopropyl- and lithiumpropylsulfonate-groups (SiO_2-NP80-CH_3, SiO_2-NP80-$C_3H_6NH_2$ and SiO_2-NP80-$C_3H_6SO_3Li$), respectively, as well as with N-methyl-N-propyl-pyrrolidinium TFSI (SiO_2-NP80-PMP-TFSI) and 1-methyl-3-propylimidazolium TFSI (SiO_2-NP80-PMI-TFSI), respectively. Mesoporous silica with a cubic pore structure (KIT-6, space group $Ia\bar{3}d$) and a hexagonal pore structure (SBA-15, space group *P6mm*) were used.

All synthetic work was carried out in the research group of Prof. Dr. Michael Fröba at the Institute of Inorganic and Applied Chemistry at University of Hamburg (Germany). The mesoporous silica were synthesized with different pore diameters [174, 175] by varying the synthesis temperature and they were surface-modified with methyl-, aminopropyl and sulfonpropyl-groups. The silica nanoparticles were prepared by Stöber synthesis [176]. Synthesis of mesoporous silica was described by Sann et al. [80]. Surface modification of the silica occurred by post-synthetic grafting with trialkoxysilane [80, 177–179]. For surface modification with N-methyl-N-propylpyrrolidinium TFSI and 1-methyl-3-propylimidazolium TFSI the silica nanoparticles were first modified with N-methyl-N-propylpyrrolidinium chloride and 1-methyl-3-propylimidazolium chloride, respectively. The precursors for post-synthetic grafting were synthesized as described in literature [178, 180]. Then, ion exchange with TFSI was performed in analogy to a reported synthesis [89].

Pore sizes and specific surface areas of the silica were determined from nitrogen physisorption in the research group of Prof. Dr. Michael Fröba. The pore sizes as well as surface areas of the silica are summarized in Table 3.1.

Table 3.1: Summary of the silica used in the present work with their average surface areas. For the mesoporous silica the average pore sizes are also shown.

Silica	**average pore size / nm**	**average surface area / m²/g**
SiO_2-NP80	-	294
SiO_2-NP80-KM	-	336
SiO_2-fumed	-	390
KIT-6	9.1	806
SBA-15	9.1	734
SiO_2-NP80-CH_3	-	317
SiO_2-NP80-C_3H_6-NH_2	-	74
SiO_2-NP80-C_3H_6-SO_3Li	-	60
SiO_2-NP80-PMP-TFSI	-	68
SiO_2-NP80-PMI-TFSI	-	125
KIT-6-110	8.5	836
KIT-6-140	10.9	491
KIT-6-140-CH_3	9.4	445
KIT-6-140- C_3H_6-NH_2	9.4	385
KIT-6-C_3H_6-SO_3H	8.8	509
SBA-15-140-CH_3	10.1	421
SBA-15-140-C_3H_6-NH_2	6.8	364
SBA-15-C_3H_6-SO_3H	8.8	507

3.2 Electrochemical experiments

For electrical characterization of the prepared electrolytes conductivity measurements were carried out by impedance spectroscopy, and electrochemical windows were determined by linear sweep voltammetry. Cyclic voltammetry was

carried out in half cells with lithium iron phosphate as cathode material. For comparison of the electrochemical response the neat IL electrolyte and the composite electrolytes were used.

3.2.1 Conductivity

Conductivity measurements of the electrolytes were performed by potentiostatic electrochemical impedance spectroscopy (PEIS). The measurements were carried out with a BioLogic SP150 potentiostat/galvanostat controlled by the software EC-Lab (BioLogic Science Instrument). A sealed micro cell purchased from TransMit – Project Division for Electrochemical Materials Research and Interface Characterization, Marburg (now: rhd instruments) was used and is pictured in Figure 3.1. The cell consists of a platinum cup acting as counter electrode where the electrolyte is kept and a cap with an integrated glass rod embedding four platinum wires which were used as working and reference electrodes. The electrolyte volume in the cell varied between 0.6 mL and 1.8 mL. The cap was sealed by an O-ring allowing to carry out the experiments outside the glovebox without contaminating the electrolyte with atmospheric humidity.

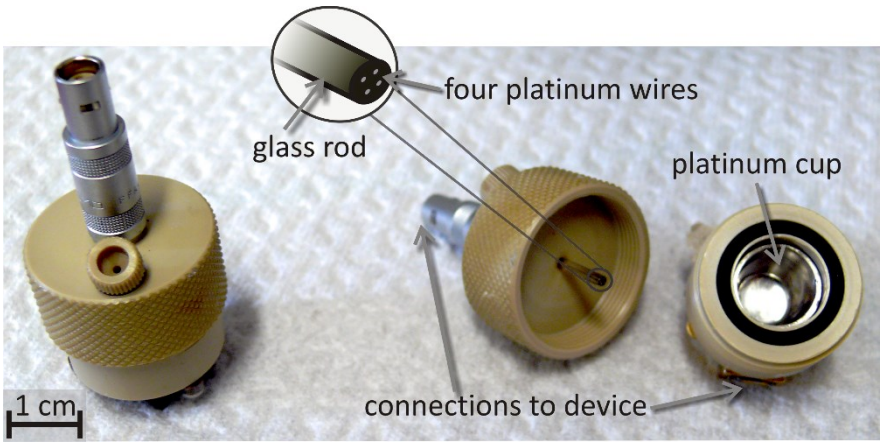

Figure 3.1: Micro cell for conductivity measurements. The electrolyte is kept in the platinum cup acting as counter electrode. Four platinum wires are embedded in a glass rod which are used as working and reference electrodes. The cap is sealed by an O-ring allowing to carry out the measurements outside the glovebox without contaminating the electrolyte with atmospheric humidity.

The cell assembling was done inside the glovebox (cf. 3.1 Electrolyte preparation) after vacuum-drying of the cell at 80 °C for at least 16 h. The PEIS measurements were carried out between 1 MHz and 1 Hz with an amplitude of 10 mV. The temperature was controlled by a Peltier element between –5.0 °C and 80.0 °C in steps of 5 K. To obtain the electrolyte resistance the spectra were fitted with an equivalent circuit consisting of a resistance and constant phase element connected in series. If an

extended frequency range with a phase of nearly 0° was observed, the fit in this frequency range was run with an ohmic resistance. The cell constant was determined by measuring the resistance of 0.1M aqueous potassium chloride solution at 25.0 °C. The potassium chloride solution (CertiPUR) was purchased from Merck KGaA with a nominal conductivity of 12.8 mS/cm at 25.0 °C. Electrolyte conductivity was calculated by deviding the cell constant with the obtained electrolyte resistance. For enhanced accuracy the cell constant was determined regularly after about ten electrolyte measurements.

The theoretical conductivity decrease was calculated by the program COMSOL Multiphysics assuming 5 vol% insulating filler material in a conducting matrix. As cell geometry a cube with 1 mm edge length was used and the filler material was simulated as 864 spherical particles with a particle size of 50 µm in an fcc lattice.

3.2.2 Electrochemical window

To determine the electrochemical window of the neat electrolyte and the composite electrolytes linear sweep voltammetry was carried out. The same cell was used as for the conductivity measurements but with a different cap. Instead of the glass rod a glassy carbon electrode was embedded into the cap. For the reference electrode a nickel wire was inserted through the cap. The cell is shown in Figure 3.2.

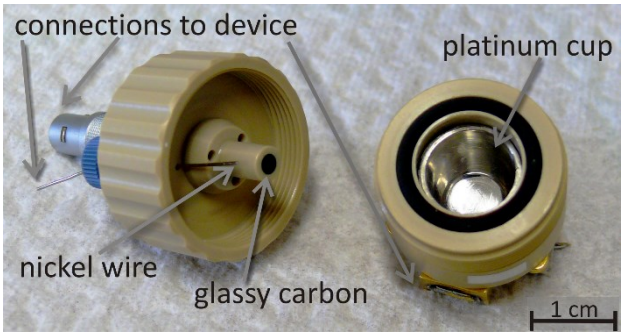

Figure 3.2: Micro cell for linear sweep voltammetry measurements. The same platinum cap was used as for the conductivity measurements. Glassy carbon is integrated into the cap and is used as working electrode. Lithium metal is pressed on the nickel wire and acts as reference electrode.

As reference electrode lithium foil (> 98 %, Chemetall) was pressed on the tip of the nickel wire. The cell was vacuum-dried at 80 °C for at least 16 h prior to assembling it in the glovebox (cf. 3.1 Electrode preparation). Linear sweep voltammetry measurements were carried out with a scan rate of 1.0 mV/s starting at the open circuit voltage using BioLogic SP150 potentiostat/galvanostat controlled by the software EC-Lab (BioLogic Science Instrument). The measurements of the anodic and cathodic limits were aborted when a current of 5 µA and –5 µA was reached, respectively. For

every measurement of anodic or cathodic limit fresh electrolytes was used. The glassy carbon electrode was polished with diamond- and alumina-suspension (purchased from BioLogic) after each measurement. As limit for electrolyte stability a current density of 5 µA/cm² was chosen.

3.2.3 Cyclic voltammetry

Cyclic voltammetry (CV) was carried out with half cells in two-electrode measurements. Lithium iron phosphate (LFP) cathodes as working electrodes and lithium foil anodes (> 98 %, Chemetall) as counter electrodes were used. Lithium iron phosphate cathodes were obtained as cathode sheets from the research group of Prof. Dr. Kwade from the Institute for Particle Technology at Technical University of Braunschweig (Germany). The LFP cathode sheets consisted of 84 wt% lithium iron phosphate, 4 wt% carbon black and 4 wt% graphite as conducting additive and 8 wt% polyvinylidene fluoride (PVDF) as binder. Loading of the sheets was 9.52 mg/cm². The measurement cell shown in Figure 3.3 was built in-house and was vacuum-dried at 80 °C for at least 16 h prior to assembling it in the glovebox (cf. 3.1 Electrode preparation). The electrolyte was kept in an acrylic glass cylinder with internal screw threads on both sides. The bottom of the cylinder was closed by a short stainless steel hexagon bolt with the cathode on it and sealed by an O-ring. An acrylic glass ring was dipped into the electrolyte on the cathode. On top of the acrylic glass ring lithium foil was placed which was stabilized by a stainless steel disk. A brass spring pin which was fixed on a stainless steel hexagon bolt contacted the anode and closed top of the acrylic glass cylinder.

The measurements were carried out with varying scan rates between 0.1 mV/s and 1.0 mV/s. Before each measurement the cell was rested for 20 h. Starting at the open circuit potential, the potential was increased to 4.2 V and decreased then to 2.1 V before returning to the open circuit potential. BioLogic SP50 and SP300 potentiostat/galvanostat controlled by the software EC-Lab (BioLogic Science Instrument) were used for the measurements. Since the acrylic glass allowed water to diffuse from atmosphere into the electrolyte the measurements were carried out inside the glovebox. The cell constant was determined geometrically being 0.7 cm^{-1}.

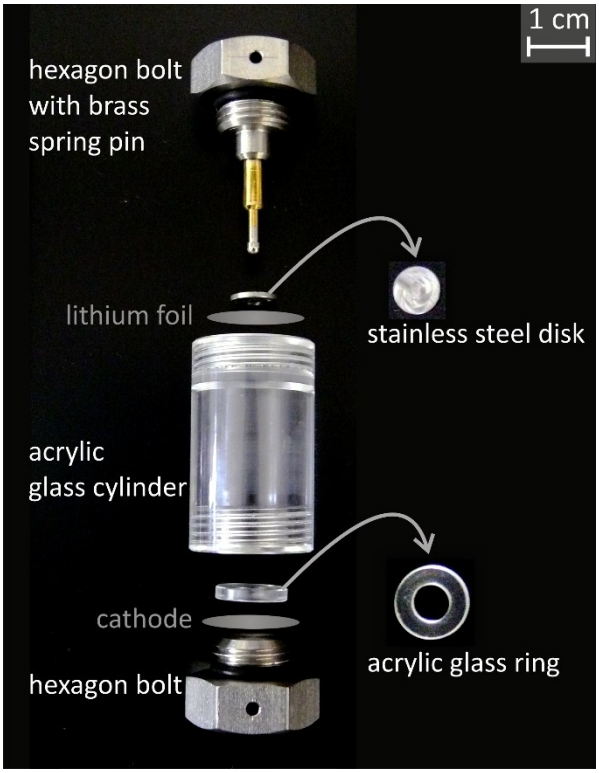

Figure 3.3: Acrylic glass cell is used for cyclic voltammetry measurements with lithium iron phosphate as working electrode and lithium metal as counter electrode. The electrodes are separated by an acrylic glass ring.

3.3 Rheological measurements

Mechanical characterization was carried out by rotational experiments achieving the electrolyte viscosities and by oscillation experiments to obtain information about the viscoelasticity of the investigated electrolytes. The measurements were carried out in the dry room (dew point –47 °C at ambient temperature of 23 °C) of Batteries and Electrochemistry Laboratory (BELLA) at Institute of Nanotechnology, KIT in Karlsruhe (Germany). As rheometer the MCR 302 of Anton Paar was used.

3.3.1 Viscosity measurements

For viscosity measurements a cone-plate geometry with an angle of 1°, diameter of 50 mm and a gap of 101 µm was used. Temperature was controlled by Peltier element and hold at 25.0 °C. The shear rate was varied logarithmically from 0.1 s^{-1} to 10000 s^{-1}. Accordingly the measuring time was varied logarithmically from 25 s to 1 s. For the measurements of 15 wt% LiTFSI/BMP-TFSI with 10 wt% SBA-15-120 the plate-plate geometry was used with diameter of 50 mm and gap of 1.000 mm. Stirring of electrolytes was interrupted approximately 15 minutes prior to measurement. After

bringing the cone in measuring position additional 15 minutes were waited before starting the measurement.

3.3.2 Mechanical properties

For oscillation experiments the same geometries were used as for the viscosity measurements. Only the gap for the measurement of 10 wt% SBA-15-120 in 15 wt% LiTFSI/BMP-TFSI was changed to 0.500 mm. Amplitude sweep experiments were carried out at angular frequency of 1 rad/s and the deformation amplitude was varied from 0.1 % to 100 %. The temperature was kept at 25.0 °C. After being stirred the composite electrolytes were rested for 15 minutes before they were brought into the measuring device. After putting the cone in measuring position another 15 minutes were waited before starting the measurement.

3.4 Scanning electron microscopy

Scanning electron microscopy (SEM) was carried out with Merlin high-resolution electron microscope (Carl Zeiss). SEM images were taken of the unmilled and ball-milled surface-unmodified silica nanoparticles (SiO_2-NP80 and SiO_2-NP80-milled), fumed silica (SiO_2-fumed) and the mesoporous silica KIT-6 and SBA-15. Before investigating the silica in the electron microscope they were platinum coated by sputtering for 60 s in an argon plasma using a sputter coater (Edwards). The images were taken using the secondary electron detector with line averaged scan. Accelerating voltage was 3.0 kV and electron current 30 pA. The working distance varied between 2.8 mm and 3.3 mm. Due to high charging accelerating voltage was decreased to 2.0 kV for the unmilled silica nanoparticles (SiO_2-NP80). The scan speed was varied between 1 and 9 for lower and higher magnitudes, respectively.

3.5 IR Spectroscopy

FTIR spectroscopy was carried out inside the glovebox (Glovebox Systemtechnik GmbH) with water and oxygen contents below 5 ppm. For the measurements the FTIR spectrometer Nicolet iS5 (Thermo Scientific) was used with iD5 ATR accessory (Thermo Scientific) which has a diamond ATR crystal with an incident angle of 45°. The sample was pressed by an integrated pressure tip onto the

ATR crystal which provides a measuring range of 1.8 mm. Atmospheric contributions to the spectra were eliminated by collecting background spectra prior to measuring the samples. ATR effect was corrected by the software Omnic. For each electrolyte 32 scans were taken with a resolution of 4 cm^{-1} and a data interval of 0.482 cm^{-1}.

3.6 Four-probe measurement to determine transference numbers

It was attempted to determine the transference number of a liquid electrolyte by a four-probe measurement. Since the transference number of silver nitrate is well known, 0.01M aqueous silver nitrate solution was used as model system for the measurements. The silver nitrate solution was prepared by dissolving an appropriate amount of silver nitrate (99.9999 %, Aldrich Chemistry) in ultrapure water which was produced by an ultrapure water system (Milli-Q Direct 8, Merck Millipore) provided by the research group of Prof. Dr. Herbert Over at the Institute of Physical Chemistry of the Justus-Liebig-University Gießen (Germany). The measurement cell depicted in Figure 3.4 was built in-house. A glass tube with flange was filled with a small amount of electrolyte (< 1 mL) and closed with a polytetrafluoroethylene-flange (PTFE-flange) which was sealed with an O-ring and flange clamp (cf. Figure 3.4). The PTFE-flange also acted as plug to minimize electrolyte volume for avoiding convections in the solution. Four silver wires were integrated into the PTFE-flange which were connected by crocodile clamps on the outside.

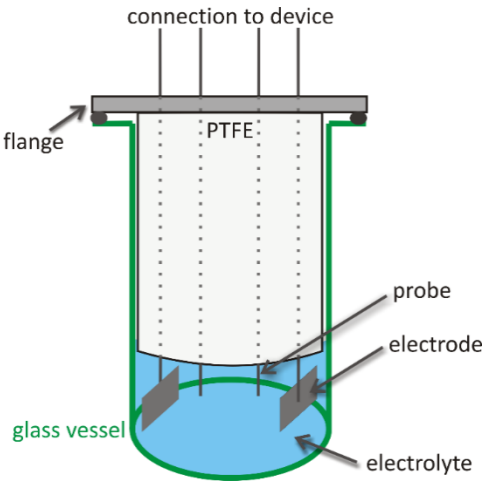

Figure 3.4: Cell with four-probe arrangement for measuring cation conduction in liquid electrolyte. Sealing with O-ring allows measuring outside the glovebox without contaminating the electrolyte with atmospheric humidity. The outer electrodes are reversible for the cations (here: silver electrodes) and are current-carrying. During galvanostatic polarization of the outer electrodes the potential drop is measured at the inner probes which are not current-carrying.

Silver sheets were spot welded on the two outer silver wires. The two inner wires were electrochemically coated by silver iodide. Therefore the cell was filled with 0.1M potassium iodide solution. The silver wire was connected as working electrode and the silver sheet as counter and reference electrode. A voltage of 1 V was applied for 30 min for coating each inner silver wire with silver iodide. As silver iodide decomposes in the presence of light the experiments were all carried out excluding light incidence. After coating of the silver wires with silver iodide the PTFE-flange was shortly washed with ultrapure water before the cell was assembled with the silver nitrate solution. The measurements were carried out with BioLogic SP150 potentiostat/galvanostat controlled by the software EC-Lab (BioLogic Science Instrument). During the measurements the cell was dipped into a temperature-controlled water bath (Julabo F25-EH) with a temperature of 25.0 °C. First potentiostatic impedance spectroscopy was carried out between 1 MHz and 1 Hz with an amplitude of 10 mV to determine the total resistance. Then galvanostatic dc measurement was carried out applying a current of 30 µA between the outer silver sheets for 50 minutes and measuring the potential drop at the silver iodide coated probes. The resulting current density was approximately 242 µA/cm². The cell constant was determined geometrically.

4 RESULTS AND DISCUSSION

As IL electrolyte N-butyl-N-methylpyrrolidinium bis(trifluoromethylsulfon)imide (BMP-TFSI) was chosen to evaluate the effect of dispersing silica in the electrolyte. Imidazolium-based ILs are discussed more often in literature as solvent for lithium electrolytes especially 1-ethyl-3-methylimidazolium bis(trifluoromethylsulfon)imide (EMI-TFSI) but they are chemically not stable to lithium metal. The chemical structures of BMP, 1-ethyl-3-methylimidazolium and TFSI are shown in Figure 4.1.

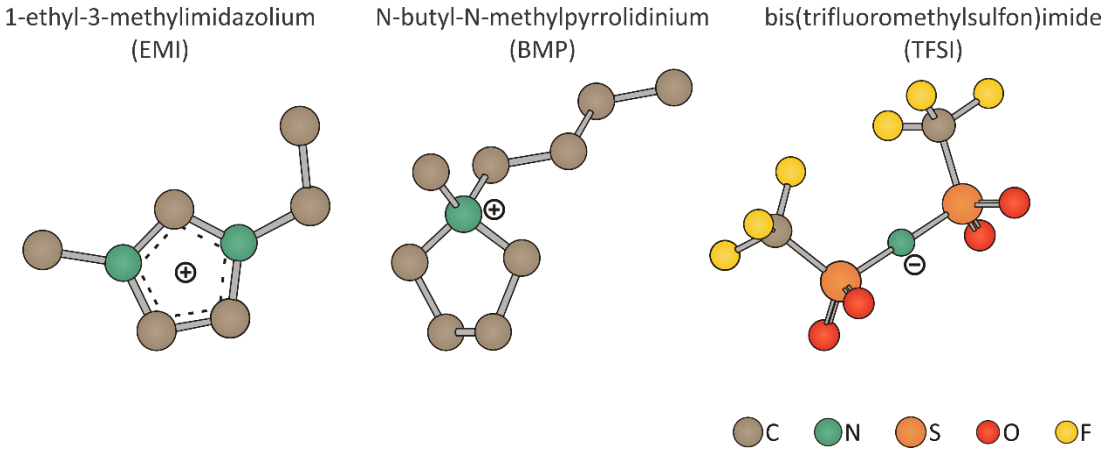

Figure 4.1: Chemical structures of the cations 1-alkyl-3-methylimidazolium (A) and N-butyl-N-methylpyrrolidinium (B) as well as of the anion bis(trifluoromethylsulfon)imide (C).

Instability of the imidazolium cation derives from the acidity in the C-2 position. The carbon atom carries a partial positive charge from the delocalized charge in the ring and is bound to two nitrogen atoms which are electron drawing. Therefore, the hydrogen atom at C-2 position of imidazolium cation tends to deprotonate easily. Pyrrolidinium-based ILs are considerably more stable since only one nitrogen atom is present in the cation which is neighboring to four carbon atoms. Figure 4.2 shows pictures of the neat BMP-TFSI and EMI-TFSI and of both ILs after contact with lithium metal for 18 h. The pyrrolidinium-based IL did optically not alter after contact

with lithium whereas the imidazolium-based IL changed its color indicating impurities in the IL which came from reactions with lithium metal. For ILs it is well known that color change occurs if impurities are present.

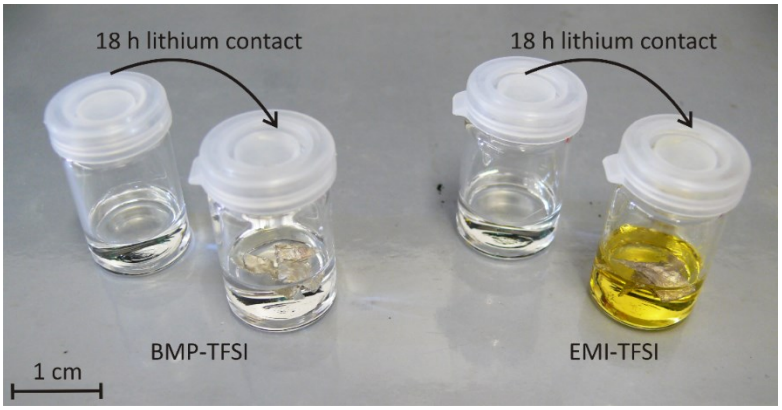

Figure 4.2: The ionic liquids N-butyl-N-methylpyrrolidinium bis(trifluoromethylsulfon)imide (BMP-TFSI) and 1-ethyl-3-methylimidazolium bis(trifluoromethylsulfon)imide (EMI-TFSI) before and after 18 hours contact with metallic lithium. The pure ionic liquids are colorless. BMP-TFSI remains optically unchanged after contact with lithium while EMI-TFSI becomes a yellow liquid due to impurities which are decomposition products from the reaction of the IL cations with lithium metal.

TFSI is a good candidate as anion due to its highly delocalized charge [181]. Hence, interactions with cations are weaker compared to anions without delocalized charge. Therefore, the anion is able to move more independently of other ions resulting in a higher conductivity [30].

4.1 Ionic liquid-based composite electrolytes with silica

Adding silica to the electrolytes led to stable dispersions (cf. Figure 4.3). It is clear from literature that IL-based dispersions are not stabilized electrostatically [182]. Due to the high ionicity of ionic liquids, Debye lengths are very short and IL dispersions cannot be considered as conventional colloids. Coulombic repulsions of dispersed particles are weak and cannot stabilize dispersions. Applying the DLVO-theory (Derjaguin-Landau-Verwey-Overbeek theory) to particles in ILs a negative interparticle potential results with a very low energy barrier for coagulation. Hence, stable IL-based dispersions cannot be described by the DLVO-theory. The stabilization of silica particles in IL electrolytes has to occur sterically and by repulsive forces of interface regions on the particles [182–184]. The ions of the ionic liquids interact with the surface of the colloidal particles as it was already shown in literature that ILs form solid-like structures in contact with silica surfaces (cf. Chapter 2.2.1). Thus, the particles cannot coagulate due to steric hindrance of the IL ions on the

particle surfaces. At the same time the ions cause repulsive forces when the particles near each other. IL electrolytes with 5 wt% fumed silica and 10 wt% mesoporous SBA-15 even formed a gel and a paste, respectively. The electrolytes are shown in Figure 4.3 together with the neat IL electrolyte and IL electrolyte containing 10 wt% silica nanoparticles of 80 nm particle size which forms a stable dispersion appearing liquid. In the cases of gel- and paste-like composite electrolytes the formed structures of IL ions on the silica surfaces seem to have a considerably longer range than the ones in the liquid appearing dispersions resulting in a more rigid structure of the composite electrolytes. This observation cannot be explained by the chemical composition of the silica surfaces since fumed silica surface is dominated by silane groups and surface of the SBA-15 contains mostly silanol groups, as it is the case for all surface-unmodified silica except fumed silica investigated in the present work. Ueno et al. also observed gelation of neat ionic liquids by adding silica and explained it by formation of a network consisting of interconnected silica particles [184, 185].

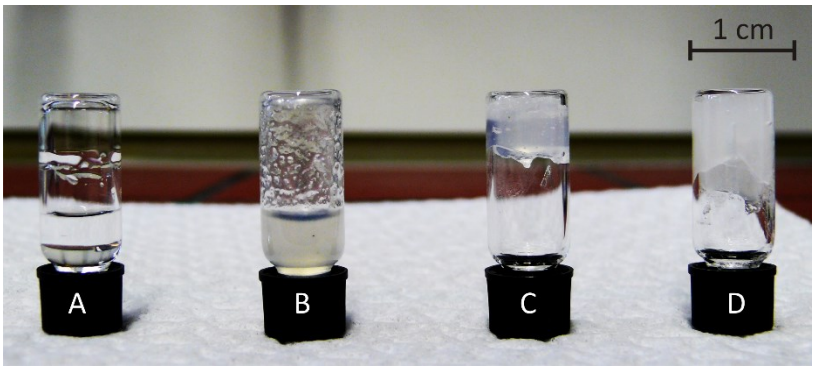

Figure 4.3: Optical appearance of 15 wt% LiTFSI/BMP-TFSI with different silica as filler materials. Vial A contains the neat IL electrolyte, vial B the IL electrolyte with 10 wt% SiO_2-NP80, vial C the IL electrolyte with 5 wt% fumed silica and vial D the IL electrolyte with 10 wt% SBA-15.

Dissolving lithium salt in ionic liquids enhances the order of the system going along with a density decrease. Since the ions are more ordered due to complexation of the lithium salt less vacancies are present in the system resulting in a decreased hole concentration. Moreover, the higher order of the ions restricts fluctuation of holes and therefore the ion mobility. Thus, viscosity increases due to the more ordered arrangement of ions [163]. Hence, the ionic conductivity decreases although the ion concentration is increased. Prior to the present work different ionic liquids with varying amount of LiTFSI as conducting salt have been investigated during the master thesis [186]. N-butyl-N-methylpyrrolidinium TFSI and 1-alkyl-3-methylimidazolium TFSI with the alkyl chain lengths varying from ethyl to hexyl were used as ionic liquids. The conductivities σ in dependence on the lithium salt mass fractions ω are presented in Figure 4.4. As expected, conductivity decreases with increasing LiTFSI concentration. Moreover, the conductivity decreases with increasing alkyl chain length

at the imidazolium cation due to higher viscosity resulting from stronger van-der-Waals interactions with longer alkyl chains. The ionic liquid with N-butyl-N-methylpyrrolidinium (BMP) cation shows conductivities similar to the ionic liquid with 1-hexyl-3-methylimidazolium (HMI) and is clearly lower than with 1-butyl-3-methylimidazolium (BMI) although the latter has the same alkyl chain length. The BMP cation is not aromatic and thus has a non-planar structure in contrast to the imidazolium cation. Hence, mobility in the BMP cation containing ionic liquid is decreased compared to the imidazolium-based ionic liquid since the pyrrolidinium cation is sterically more demanding and accordingly less mobile [187].

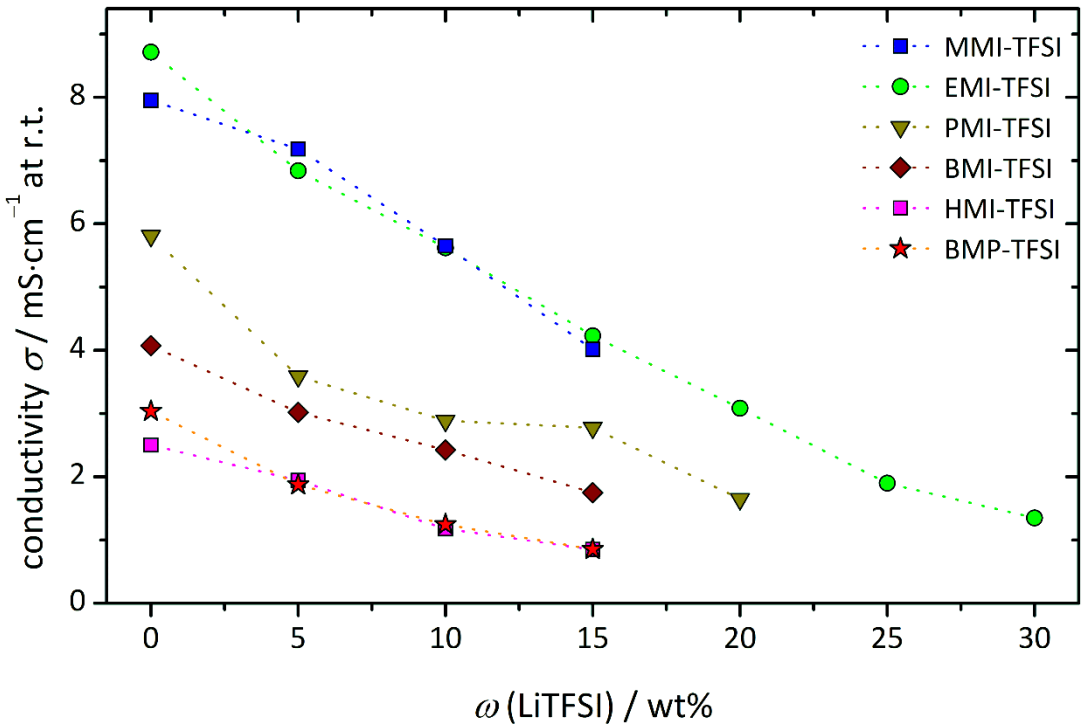

Figure 4.4: Room temperature conductivities σ of different ionic liquids in dependence on mass fractions ω of LiTFSI. As ILs N-butyl-N-methylpyrrolidinium TFSI (BMP-TFSI) and 1-alkyl-3-methylimidazolium TFSI (alkyl-MI-TFSI) with varying alkyl chain lengths were used (M: methyl, E: ethyl, P: propyl, B: butyl, H: hexyl). The diagram was modified after [186]. The dotted lines are shown as guides for the eye.

Aim of the present work was to investigate the interface effect of the IL electrolyte with isolating filler material. In particular, it was an open question whether introduction of an isolating material to the IL electrolyte results in an enhanced lithium conductivity due to an interface effect suppressing lithium complex formation as reported in literature [11, 25] (cf. Chapter 2.2.2). It is known that the dominating species of lithium in ILs are $[Li(TFSI)_2]^-$ complexes for mole fractions smaller than 0.2. For higher mole fractions of lithium salt the ion species become more complex and multinuclear aggregates are formed. Thus, in the present work BMP-TFSI with 15 wt% LiTFSI was chosen as standard electrolyte equaling a mole fraction of 0.26

for the conducting salt. If the filler material avoids lithium complexation the effect should be most expressed at mole fractions above 0.2 where lithium complexation is strongly pronounced. Moreover, with 15 wt% conducting salt the viscosity increase and conductivity decrease is in an acceptable limit and the concentration of lithium ions is adequate. Table 4.1 summarizes the concentration, mole fraction and molality of the standard electrolyte. The water content of the electrolyte was always lower than 10 ppm.

Table 4.1: Mole fraction, concentration and molality of the standard electrolyte 15 wt% LiTFSI/BMP-TFSI in the present work.

	mass fraction	**mole fraction**	**concentration**	**molality**
LiTFSI in BMP-TFSI	15 wt%	26 mol%	0.76 mol/L	0.62 mol/kg

Since the anion coordination to lithium ions should be avoided by the filler material and lithium ion mobility should not be hindered, material with Lewis acidic surface is assumed to be most promising to achieve the desired effect. The Lewis acidity of the surface avoids adsorption of lithium cations and hence, does not hinder them in their mobility. Moreover, the acidic surface could be able to capture anions resulting in a decreased anion concentration in the interface region where less anions are present to coordinate to the lithium ions. The literature-known conductivity enhancement in heterogeneous doped solid electrolytes as well as in dispersed liquid and polymer electrolytes was also achieved using filler materials with Lewis acidic surfaces (cf. Chapter 2.2). Thus, in the present work silica was chosen as filler material. To investigate the influence of silica surfaces on the properties of 15 wt% LiTFSI/BMP-TFSI different silica were used: surface-unmodified silica particles with particle size of 80 nm (SiO_2-NP80) which were also used after ball-milling (SiO_2-NP80-milled), fumed silica particles with a mean particle size of 7 nm, mesoporous surface-unmodified silica KIT-6 and SBA-15 with cubic and hexagonal pore structure, respectively, and average pore sizes of 9 nm as well as surface-modified silica nanoparticles with a particle size of 80 nm and methyl (SiO_2-NP80-CH_3), aminopropyl (SiO_2-NP80-$C_3H_6NH_2$), lithiumpropylsulfonate (SiO_2-NP80-$C_3H_6SO_3Li$), N-propyl-N-methylpyrrolidinium TFSI (SiO_2-NP80-PMP-TFSI) and 1-methyl-3-propylimidazolium (SiO_2-NP80-PMI-TFSI) as surface groups. KIT-6 silica with different pore sizes and varying surface modification as well as SBA-15 with different surface modifications were also used as filler materials in the IL electrolyte 15 wt% LiTFSI/BMP-TFSI. The corresponding results of the electrolytes with the different KIT-6 and SBA-15 silica are shown in the appendix.

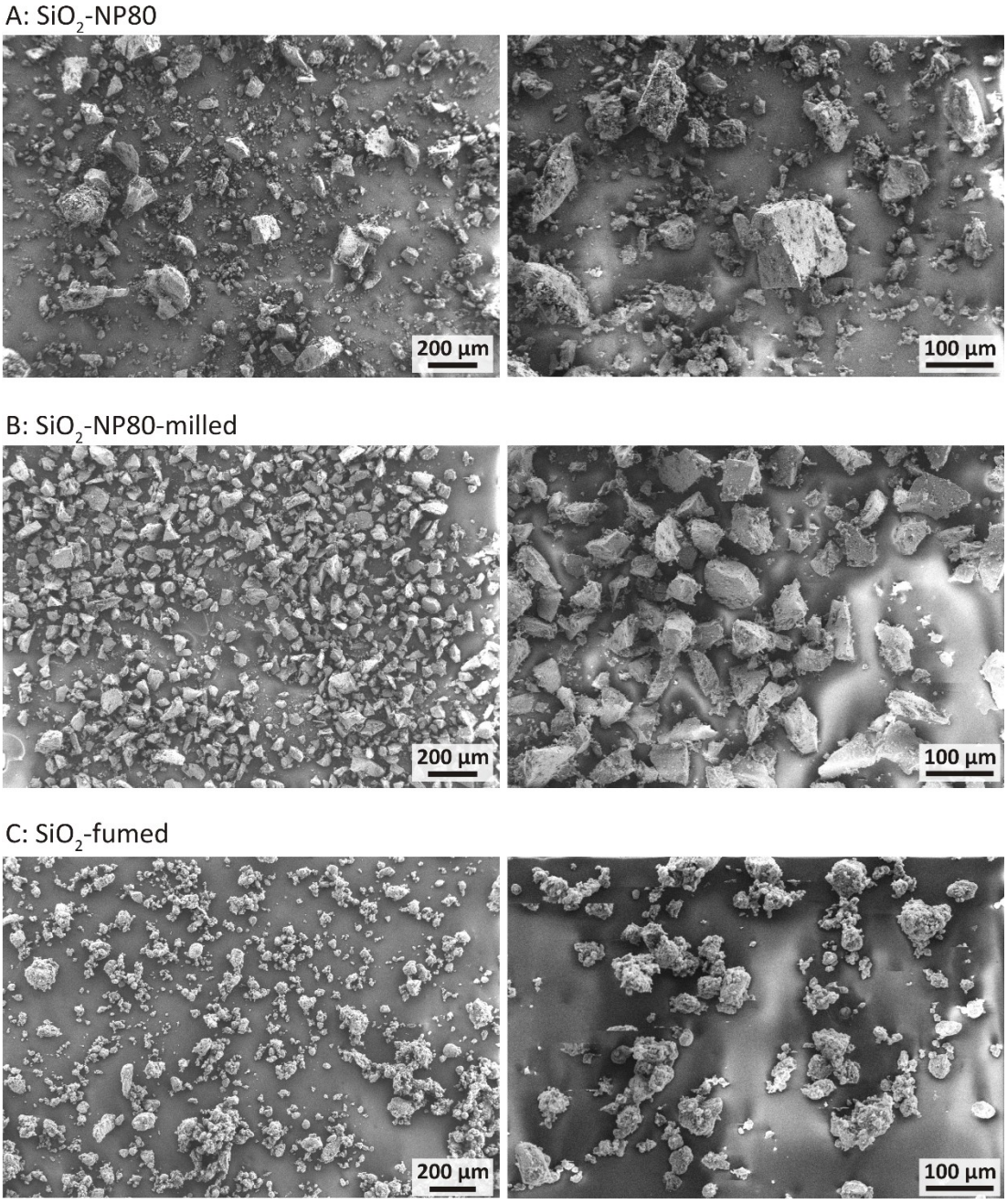

Figure 4.5: Secondary electron microscope (SEM) images of the surface-unmodified silica nanoparticles. Unmilled silica nanoparticles with particle size of 80 nm (A) and the same silica after ball-milling (B) are presented as well as fumed silica (C).

The difference of the unmilled and ball-milled silica nanoparticles with particle size of 80 nm (SiO_2-NP80 and SiO_2-NP80-milled, respectively) is their particle size distribution and morphology. The scanning electron microscope (SEM) images of the silica particles are shown in Figure 4.5. The particle size distribution of the unmilled particles is very broad whereas the ball-milled silica particles show quite uniform morphologies. Fumed silica is also depicted in the SEM images of Figure 4.5. The particles of fumed silica agglomerate and exhibit a broad particle size distribution.

Moreover, it becomes obvious that fumed silica agglomerates appear spongy indicating that the agglomerates are not packed densely.

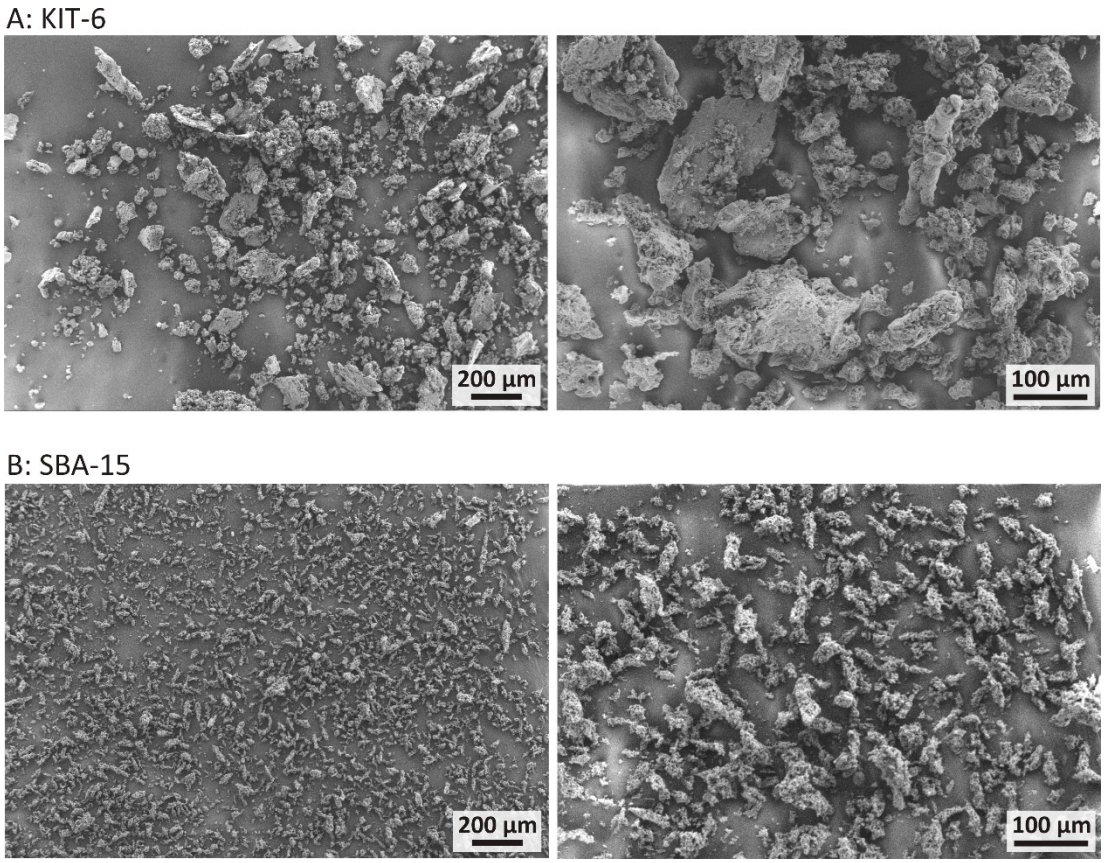

Figure 4.6: SEM images of the mesoporous silica KIT-6 (A) and SBA-15 (B).

The mesoporous silica KIT-6 and SBA-15 with average pore width of 9 nm are shown by SEM in Figure 4.6. KIT-6 forms large agglomerates and has significantly larger particle sizes than SBA-15. The SBA-15 silica appears also spongy as it is the case for fumed silica indicating high porosity. Both SBA-15 and fumed silica form gel- and paste-like composite IL electrolytes. Hence, it may be assumed that in these composite electrolytes the IL electrolytes are more confined resulting in larger interface regions where a solid-like ordering is rather expected from literature. Thus, the resulting composite electrolytes appear more solid than liquid. SEM images of the mesoporous silica with higher magnitude are shown in the appendix.

4.2 Conductivity behavior of composite electrolytes

Figure 4.7 shows the temperature dependent conductivities σ of 15 wt% LiTFSI/BMP-TFSI with 2.5 wt%, 5 wt%, 7.5 wt% and 10 wt% of surface-

unmodified silica. Assuming a density of 2.2 g/mL for all silica the mass fractions 2.5 wt%, 5 wt%, 7.5 wt% and 10 wt% of silica in the IL electrolyte correspond to volume fractions of 1.7 vol%, 3.5 vol%, 5.4 vol% and 7.4 vol%, respectively.

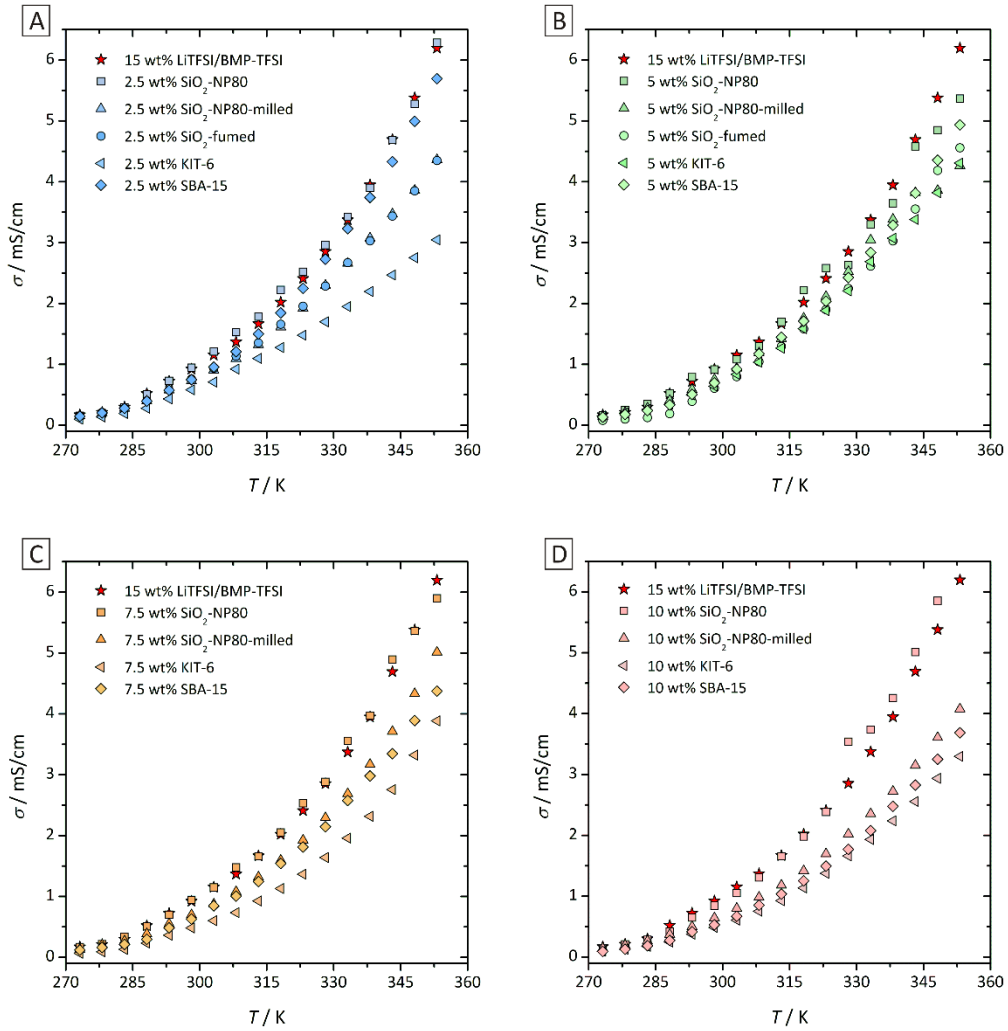

Figure 4.7: Temperature dependent conductivities σ of 15 wt% LiTFSI/BMP-TFSI with surface-unmodified silica. Conductivities of the IL electrolytes with 2.5 wt%, 5 wt%, 7.5 wt% and 10 wt% filler material containing IL electrolytes are presented in part A, B, C and D, respectively.

As expected, the conductivities increase with rising temperature. By adding filler material the conductivities decrease with respect to the neat IL electrolyte but in a different manner for different silica as filler materials. This decrease is pronounced and strongest for 10 wt%. An exceptional behavior is observed in those electrolytes with unmilled silica nanoparticles with a particle size of 80 nm (SiO_2-NP80). The conductivities of these electrolytes hardly change with respect to the neat electrolyte with increasing silica fraction. The room temperature conductivities σ of the electrolytes are presented as function of the content of filler mass fraction ω in Figure

4.8. The error bars are not shown in Figure 4.7 for graphical reasons but are presented for the room temperature conductivities in Figure 4.8. The scattering of the measured resistance in repeated measurements of the same electrolyte was always less than 1 %. The electrolyte conductivity is calculated from the measured resistance and the cell constant which also is determined from resistance measurements. Assuming the conductivity of the standard electrolyte used for determining the cell constant as error free, an error of 1 % results for the cell constant due to resistance measurements. The total error of the conductivities is composed of the sum of the errors of conductivity and cell constant. Thus, conductivities are determined with an uncertainty of ±2 %.

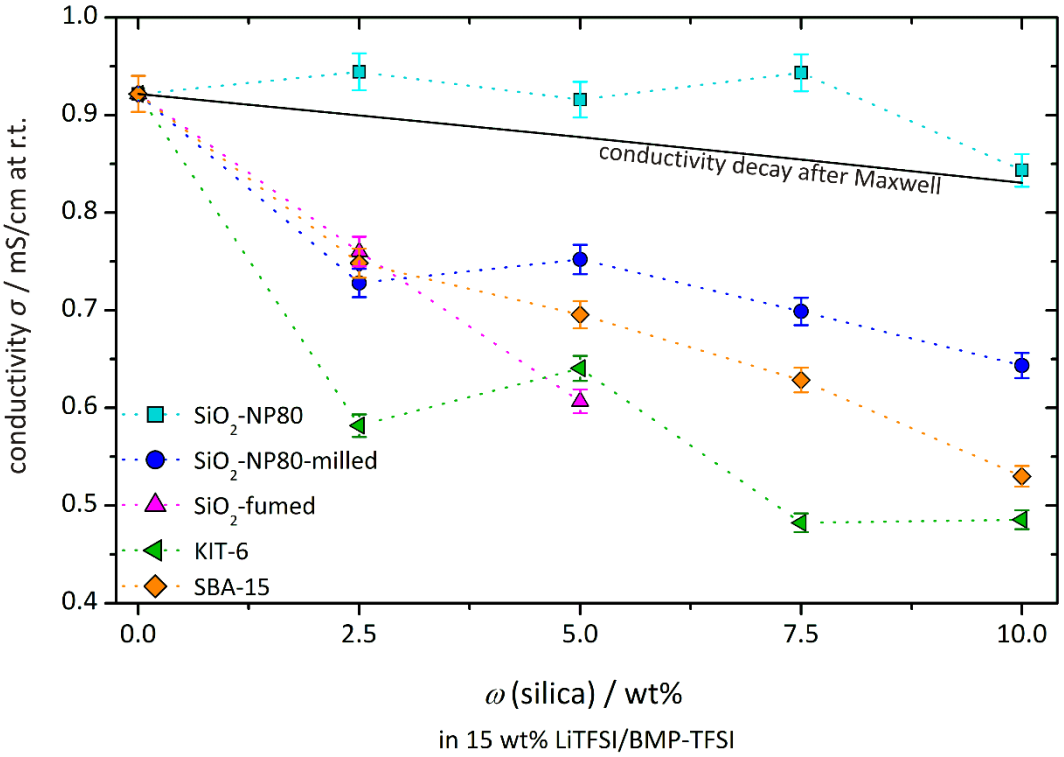

Figure 4.8: Room temperature conductivities σ of 15 wt% LiTFSI/BMP-TFSI with different surface-unmodified silica in dependence on the silica mass fraction ω. Conductivity decay predicted by Maxwell if the filler material represents solely an exclusion volume without occurring interface effect is depicted as solid black line. The dotted lines are presented as guides for the eye.

From Figure 4.8 it is obvious that the conductivities of 15 wt% LiTFSI/BMP-TFSI containing unmilled silica particles with a particle size of 80 nm (SiO_2-NP80) hardly change with respect to the neat electrolyte up to a silica content of 10 wt%. All other surface-unmodified silica presented in Figure 4.8 cause an initial steeper conductivity decay for a content of 2.5 wt% with respect to the neat electrolyte. The conductivities of the electrolytes with 2.5 wt% filler material are equal for the ball-milled nanoparticles, fumed silica and SBA-15. By further increasing the silica fraction the conductivity decay for all electrolytes is less pronounced compared to the decay from neat electrolyte to the IL electrolytes with 2.5 wt% filler materials. For the electrolyte

with KIT-6 even a small increase in conductivity occurs from 2.5 wt% to 5 wt% KIT-6 in IL electrolyte. Only the conductivity of the electrolyte with fumed silica decreases linearly but it is in the same range as the conductivities of the other composite electrolytes although the electrolyte with 5 wt% fumed silica is a gel and thus, has a high viscosity. The lowest conductivities are reached for IL electrolytes with KIT-6 as filler material. SiO_2-NP80 and SiO_2-NP80-milled are the same compounds with the only difference that one is unmilled and the other one is ball-milled. Nevertheless, they induce clearly different conductivity behaviors in the composite electrolytes. Conductivities of the electrolytes with the unmilled nanoparticles hardly change with respect to the neat electrolyte. For the electrolytes with the ball-milled nanoparticles the conductivity first decreases and hardly changes for silica fractions above 5 wt%. Thus, with the ball-milled particles considerably lower conductivities are observed in comparison to the unmilled nanoparticles. Hence, the morphology of the aggregates and the type of particle network is crucial for the conductivity behavior. Since it is known that ILs form ordered structures on silica surfaces (cf. Chapter 2.2.1), varying particle morphology and surface curvature may induce different structures with different conductivity behaviors.

If the filler material represents an exclusion volume solely the conductivity decay should behave as described by Maxwell (cf. equation (2.8)). This conductivity decrease is depicted in Figure 4.8 by the continuous black line and is not in accordance with the conductivity behaviors of the composite electrolytes. Thus, the silica clearly induce an effect which influences the ion mobilities in the composite electrolytes. Except the fumed silica which is mostly silanized and contains hardly silanol groups on its surface all other silica presented in Figure 4.7 and Figure 4.8 have more or less the same surfaces with mainly silanol groups on it. If the conductivity behavior resulted only from the interface effect, the electrolytes with the mesoporous silica would show a different behavior since they have a considerably higher total surface area (inner and outer surface). As the conductivities of the electrolytes containing the mesoporous silica are similar to conductivities of the electrolytes with non-porous nanoparticles, it can be assumed that the conductivity is not dominated by the interface effect. Again this indicates that the conductivity behavior is mainly influenced by the formed particle network.

The temperature dependent conductivities σ of 15 wt% LiTFSI/BMP-TFSI with surface-modified silica nanoparticles are shown in Figure 4.9. Again the error bars are not presented for graphical reasons.

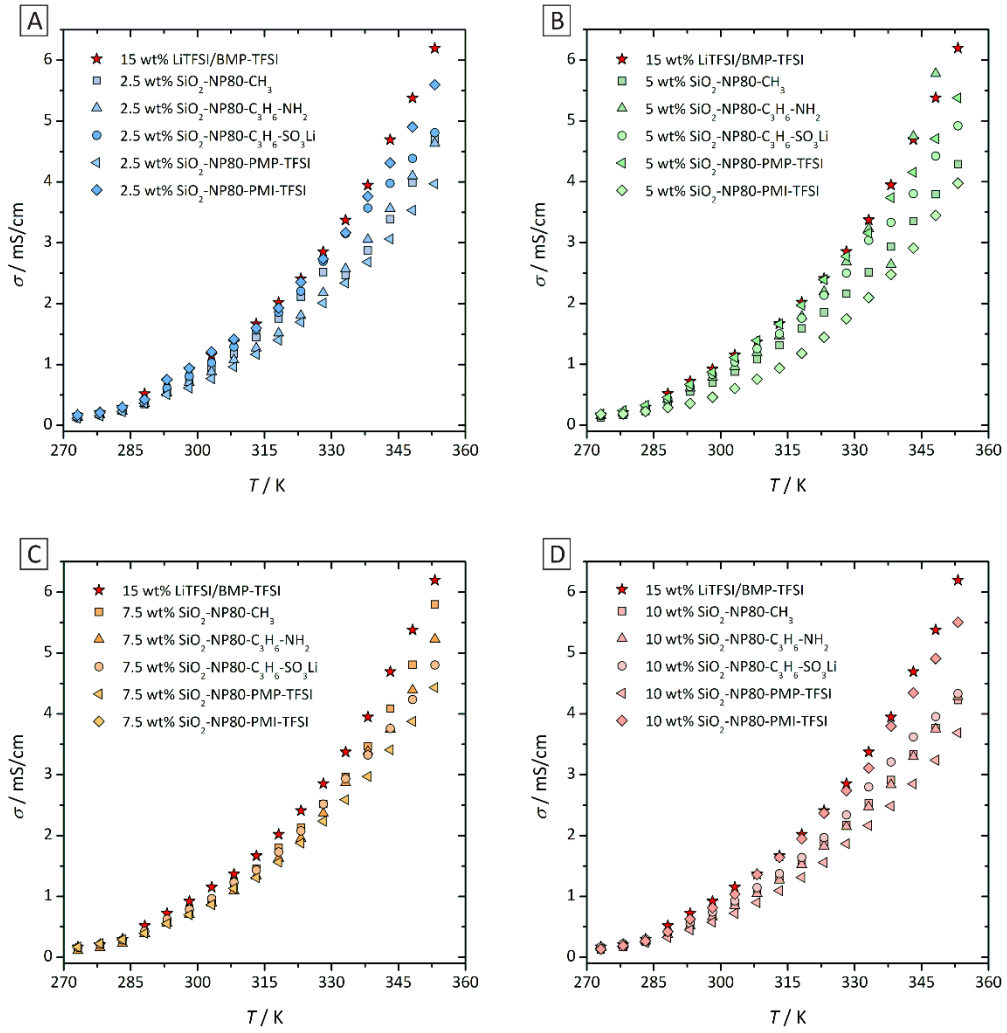

Figure 4.9: Conductivities σ in dependence on temperature of 15 wt% LiTFSI/BMP-TFSI with surface-modified silica nanoparticles. In part A, B, C and D results of IL electrolytes containing 2.5 wt%, 5 wt%, 7.5 wt% and 10 wt% surface-modified silica nanoparticles, respectively, are shown.

With rising temperature conductivities of all electrolytes increase as expected. In contrast to the electrolytes containing surface-unmodified silica (cf. Figure 4.7), differences in conductivities of composite electrolytes with surface-modified silica are very small. For a better comparison of the electrolytes their room temperature conductivities are shown in dependence on the silica fraction in Figure 4.10.

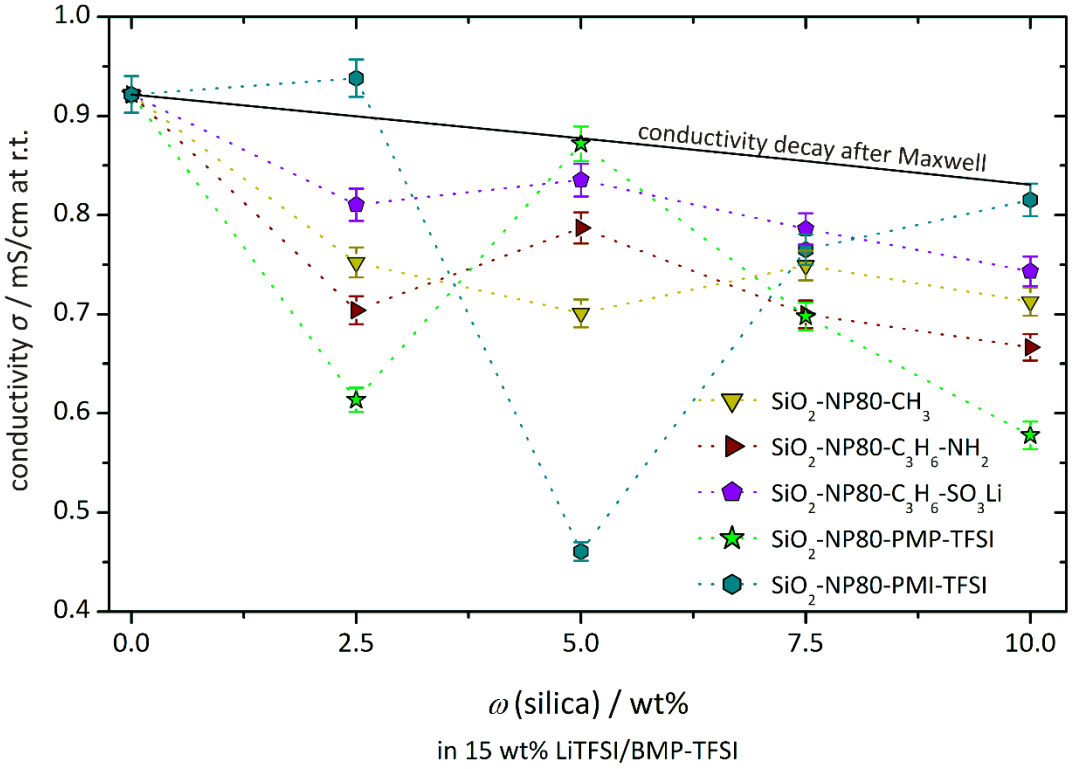

Figure 4.10: Room temperature conductivities σ of 15 wt% LiTFSI/BMP-TFSI with different surface-modified silica nanoparticles in dependence on the filer material mass fraction ω. The solid black line describes the conductivity decay predicted by Maxwell if the filler material represents solely an exclusion volume without respecting interface effects. The dotted lines are inserted as guides for the eye.

All surface-modified silica despite the silica with imidazolium-functionalization (SiO_2-NP80-PMI-TFSI) induce a conductivity decay in the IL electrolyte with 2.5 wt% silica with respect to the neat electrolyte. The electrolytes containing silica with lithiumpropylsulfonate- and aminopropyl-functionalization show a slight increase in conductivity for 5 wt% silica with a following conductivity decay for silica fractions above 7.5 wt%. The methyl-modified silica induce a conductivity decrease up to a silica fraction of 5 wt%. IL electrolyte with 7.5 wt% methyl-modified silica show a slight increase in conductivity followed by a small conductivity decrease for 10 wt% silica. The composite electrolyte with 5 wt% pyrrolidinium-modified silica shows a comparably high conductivity increase followed by a conductivity decrease for 7.5 wt% and 10 wt% silica with conductivity values very similar to the electrolyte with aminopropyl-modified silica. The silica with imidazolium-functionalization shows a quite different conductivity behavior. With 2.5 wt% imidazolium-modified silica the electrolyte conductivity hardly changes followed by a high conductivity decay for the electrolyte with 5 wt% imidazolium-modified silica reaching the smallest conductivity value of all presented electrolytes in the present work. Increasing the silica fraction up to 7.5 wt% a high conductivity increase follows resulting in conductivity values similar to the electrolytes with methyl- and lithiumpropylsulfonate-functionalization.

Increasing the silica fraction of imidazolium-modified nanoparticles to 10 wt% in the electrolyte induces a further conductivity increase. Disregarding the electrolyte with imidazolium-modified silica, conductivity behavior of composite electrolytes with surface-modified silica is similar for all modified silica investigated in the present work. Moreover, these electrolytes show higher conductivities compared to the composite electrolytes with unmodified silica.

Again the conductivity decay predicted by Maxwell if the filler material represents solely an exclusion volume is shown in Figure 4.10 as continuous black line. The conductivity behaviors of the composite electrolytes with surface-modified silica resemble more the predicted conductivity decay than the electrolytes with surface-unmodified silica. Nevertheless, the conductivity behavior is not described exactly by Maxwell's prediction. Hence, it may be assumed that interactions between filler material and electrolyte occur. The morphologies of the surface-unmodified silica were clearly different leading to quite different conductivity behaviors in the composite electrolytes. Since for the surface-modified the same silica were used for modification their morphologies are very similar just as their conductivities are. Again the hypothesis is supported that morphology of filler material is crucial for the electrolyte properties. For a composite electrolyte consisting of a conducting matrix with a conductivity of 0.92 mS/cm (as it is the case for 15 wt% LiTFSI/BMP-TFSI) and 5 vol% of insulating spherical silica particles with particle sizes of 50 µm it was simulated that conductivity decrease is 71 % along the particles. Since the nanoparticles are agglomerated in the dispersed electrolytes the particle size of 50 µm should be in the magnitude of the agglomerates. Hence, the changes in conductivity observed in the present work cannot be described by simple geometric current interruption as a relatively small conductivity decrease was observed.

If an interface effect would influence the electrolyte properties, composite electrolytes containing filler materials with varying surface modifications would have led to clearly different conductivity behaviors. Since the conductivities are varying with the morphology of the filler materials, it can be assumed that the different silica lead to different networks and hence, to varying mobility mechanisms in these networks. If the mechanism for ion mobility changes, a different activation energy is expected. The activation energy describes the required energy for an ion to change its position in the electrolyte and is influenced by the ion environment which should be different in different networks. To determine the activation energy E_A the Arrhenius equation (cf. equation (4.1)) is used which describes the temperature dependency of conductivity.

$$\sigma = \frac{A}{T} \cdot e^{-\frac{E_A}{RT}} \tag{4.1}$$

The preexponential factor A describes the jump frequency and activation entropy. The energy barrier which the ion has to overcome for the jump is depicted by the activation energy E_A. R describes the universal gas constant, T the temperature and σ the conductivity. Since the mobility of ions in ionic liquids resembles the mobility in solid electrolytes the preexponential factor for ionic liquids is assumed to be antiproportional to temperature as it is the case for solid electrolytes. Taking the natural logarithm of the Arrhenius equation and combining the temperature dependence of the preexponential factor with the conductivity, results in equation (4.2).

$$\ln(\sigma \cdot T) = \ln A - \frac{E_A}{R} \frac{1}{T} \tag{4.2}$$

Plotting the natural logarithm of the product of conductivity and temperature against the reciprocal temperature allows the determination of activation energy from the slope of the plot which equals the quotient of activation energy E_A and universal gas constant R. ILs near the glass temperature do not follow Arrhenius behavior and are mostly described by the Vogel-Fulcher-Tamman (VFT) equation which is used for glass-forming systems near the glass temperature. The VFT equation is shown in equation (4.3) with the preexponential factor A and the glass temperature T_g.

$$\sigma = A \cdot e^{-\frac{E_A}{R(T-T_g)}} \tag{4.3}$$

In the present work the activation energies were determined by Arrhenius equation for temperatures above 293 K, considerably above the glass temperature T_g. The VFT equation is not applied for determination of activation energy since a linear behavior in the Arrhenius plot was found for conductivities above 293 K. Moreover, the VFT equation contains two unknown parameter, being the preexponential factor A and the glass temperature T_g instead of one as it is the case for the Arrhenius equation. Thus, applying VFT does not offer more information than using the Arrhenius equation. The activation energies of the presented composite electrolytes are shown in Figure 4.11 and Figure 4.12 in dependence of the filler material fraction.

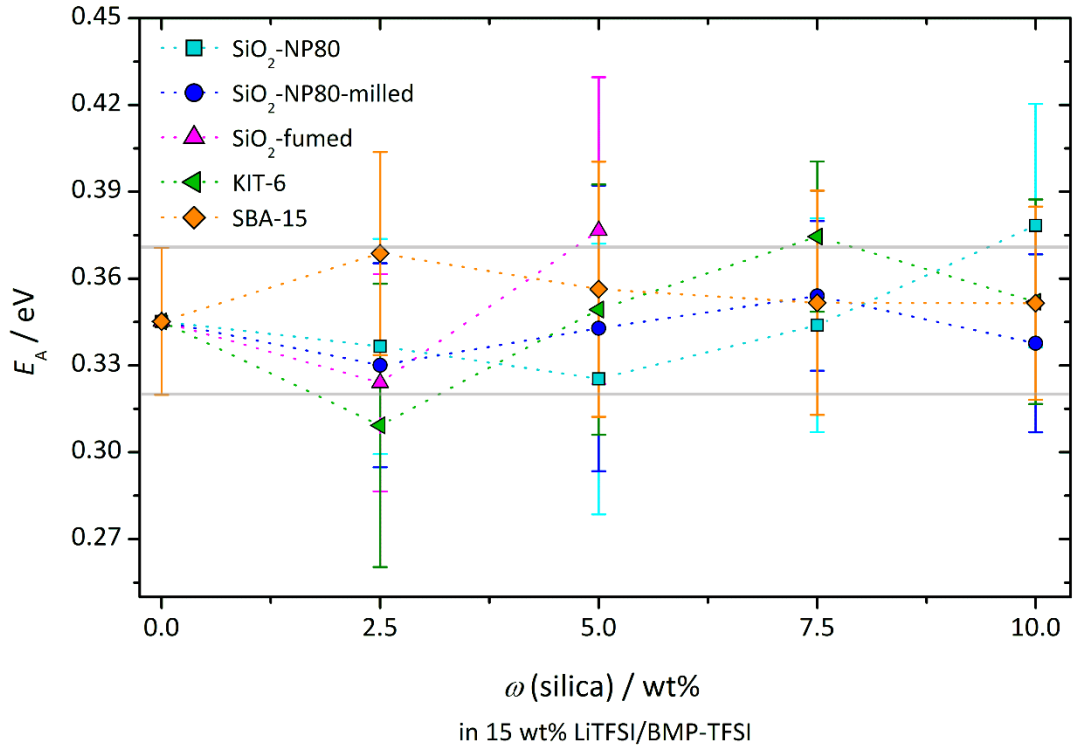

Figure 4.11: Activation energies E_A of 15 wt% LiTFSI/BMP-TFSI with different surface-unmodified silica in dependence on the mass fraction ω of filler material. Dotted lines are presented as guides for the eye.

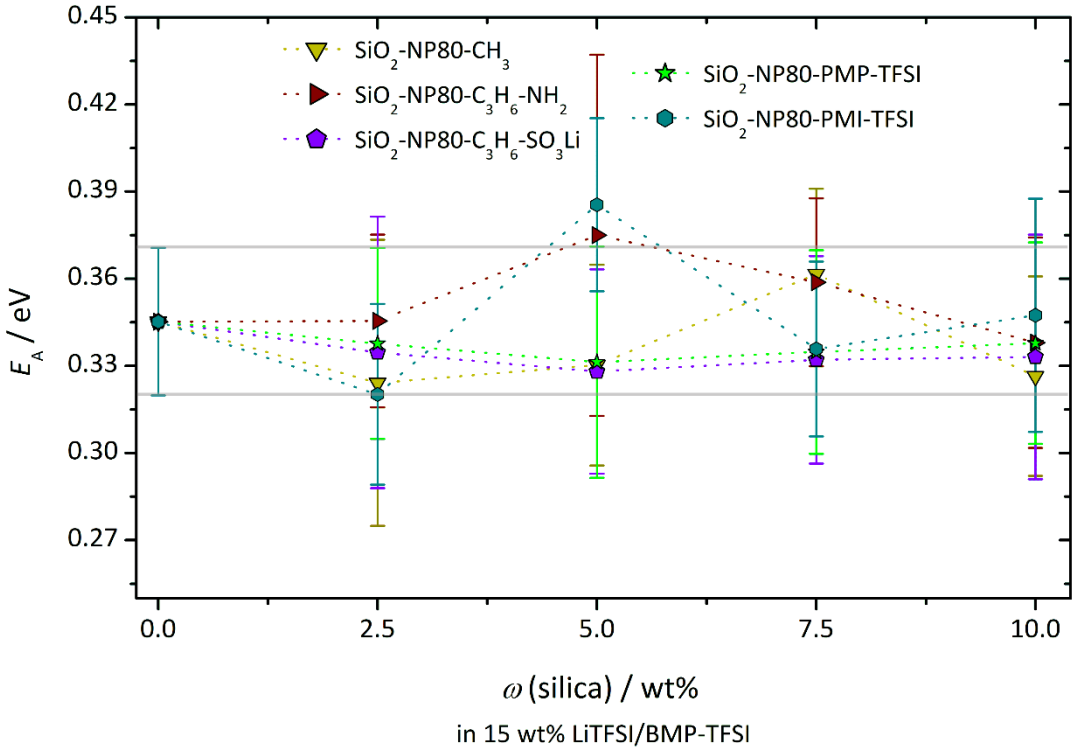

Figure 4.12: Activation energies E_A of 15 wt% LiTFSI/BMP-TFSI with different surface-modified silica in dependence on the mass fraction ω of filler material. Dotted lines are shown as guides for the eye.

The calculated activation energies contain errors from the fit of the plot, the conductivity and temperature. The temperature was adjusted with an uncertainty of 0.1 K resulting in a mean error of 0.03 %. The error of conductivity is 2 % as shown above and the error of the fit was determined for every electrolyte by the ratio of the absolute error of slope and the absolute value for the slope. The resulting error bars of activation energies are presented in Figure 4.11 and Figure 4.12. Obviously, the uncertainty of activation energies is higher than their difference to each other. Thus, no quantitative conclusion is possible but there are a few noticeable trends.

Regarding the conductivities of electrolytes with surface-unmodified silica (cf. Figure 4.8) for 2.5 wt% of filler material, almost the same conductivity values are reached for all composite electrolytes except the electrolytes with the unmilled nanoparticles being quite high and with the mesoporous SBA-15 being very low. In the activation energies this trend is not obvious. The electrolyte with 2.5 wt% SBA-15 shows as expected the highest activation energy but all other electrolytes show more or less the same values of activation energy. For 10 wt% unmilled nanoparticles in the IL electrolyte the highest activation energy is determined with respect to the other composite electrolytes having the same silica fraction, but this electrolyte shows also the highest conductivity among the composite electrolytes with 10 wt% silica fraction. The electrolytes with 10 wt% imidazolium-modified silica shows the highest conductivity among the electrolytes with 10 wt% surface-modified silica. At the same time this electrolyte has the highest activation energy compared to the ones of composite electrolytes with surface-modified silica. For electrolytes with 2.5 wt% surface-modified silica the activation energies are more or less the same whereas the conductivities are clearly different.

Due to the high error bars no significant conclusions can be drawn. But it may be assumed that conductivity mechanisms vary in the different composite electrolytes with surface-unmodified silica. In the electrolytes with surface-modified silica the mobility mechanisms seem to resemble more each other than in the electrolytes with surface-unmodified silica. As known from literature stabilization of IL dispersions occurs sterically due to solid-like regions on the particles (cf. Chapter 4.1). Hence, there is an interface effect but it seems not to influence directly electrolyte properties as it was shown in the literature-known heterogeneous doped electrolytes (cf. Chapter 2.2). Nevertheless, the formed particle network stabilized by these solid-like regions at the interfaces appears to be crucial for the electrolyte properties. The question arises how the chemical composition of the interface regions looks like. Therefore, the interface was analyzed by IR spectroscopy. As reference the neat ionic liquid as well as the IL electrolyte was investigated. By using the liquid composite electrolytes for spectroscopic measurements the resulted spectra show only the bulk

electrolyte due to low concentrations of the filler material. To investigate the interface region the amount of bulk electrolyte has to be minimized. Therefore, 90 wt% silica in 15 wt% LiTFSI/BMP-TFSI was used as composite material as it can be expected that the silica particles are coated by a thin electrolyte film. The IR spectra are shown in Figure 4.13.

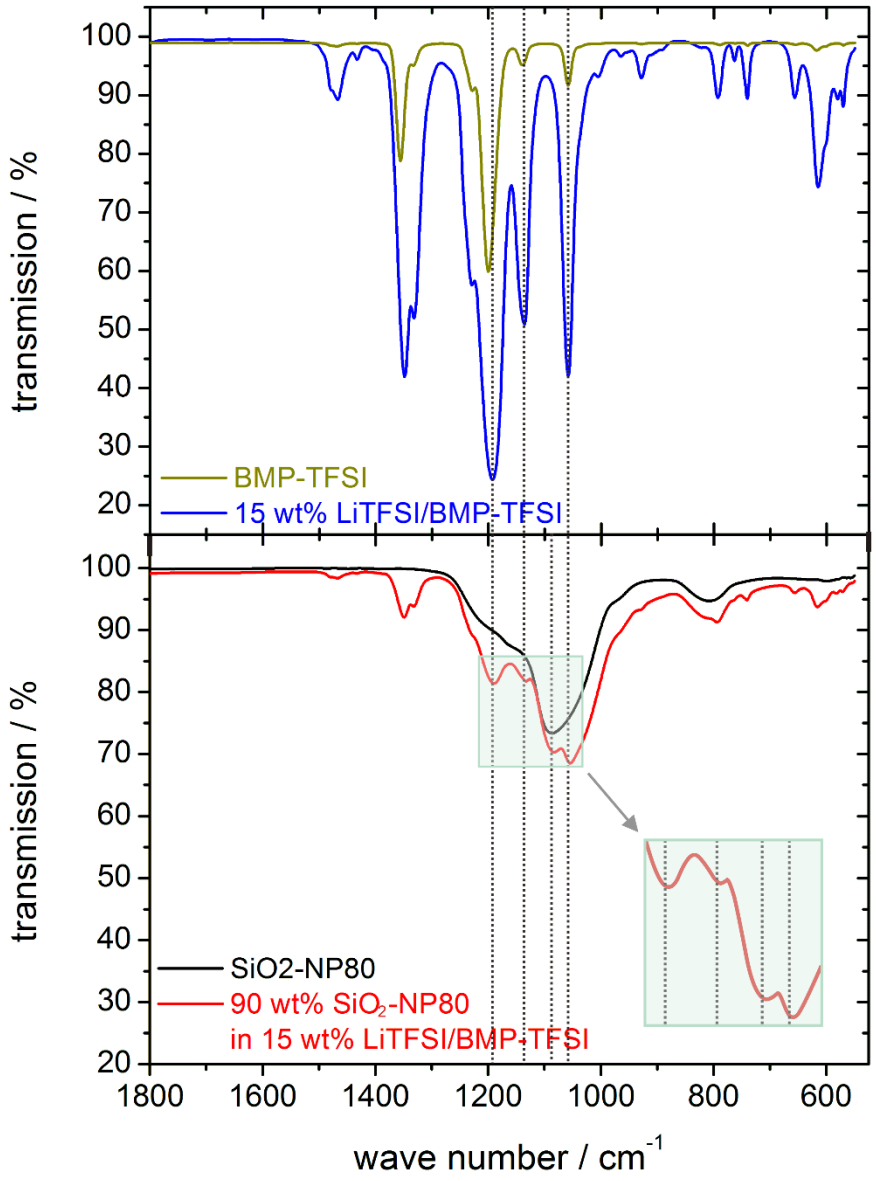

Figure 4.13: IR spectra of N-butyl-N-methylpyrrolidinium TFSI (BMP-TFSI) with and without LiTFSI as conducting salt (top), of the neat silica particles (SiO_2-NP80) and the particles coated with IL electrolyte (bottom). The dotted lines are shown as guides for the eye to display the slight peak shifts discussed below.

Slight peak shifts of the electrolyte coated silica occurred with respect to the neat IL electrolyte in the IR spectra. The shifts are correlated to vibrations of electrolyte

species. Each sample was measured systematically at least five times to ensure that the phase shifts do not contribute to measurement errors. Thus, it is clear that an interface effect influencing the network formation occurs but it remains unclear which ions are involved in which manner in the interface region.

Conductivities, activation energies and IR-spectra show that an interface effect occurs in the IL composite electrolytes. Hence, a network is formed by the silica particles which influences the electrical transport properties of the electrolytes.

4.3 Mechanical properties of composite electrolytes

Viscosities were measured by rotational rheology experiments in dependence on shear rate. The neat IL electrolyte is a Newtonian fluid and does not change its viscosity with increasing shear rate as shown in the flow curve in Figure 4.14. The composite electrolytes show shear thinning behavior as their viscosities decrease with increasing shear rate.

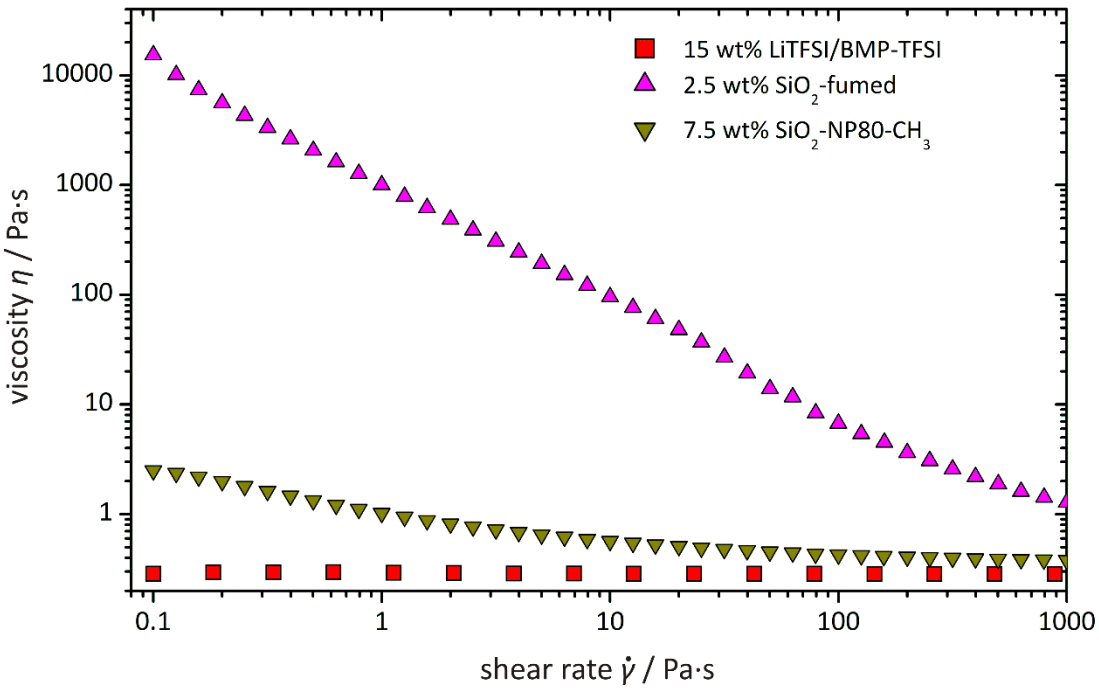

Figure 4.14: Flow curves showing the dependence of viscosity on the shear rate for the neat electrolyte which is a Newtonian liquid and the IL electrolytes containing fumed silica and methyl-modified silica nanoparticles, respectively, both being shear thinning materials.

In Figure 4.14 the flow curves of IL electrolytes with 2.5 wt% fumed silica and 7.5 wt% methyl-modified silica nanoparticles are exemplarily shown. The silica particles are agglomerated in the dispersed electrolytes as long as they are in rested

state. Upon applying a force by rotating the cone during measurement, the agglomerates break forming mainly primary particles. Thus, the intermolecular forces making the dispersions stable are weakened and the viscosity decreases as the flow resistance is decreased due to lower intermolecular forces.

Since non-Newtonian liquids show a strong dependence of viscosity on shear rate and shear stress, absolute viscosity values can only be determined for Newtonian liquids. For non-Newtonian liquids the sample history has to be respected and is crucial for resulting viscosity values as the sample experiences forces during application on the measuring device and during the initial operation to bring the cone in measuring position. Due to the forces during the measurement preparation, the sample is in a non-rested state and may have already a decreased viscosity in case of shear thinning materials. Nevertheless, viscosities are presented for non-Newtonian liquids, too. Here, it is important to note all measurement conditions, information on the shear history and at which shear rate or stress the presented viscosity values were collected.

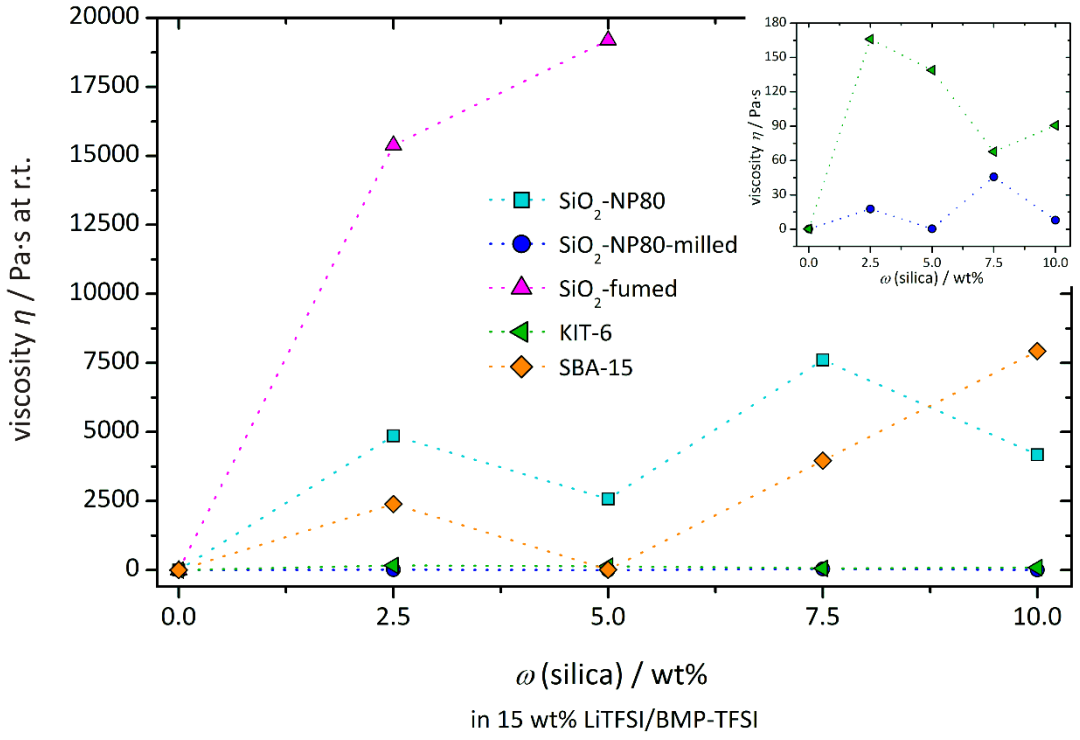

Figure 4.15: Room temperature viscosities η of 15 wt% LiTFSI/BMP-TFSI with surface-unmodified silica in dependence on the silica mass fraction ω. Dotted lines are shown as guides for the eye.

For the viscosity measurements presented here attention was paid to treat all electrolytes in the same manner prior to measurement with respect to their shear history. Stirring was interrupted 15 minutes before measurement and the electrolyte was poured onto the plate directly from the sample vial without using pipettes or syringes. Only for the gel-like electrolytes with 5 wt% fumed silica and 10 wt%

mesoporous SBA-15 a spatula was used. After putting the cone in measuring position the sample was rested for another 15 min before starting the measurement. Figure 4.15 and Figure 4.16 show the viscosities at a shear rate of 0.1 s^{-1} and 25.0 °C in dependence on the silica fraction in the electrolyte. The lowest measured shear rate was chosen for presenting viscosities since there the system is in the most rested state.

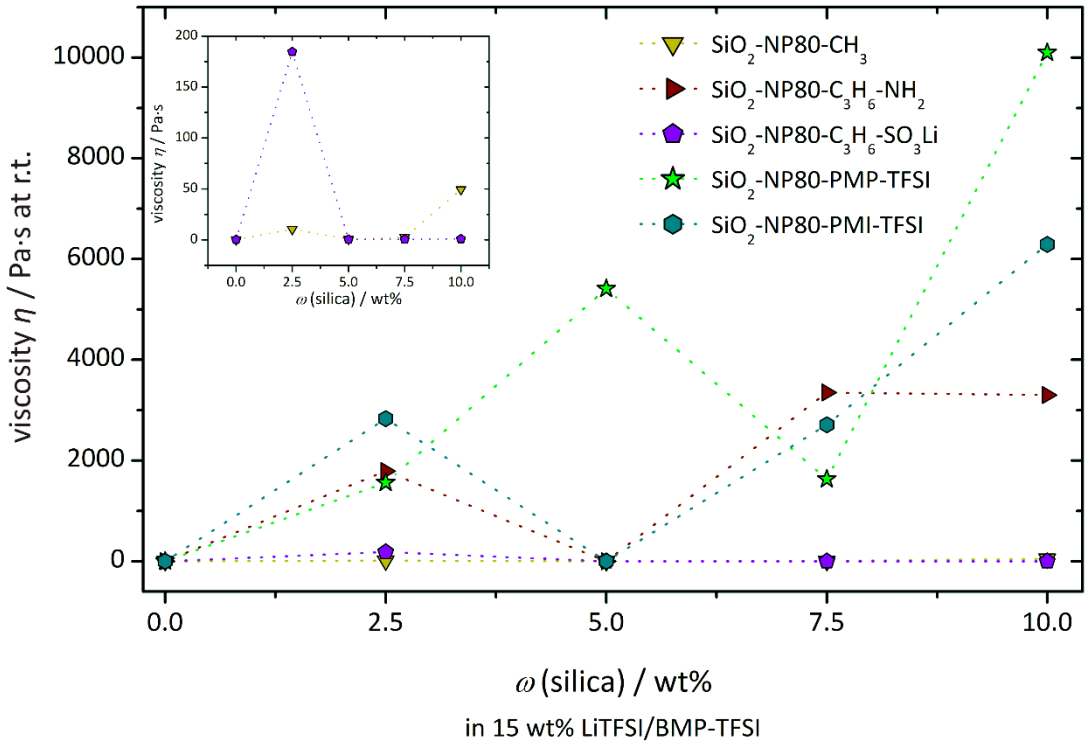

Figure 4.16: Room temperature viscosities η of 15 wt% LiTFSI/BMP-TFSI with surface-unmodified silica in dependence on the silica mass fraction ω. Dotted lines are presented as guides for the eye.

For all electrolytes the viscosity increases by addition of filler material but no clear trend of the viscosity as function of the silica fraction was observed. A possible explanation is that the sample history slightly varied for the electrolytes and the networks of some electrolytes were not stable enough to maintain. Thus, the viscosities should be treated carefully and regarded more as relative values than absolute ones. Since the errors in viscosity resulting from sample history are much larger than measuring errors and cannot be calculated, error bars are not presented for rheological measurements. For the electrolytes with surface-unmodified silica (cf. Figure 4.15) it is clear that electrolytes with fumed silica have the highest viscosity followed by the electrolytes with unmilled nanoparticles. Disregarding the electrolyte with 5 wt% SBA-15 it can be concluded that SBA-15 induce a linear viscosity increase with rising filler amount in the electrolyte. For KIT-6 containing electrolytes the viscosity strongly increases with 2.5 wt% KIT-6 and decreases then up to an amount of 7.5 wt% before slightly increasing for 10 wt%. KIT-6 also stood out in the conductivity measurements

(cf. Figure 4.8) as it showed the lowest conductivities among the electrolytes with surface-unmodified silica and caused the highest conductivity decrease for an amount of 2.5 wt%. The ball-milled silica nanoparticles increase the viscosity of the IL electrolyte only slightly. Thus, no direct correlation of viscosity and conductivity occurs as composite electrolytes with low viscosities do not show high conductivities. Since silica with similar surfaces influence electrolyte viscosities differently, the hypothesis is underlined that electrolyte properties depend strongly on the particle morphology as the main differences of the unmodified silica are their morphologies. The viscosities of electrolytes with methyl-modification hardly change with varying silica fractions up to 10 wt% where a considerable viscosity increase occurs (cf. Figure 4.16). Electrolytes with aminopropyl- and imidazolium-modified silica show very similar viscosity behavior although conductivities of these electrolytes are clearly different. The pyrrolidinium-modified silica induces at an amount of 5 wt% a very high viscosity increase in the electrolyte. The same electrolyte has the highest conductivity under all composite electrolytes containing 5 wt% surface-modified silica.

From the conductivity results it was concluded that the chemical composition of silica surface hardly influences the electrolyte properties and that the conductivity behavior varied only with different particle morphologies. For the viscosities varying silica surfaces influenced the electrolyte behavior in a different manner. As the conductivity behavior of composite electrolytes with surface-modified silica is very similar and their viscosities differ each other, it may be concluded that the conduction mechanisms remain similar in the different composite electrolytes but the mechanical properties vary due to varying interface regions resulting from different surfaces. This conclusion is in good agreement with the works of Ueno et al. [183–185]. They reported a gelation in ionic liquids by adding silica particles due to interconnected networks of the silica nanoparticles. This network formation was dependent on the particle surface. They assumed a multilayered IL structure on the silica surfaces which inhibit aggregation of the particles. Moreover, they reported a high ionic conductivity in the ion gels which they explained by phase separation of ionic liquid in an interconnected silica network. Thus, interface regions have to be established on the silica surfaces which stabilize the dispersion. These regions may also be dependent on the particle morphologies resulting in slightly different networks. If mobility mechanisms of ions did not change in the composite electrolytes decreasing conductivity should went along with increasing viscosity. Then, it would be expected that electrolytes with highest conductivities show lowest viscosities and vice versa. Since it is not the case and no obvious correlation of viscosity and conductivity is present, it may be assumed that ion mobility mechanism is directly influenced by the

formed network of filler material. Hence, viscosity measurements support the conclusions drawn from the activation energies of the composite electrolytes that ion mobility mechanisms vary in the different composite electrolytes.

Walden proposed an empirical equation which states that the product of the equivalent conductivity Λ and viscosity η is constant for ideal electrolytes. Angell et al. [188] and Gores et al. [189] showed that ionic liquids also fulfill the Walden rule since the product of equivalent conductivity and viscosity is constant with varying temperature. Combining the Walden equation with Stokes equation it becomes clear that the Walden product is a constant, only varying with the hydrodynamic ion radii r_i of electrolyte ions. The Faraday constant F, charge number z and elementary charge e are constants (cf. equation (4.4)).

$$\Lambda\eta = \frac{Fz^2e}{6\pi\sum r_i} \tag{4.4}$$

Thus, as long as the coordination of the ions in the IL composite electrolytes does not change the product of equivalent conductivity and viscosity should be constant. The equivalent conductivity Λ was determined from conductivity σ, concentration c of conducting salt and charge number z by equation (4.5). The charge number is one since all ions are monovalent. The volume of the electrolyte is not known as masses m were used to prepare electrolytes. Therefore, the density ρ of the IL electrolyte was determined by a pycnometer being 1.46 g/mol. The conducting salt concentration c in electrolyte was calculated from the amount n_{LiTFSI} of LiTFSI. To obtain the concentrations of the composite electrolytes the silica mass fractions were converted into volume fractions using 2.2 g/mL as density for the silica. Since the density of silica may vary for the different filler materials an error is made by using the same silica density for all composite electrolytes. Nevertheless, the density changes should be very small for the different silica and the resulting error is made systematically which does not change in composite electrolytes with same silica. Moreover, volume change due to intermolecular interactions was not considered resulting in an additional error which is made systematically. Hence, the equivalent conductivities should be treated more as relative values than absolute ones.

$$\Lambda = \frac{\sigma}{z \cdot c} = \frac{\sigma \cdot V_{\mathrm{tot}}}{z \cdot n_{\mathrm{LiTFSI}}} = \frac{\sigma(V_{\mathrm{electrolyte}} + V_{\mathrm{silica}})}{z \cdot n_{\mathrm{LiTFSI}}} = \frac{\sigma\left(\frac{m_{\mathrm{electrolyte}}}{\rho_{\mathrm{electrolyte}}} + \frac{m_{\mathrm{silica}}}{\rho_{\mathrm{silica}}}\right)}{z \cdot n_{\mathrm{LiTFSI}}} \tag{4.5}$$

Thus, equivalent conductivities could be obtained as shown in Figure 4.17 and Figure 4.18. The product of molar conductivity and viscosity was determined for the neat IL electrolyte. If complexation and therefore mobility mechanisms of ions in

composite electrolytes do not change with respect to the neat IL electrolyte the product of equivalent conductivity and viscosity should be the same for all electrolytes investigated in the present work. Hence, the expected equivalent conductivities were determined from the measured viscosities of the composite electrolytes and the product of equivalent conductivity and viscosity of the neat IL electrolyte. The expected values are depicted in light colors together with the measured values (cf. Figure 4.17 and Figure 4.18).

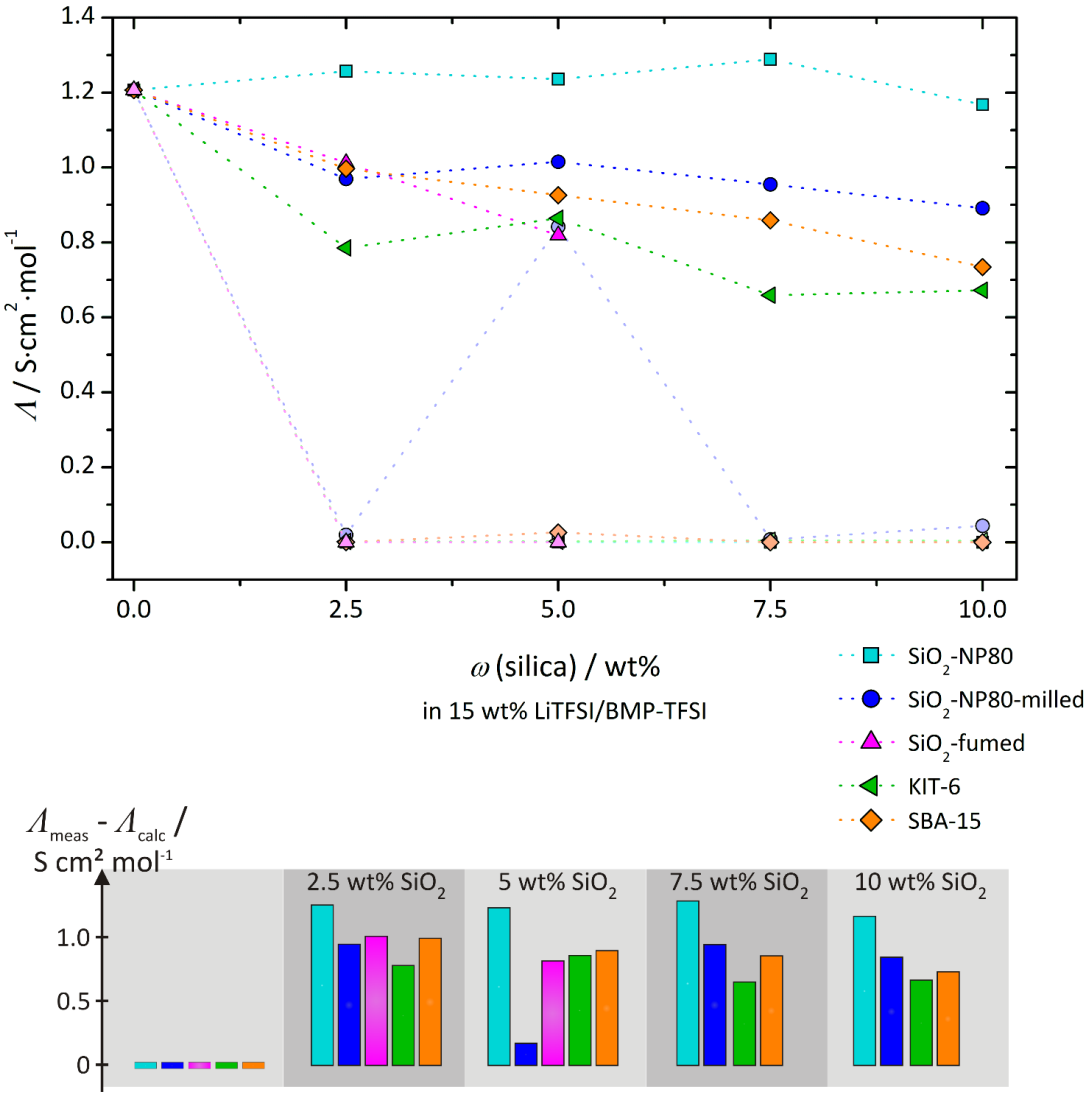

Figure 4.17: Equivalent conductivities Λ normalized to conducting salt concentration of IL electrolyte with surface-unmodified silica in dependence on the silica mass fraction ω are shown (top). In light colors calculated equivalent conductivities are presented determined from Walden's rule with the assumption of not varying hydrodynamic ion radii in the composite electrolytes. Dotted lines are shown as guides for the eye. For clarity the difference of measured and calculated equivalent conductivities is shown (bottom).

The measured conductivities are higher than the expected values if ion coordination does not change in the electrolytes. The Stokes equation cannot be used to determine

the absolute radii of the ions since it is only valid for spheres moving in an incompressible continuum fluid. But it is obvious that complexation and hence, ion mobility mechanism is changed in the composite electrolytes with respect to the neat IL electrolyte. Since the measured equivalent conductivities are considerably higher than expected from the corresponding viscosities, a clear evidence on ion mobility enhancement is given.

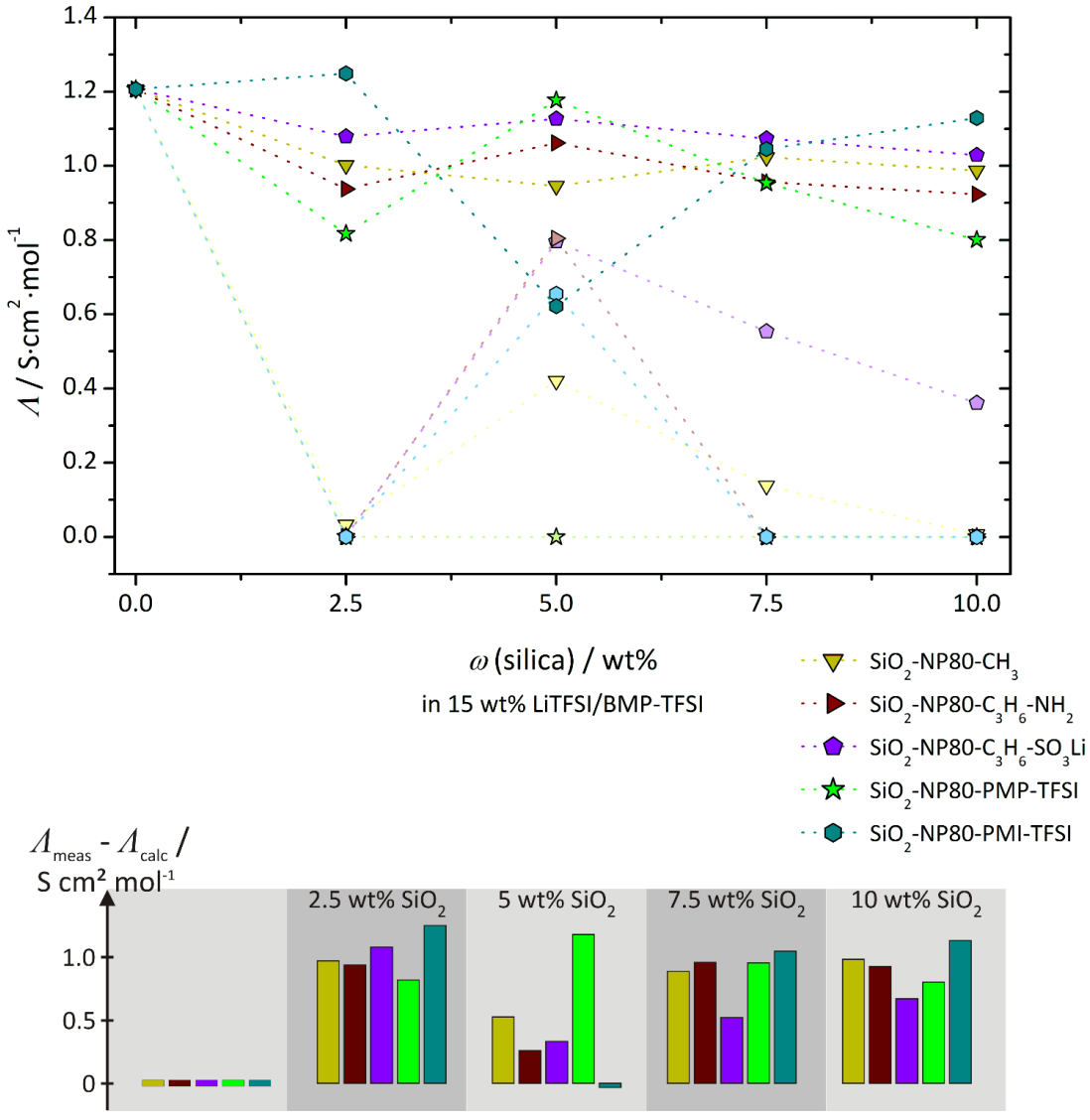

Figure 4.18: Measured and calculated values of equivalent conductivity Λ for the IL electrolyte with surface-modified silica in dependence on silica mass fraction ω are presented (top). The measured equivalent conductivities are normalized to the conducting salt concentration. The calculated equivalent conductivities (light color) are determined from Walden's rule assuming the hydrodynamic ion radii to be unchanged in the composite electrolytes with respect to the neat IL electrolyte. Dotted lines are shown as guides for the eye. Difference of measured and calculated equivalent conductivities is presented for clarity (bottom).

It is well known from literature that ILs form solid-like structures on solid surfaces. Hence, it is most likely that the IL ions are incorporated into the network formed by

the silica since there is no other way to understand the stability of the dispersions. This allows the assumption that the observed ion mobility enhancement is caused primarily by the lithium ions. Moreover, it is known that IL cations have the highest transference number in IL electrolytes as they exist mainly as single ions. Thus, the ion mobility of the IL cations can hardly be further increased. Hence, the increased ion mobility most likely is caused by the lithium ions or anions. The anions are mainly involved in lithium complexes as the IL cations exist as single ions. Though, anion mobility enhancement, which equals concentration enhancement of free anions, results in decomplexation of lithium ions going along with mobility enhancement of lithium ions.

So far it seems as network formation is crucial for the electrolyte properties which is assumed to depend more on particle morphology than on chemical composition of particle surface. It was tried to further characterize the network by rheological oscillation experiments. Up to now, it became clear that addition of 2.5 wt% silica induces an increase in viscosity and the strongest decrease in conductivity. Further addition of filler material hardly affects the conductivity compared to the changes in viscosity. Thus, for network characterization by oscillation experiments in addition to the neat IL electrolyte the electrolytes with 2.5 wt% and 10 wt% silica were investigated. Again attention was paid to keep sample history the same for all composite electrolytes. In Figure 4.19 the shear moduli *G* of the neat IL electrolyte and the composite electrolytes are shown which were determined by amplitude sweep experiments. The shear modulus gives evidence on the rigidity of the system.

Comparing the neat ionic liquid N-butyl-N-methylpyrrolidinium TFSI (BMP-TFSI) with the IL electrolyte, being the same ionic liquid with 15 wt% LiTFSI, the shear modulus is increased for the IL electrolyte indicating a higher rigidity. Thus, the microscopic structure of the IL electrolyte becomes more ordered (cf. Chapter 4.1) resulting in a more rigid network which still is weak. Thus, the liquid behavior is maintained. The increased rigidity of the IL electrolyte with respect to the neat ionic liquid can be explained by the complexation of lithium ions which induces a higher order. Except the electrolytes with 2.5 wt% ball-milled silica nanoparticles and amino-functionalized silica, respectively, all other composite electrolytes with 2.5 wt% silica showed increased shear moduli with respect to the neat IL electrolyte.

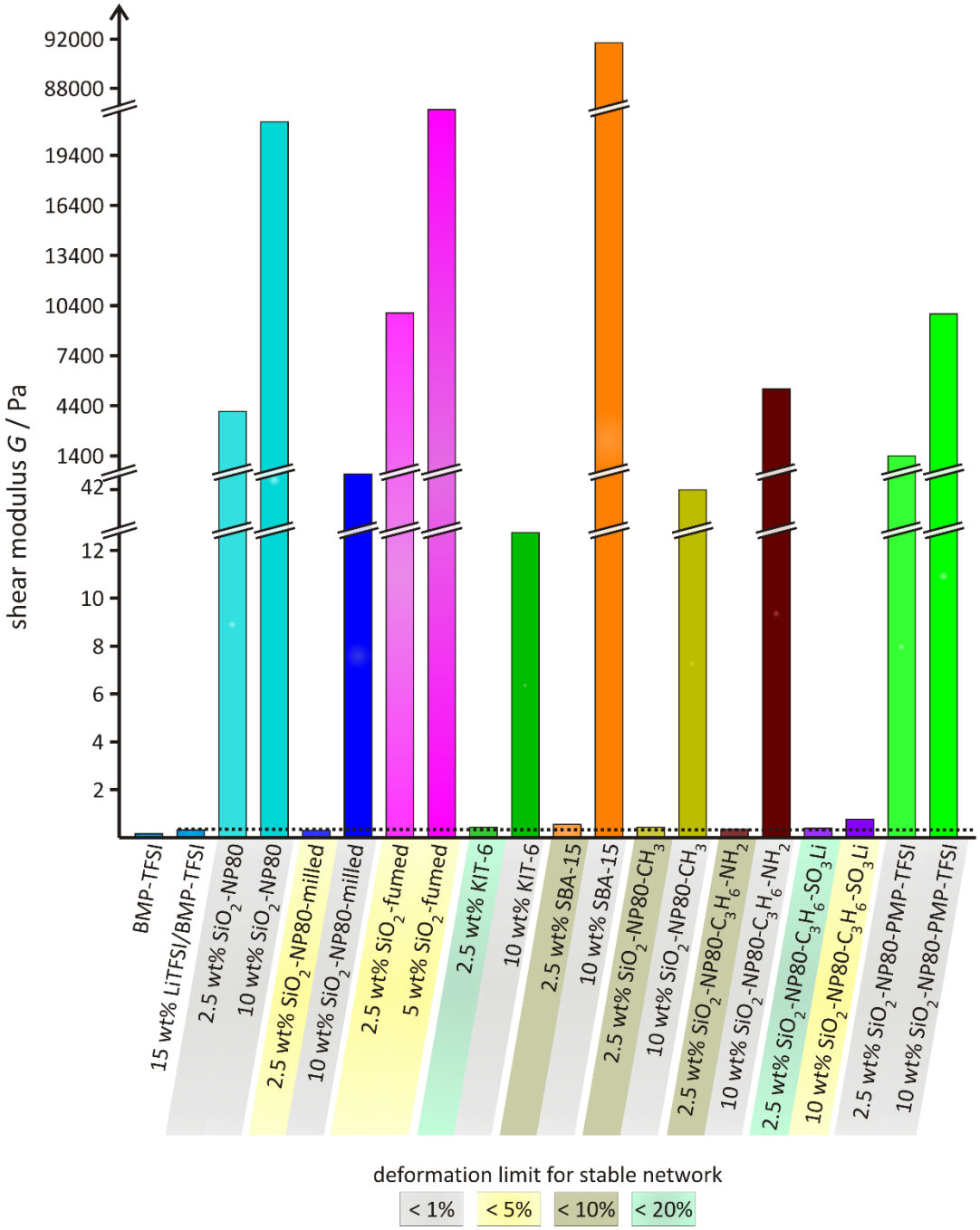

Figure 4.19: Shear moduli *G* of the IL electrolyte and the different composite electrolytes determined by amplitude sweep at angular frequency of 1 rad/s. The color code in *x*-axis labeling depicts the limit of deformation amplitude where the network collapses.

Hence, addition of filler material induces additional ordering of the IL ions which is attributed to solid-like interface regions on the particle surfaces as already reported in literature. As the transition from the solid-like structures to the bulk electrolyte does not occur as an abrupt junction, an ordered microstructure of the IL ions may exist even in a long range resulting in higher rigidity and shear moduli. The composite electrolytes containing 10 wt% silica show all higher shear moduli than the electrolytes with 2.5 wt% filler material. Since the concentration of silica particles is enhanced in

the electrolytes, more interface regions occur which induce a larger volume fraction of more ordered regions in the bulk material. Thus, a network is established with higher rigidity due to increased long-range order based on intermolecular interactions. Since more ions are involved in the network less liquid phase remains to consume the deformation energy. Hence, the network is destroyed at lower deformation amplitudes compared to the networks of composite electrolytes with 2.5 wt% filler material.

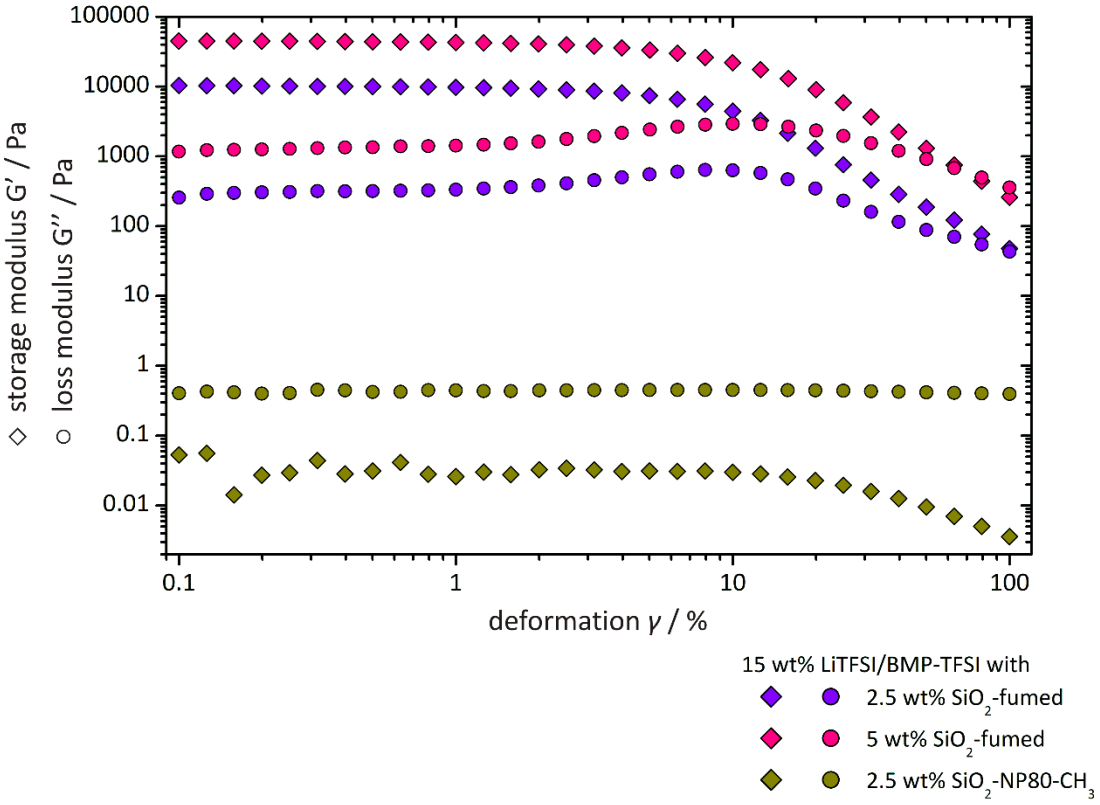

Figure 4.20: Storage and loss moduli in dependence on deformation amplitude during an amplitude sweep with an angular frequency of 1 rad/s for the IL electrolytes with 2.5 wt% and 5 wt% fumed silica as well as with 2.5 wt% methyl-modified silica nanoparticles.

Figure 4.20 shows typical results of storage and loss moduli in dependence on the deformation amplitude for viscoelastic solid composite electrolytes containing fumed silica and a liquid composite electrolyte containing 2.5 wt% methyl-modified silica nanoparticles. Due to the liquid behavior the loss modulus of the electrolyte with 2.5 wt% methyl-modified silica is constant and always higher than the storage modulus. At high deformation amplitudes the storage modulus deviates from its constancy and decreases. This indicates the presence of a network-like structure in the dispersion which is destroyed at higher deformation amplitudes. Thus, the electrolyte with 2.5 wt% methyl-modified silica is a viscoelastic liquid. A completely liquid material without elastic part shows constant loss and storage modulus independent of

the deformation amplitude with the loss modulus being higher than the storage modulus.

For the electrolytes with fumed silica the storage modulus is considerably higher than the loss modulus indicating the material to be more elastic than liquid. At higher deformation amplitudes the storage and loss moduli start to decrease due to the collapsing network of the electrolyte. The loss modulus deviates from constancy earlier than the storage modulus going through a very small minimum before reaching a maximum. This behavior is typical for strong dispersions. If the deformation amplitude is high enough, the network collapses. First the network is destroyed only locally resulting in micro cracks which reduce the flow resistance for the liquid part of the dispersion leading to decreased loss moduli. Then, the micro cracks grow to macro cracks and interrupt the flowing behavior leading to increased loss moduli. Finally the crack crosses the whole gap destroying the structure and reducing the resistance for the cone to move. Hence, the loss modulus decreases. Further increasing the deformation amplitude results in destroying the agglomerates of the dispersed phase and accordingly in lower viscosities and loss moduli.

The relation of storage and loss modulus is expressed in the phase shift. Dominating storage moduli result in small phase shifts indicating elastic behavior. Materials with viscous behavior show dominating loss moduli going along with high phase shifts near to 90°. A phase shift of 45° indicates the transition from viscous to elastic material. The obtained phase shifts of the electrolytes investigated in the present work are demonstrated in Figure 4.21.

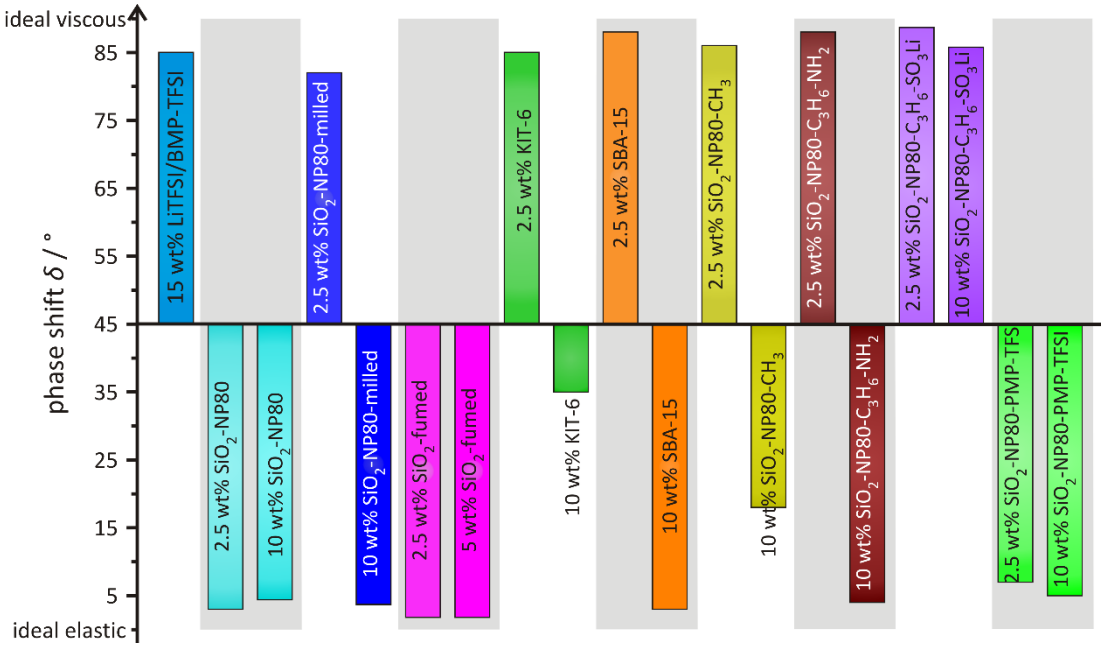

Figure 4.21: Phase shifts of the IL electrolyte and composite electrolytes determined in an amplitude sweep with an angular frequency of 1 rad/s.

As expected the neat IL electrolyte shows almost ideal viscous behavior indicating the electrolyte to be liquid with microscopic short-range order. The composite electrolytes with 2.5 wt% silica are viscoelastic liquids except the electrolytes containing unmilled silica nanoparticles, fumed silica and pyrrolidinium-modified silica nanoparticles. With 10 wt% filler material all composite electrolytes are viscoelastic solids with clearly pronounced network. Only the electrolytes with 10 wt% KIT-6 and 10 wt% methyl-modified silica show weak network formation. Network formation appears to depend on morphology and chemical composition of surface. Surfaces of unmilled and ball-milled silica nanoparticles are identical but clearly different mechanical properties are achieved since the electrolyte with unmilled nanoparticles shows dominating elastic behavior for 2.5 wt% and 10 wt% of silica and the ball-milled nanoparticles containing electrolyte is almost liquid for 2.5 wt% filler material. The mechanical properties of the electrolyte with unmilled silica nanoparticles resembles more the behavior of the electrolyte with fumed silica which has a different surface containing mainly silane groups in contrast to the silanol groups dominating surface of the unmilled and ball-milled silica nanoparticles. The surface-modified silica have all very similar morphologies since modification occurred using the same silica nanoparticles but establish clearly different mechanical properties.

Hence, neither the morphology is clearly dominating the mechanical properties nor the chemical composition of surface since the ball-milled and unmilled nanoparticles also showed different behaviors. The results of oscillation experiments give evidence on network formation in the composite electrolytes which most likely derive from solid-like structures at the interface regions of silica particles and electrolyte inducing a long-range order into the bulk electrolyte. Formation of the solid-like structures appears to depend on the chemical composition of the filler surfaces which directly influence the composition of the interface region and on the morphology influencing the established network due to different curvatures of particle surfaces. The correlation of mechanical and electrical properties allows to conclude that the mobility of at least one ion species is enhanced in the composite electrolytes with respect to the neat IL electrolyte.

4.4 Electrochemical behavior of composite electrolytes

Although it is obvious from the correlation of electrical and mechanical properties that ion mobility of at least one ion species is enhanced by the silica particles no conclusion can be drawn, yet, which ion species is addressed. Thus, electrochemical measurements in half cells with lithium anode and lithium iron phosphate (LFP)

cathode were carried out. Comparison of the results with the ones obtained with neat IL electrolyte give evidence whether lithium ion conductivity is influenced by the filler material.

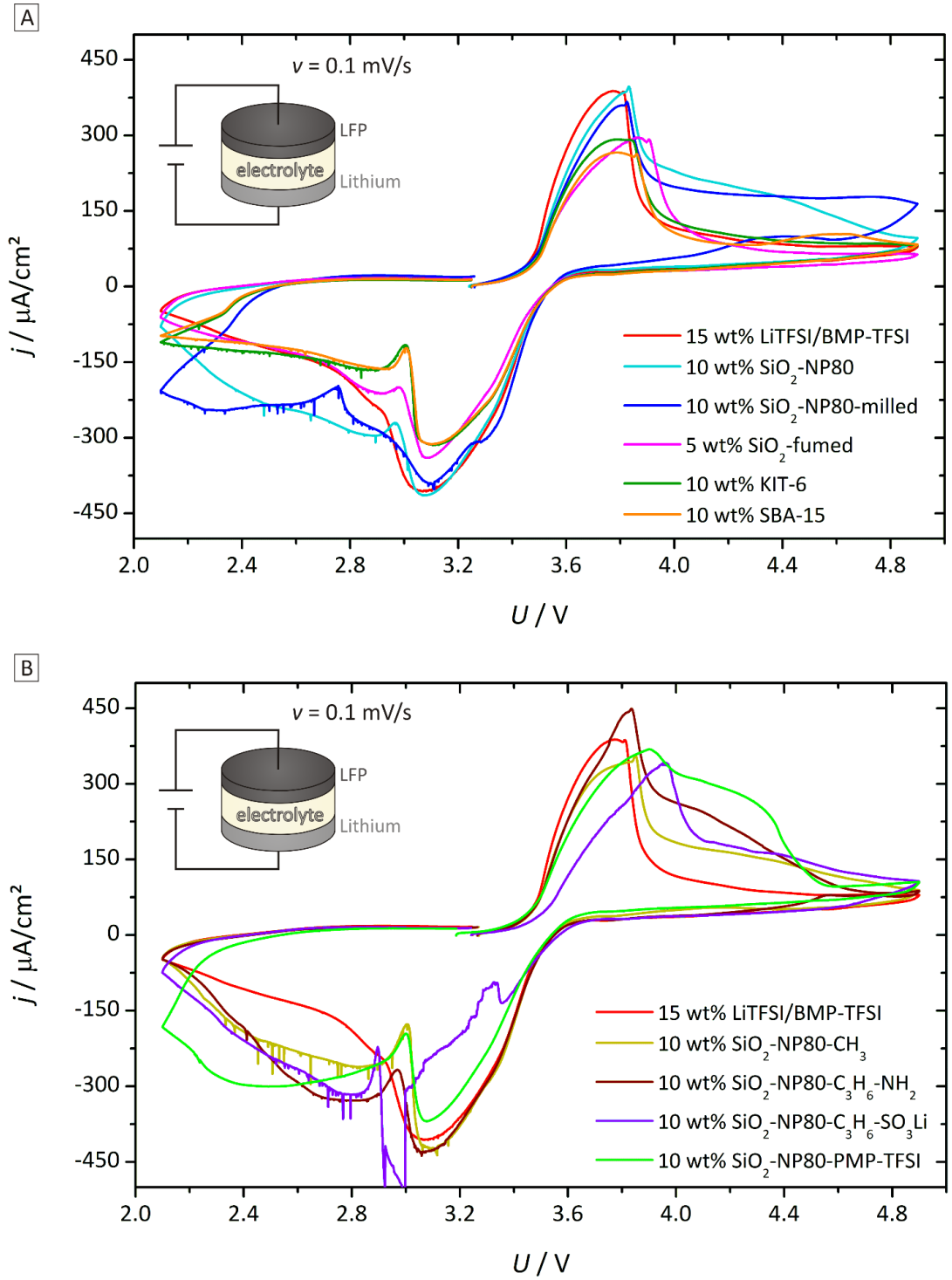

Figure 4.22: Cyclic voltammetry results in cells with lithium iron phosphate and lithium as electrodes and the ionic liquid-based composite electrolytes (scan rate *v* was 0.1 mV/s). Current fluctuation might be explained with expansion of the cathode or inhomogeneities at the anode.

If the formed network in the composite electrolytes does not influence lithium ion mobility, decreased electrochemical performance is expected in the half cells with composite electrolytes due to steric hindrance of lithium ions by the network. An increased or unchanged electrochemical response in the half cells proves that lithium ion mobility is increased. Since rheological measurements showed that network formation is stronger with increasing silica fraction and conductivity decay was poor for all silica fractions above 5 wt% filler material, composite electrolytes with 10 wt% silica were chosen for the experiments in half cells. The results obtained with very low scan rate of 0.1 mV/s where the system is mainly in equilibrium are shown in Figure 4.22. The different composite electrolytes show slightly different overvoltages which were higher for electrolytes with poor electrochemical response, as expected. The composite electrolytes with the two positively polarized surface functionalizations being aminopropyl- and pyrrolidinium-groups show parasitic side reaction which occurs with the iron phosphate of LFP as it also occurs in cells with steel as cathode and lithium as anode (cf. Figure 4.23). Electrolyte decomposition can be excluded as in this case a continuous current increase would be obvious and no current decrease due to diffusion limitation would occur. Moreover, the electrolyte was not changed between measurements with varying scan rates and reasonable voltammograms were still achieved.

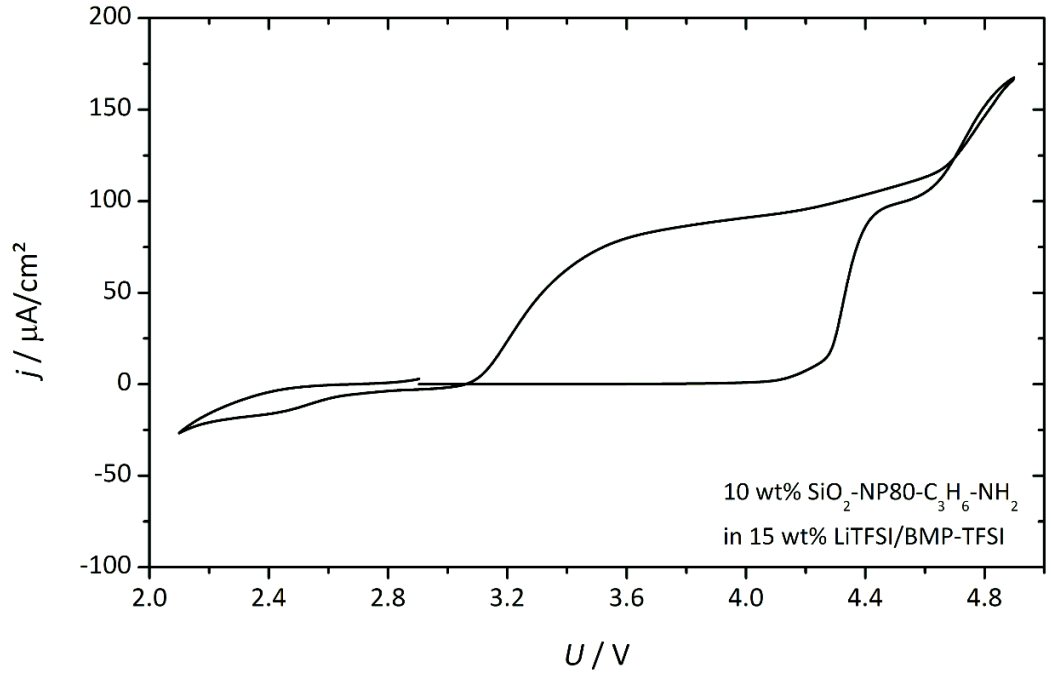

Figure 4.23: Cyclic voltammetry with a scan rate of 0.4 mV/s. 10 wt% aminopropyl-modified containing IL electrolyte was used with steel and lithium as electrodes.

With electrolytes containing the unmilled and ball-milled nanoparticles very similar results as for the neat IL electrolyte were obtained. Especially the electrochemical response of the electrolyte with unmilled nanoparticles was very close to the one of the neat IL electrolyte. The electrochemical response of electrolytes containing the surface-modified silica is only slightly decreased with respect to the neat IL electrolyte and shows a dependence on the silica surface, as already observed in the mechanical properties but not obvious from the conductivity results. The comparison of mechanical and electrical properties of the composite electrolytes showed that mobility of at least one ion species is enhanced. In Chapter 4.3 it was assumed that the lithium ion conductivity is increased in the composite electrolytes. The cyclic voltammetry results with LFP give a further evidence on an enhancement of the lithium ion conductivity since the electrochemical response in the half cells decreases hardly despite a severe viscosity increase and the decrease in total conductivity. The electrochemical response in the half cells with electrolytes containing mesoporous and fumed silica was considerably more decreased than in the case of the other investigated composite electrolytes, but no side reactions occurred. It seems as in these electrolytes the IL electrolyte is confined stronger avoiding side reactions with the iron phosphate. At the same time this confinement seems to restrict the ion mobility resulting in a poor electrochemical response.

The same experiments were also carried out with faster scan rates being 0.4 mV/s. The results are shown in Figure 4.24. With the faster scan rate the electrolytes containing the unmilled and ball-milled nanoparticles show improved electrochemical response in the half cells with lithium iron phosphate with respect to the neat IL electrolyte. The cells with composite electrolytes containing KIT-6 and fumed silica show slightly decreased electrochemical response compared to the neat IL electrolyte. The lowest performance was achieved in the half cells with SBA-15 containing composite electrolyte. Hence, the assumption is underlined that fumed and mesoporous silica confine the IL electrolyte stronger and damp the mobility of lithium ions. Moreover, in the composite electrolytes with mesoporous silica a plateau is established at peak maximum during charging. Peaks in cyclic voltammograms occur due to diffusion limitations as the concentration of active species in the electrolyte depletes near the electrode. A plateau at peak maximum indicates that the concentration of active species remains constant at electrode surface in this voltage range. Since the reaction occurs without depletion of active species it may be assumed that a stronger confinement of the IL electrolyte results in forming a special interface on the electrode which does not retard lithium ion mobility. The composite electrolytes with surface-modified silica show all similar electrochemical response in half cells with lithium iron phosphate as the neat IL electrolyte with only slight differences.

Thus, at higher scan rates no influence of the silica surface on the electrolyte performance is observed. Again side reactions with iron phosphate occur as already discussed for the cyclic voltammograms with a scan rate of 0.1 mV/s.

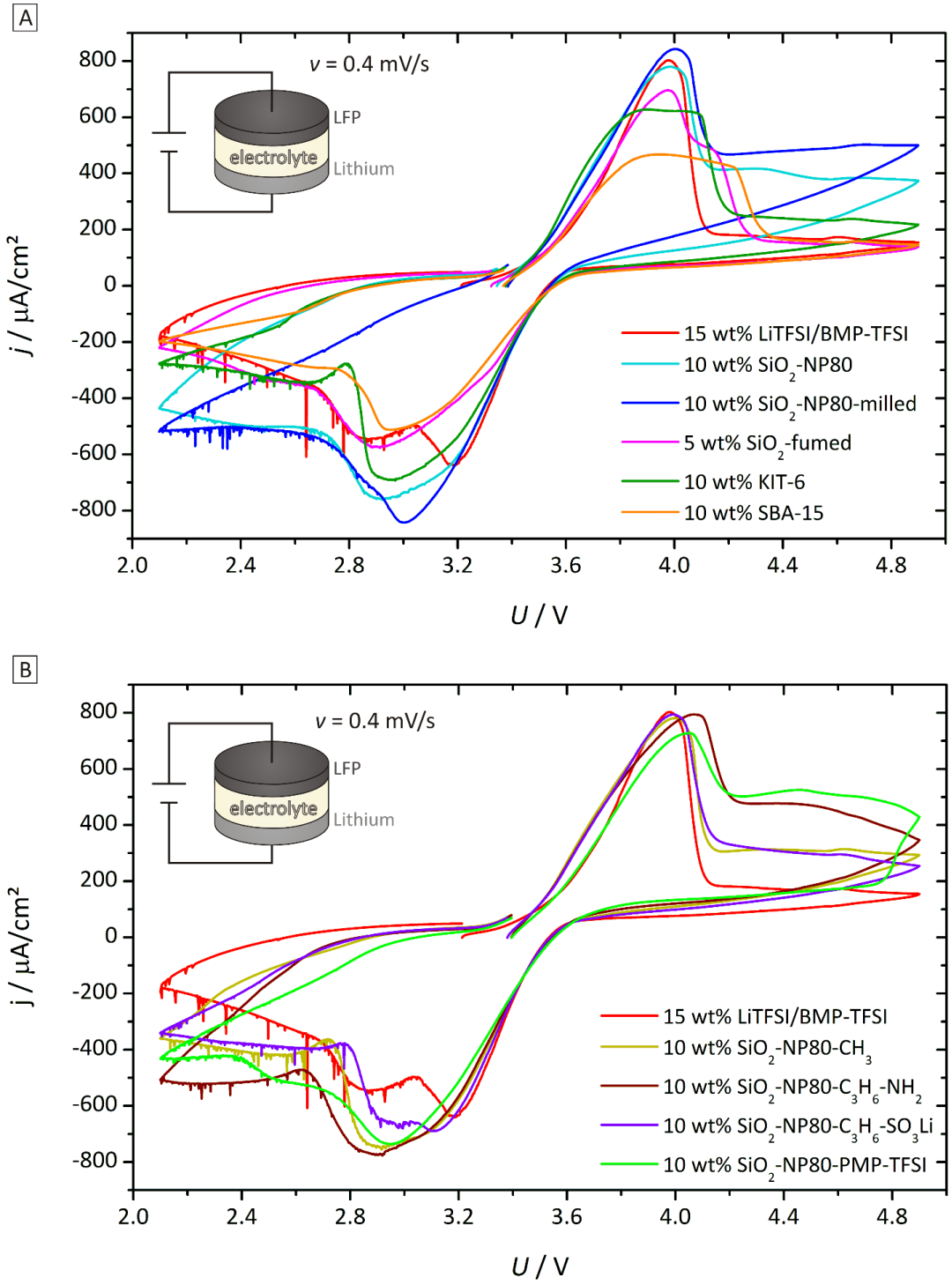

Figure 4.24: Cyclic voltammetry with a scan rate *v* of 0.4 mV/s for the composite electrolytes with lithium iron phosphate and lithium as electrodes. The current fluctuations may occur due to expansion of cathode material and due to inhomogeneities at the anode.

From the cyclic voltammetry experiments it can be summarized that the enhancement in ion mobility which was concluded from the correlation of electrical and mechanical properties concerns the lithium ion mobility. If only the IL cation or anion mobility were improved by the filler material the electrochemical response in the half cells should have been very poor since silica represents an exclusion volume and increases the viscosity of the electrolyte.

4.5 Electrochemical stability of composite electrolytes

Since IL electrolytes are discussed for lithium (ion) batteries due to their high stability it is interesting to investigate whether the filler material influences the electrochemical stability of the electrolyte. For lithium ion batteries and next generation batteries various electrode combinations are under consideration which all influence electrolyte stability in a different manner. Therefore, it is helpful to have a standard system concerning the electrode materials for determining the electrolyte stability to allow the comparison of different electrolytes. Hence, glassy carbon and platinum were chosen as working and counter electrodes, respectively, since they have defined surfaces allowing reproducible results. The neat IL electrolyte has an electrochemical window of 4.3 V with a cathodic limit at 0.8 V and anodic limit at 5.1 V versus lithium, respectively.

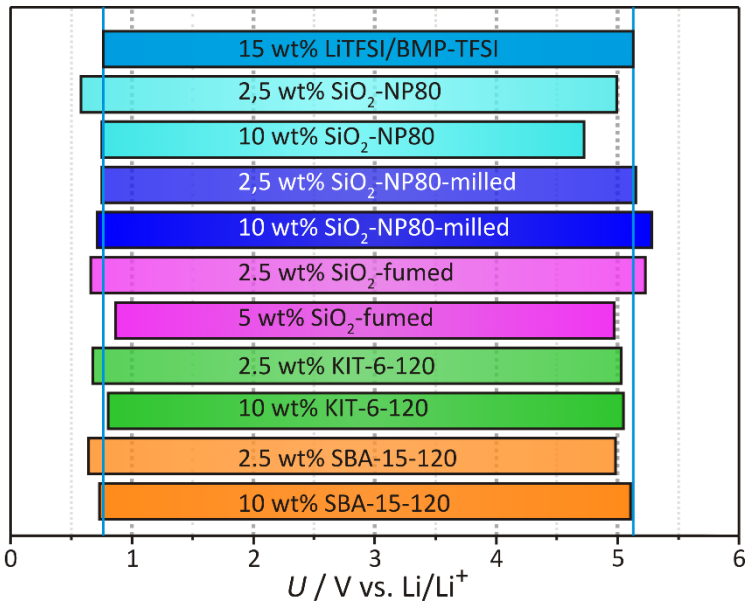

Figure 4.25: Electrochemical windows of the IL electrolytes with surface-unmodified silica. The measurements were carried out with glassy carbon and platinum as working and counter electrodes, respectively.

Addition of 2.5 wt% surface-unmodified silica enhances the cathodic stabilities of the composite IL electrolytes. The anodic limits are decreased for 2.5 wt% of surface unmodified silica in the electrolytes except the composite electrolyte with 2.5 wt% fumed silica which shows an improved stability in anodic and cathodic direction. The composite electrolyte with 2.5 wt% ball-milled silica nanoparticles shows a very similar electrochemical window as the neat electrolyte. For 10 wt% ball-milled silica nanoparticles in IL electrolytes the electrochemical windows are improved in cathodic and anodic direction. With 10 wt% unmilled silica nanoparticles the cathodic limit remains unchanged whereas the anodic limit is considerably decreased. The gel-like electrolyte with 5 wt% fumed silica shows a decreased electrochemical stability at both the cathodic and anodic limit. The same occurs for the electrolyte with 10 wt% mesoporous KIT-6 but with the decrease of the electrochemical window being less pronounced. The electrolyte containing 10 wt% mesoporous SBA-15 has a very similar cathodic and anodic stability as the neat IL electrolyte. Hence, the stronger confinement of IL electrolyte influences the electrochemical window negatively.

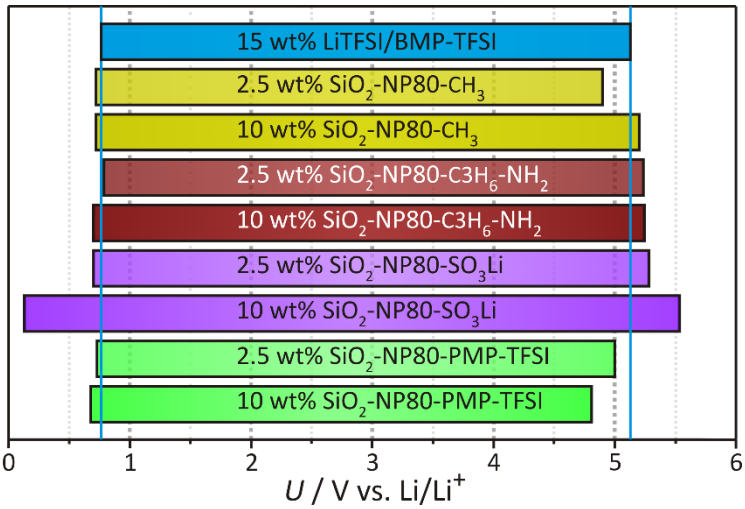

Figure 4.26: Cathodic and anodic stability limits of the IL electrolytes with surface-modified silica determined with glassy carbon and platinum as working and counter electrodes, respectively.

The composite electrolytes with surface-modified silica show all at least an enhanced cathodic limit which is notably increased for the electrolyte with 10 wt% lithiumpropylsulfonate-modified silica. The anodic limit is also increased in electrolytes with surface-modified silica except the electrolytes with pyrrolidinium-modified silica and 2.5 wt% methyl-modified silica where the potential of anodic decomposition occurs at lower potentials compared to the neat electrolyte. Since the surface-modification occurred only with the synthesized silica nanoparticles having a particle size of 80 nm a comparison should be carried out with the ball-milled silica nanoparticles containing electrolytes. It is obvious that a remarkable change in

electrochemical stability occurs for the electrolytes with pyrrolidinium-modified silica and 2.5 wt% methyl-modified silica where the anodic limit is considerably decreased and for the electrolyte with 10 wt% lithiumpropylsulfonate-functionalized silica which shows a considerably improved electrochemical window. Hence, no clear trend is obvious for the electrochemical stability of the composite electrolytes. It looks as if the nature of the network formed by the filler material directly influences the electrochemical stability of composite electrolytes. Nevertheless, even the composite electrolytes with lower electrochemical windows have a sufficient stability to be used with most electrode materials.

4.6 Cation conductivity

The combination of the electrical and mechanical properties in combination with cyclic voltammetry tests in half cells using lithium iron phosphate as cathodes allows to conclude that the lithium ion conductivity is enhanced at least in most composite electrolytes with silica as filler materials. To obtain an absolute value for the lithium ion conductivity the transference number of lithium ions has to be determined. As discussed in the second chapter the established methods for determining transference numbers in liquid electrolytes are valid for binary electrolytes or overestimate them considerably. Thus, it was tried to measure the cation conductivity directly by a four-probe measurement using an approach which is well established for solid electrolytes. The electrolyte is assembled between two reversible electrodes where the current is applied. Between the polarized electrodes two potential probes are placed within the electrolyte which measure the potential drop in the electrolyte without overvoltages. For the probes a material is used which is only conducting for the ion of interest, being lithium in this case. Thus, the probes measure the electrochemical potential drop of the cations in the electrolyte while the current is applied between the outer electrodes. The total resistance can be measured by impedance spectroscopy prior to polarization with the same set-up. If the set-up is not changed between the measurements the transference number can be determined by the directly measured values excluding the error of the cell constant.

This approach was tested with an aqueous silver nitrate solution to check whether the method works with liquid electrolytes since the transference number of silver ions in silver nitrate solution is well known from literature [190]. To minimize convection in the liquid electrolyte which would disturb the established ion gradient, a set-up was chosen which uses a very small amount of electrolyte and the cell was temperature-controlled in a water bath during the measurement. As outer electrodes silver was used

and as probes silver iodide coated silver wire. Mostly a transference number close to unity was obtained. For the used 0.01 M silver nitrate solution a transference number of 0.48 is expected. In some cases transference numbers close to 0.5 were achieved. A typical measurement is shown in Figure 4.27. Firstly, impedance measurement was carried out to obtain the total resistance of the electrolyte being 287 Ohm. Then the outer electrodes were polarized galvanostatically with a current density of 242 µA/cm². A stable potential was established being 13 mV resulting in a resistance of 433 Ohm and an overestimated transference number of 0.66 for the silver ions.

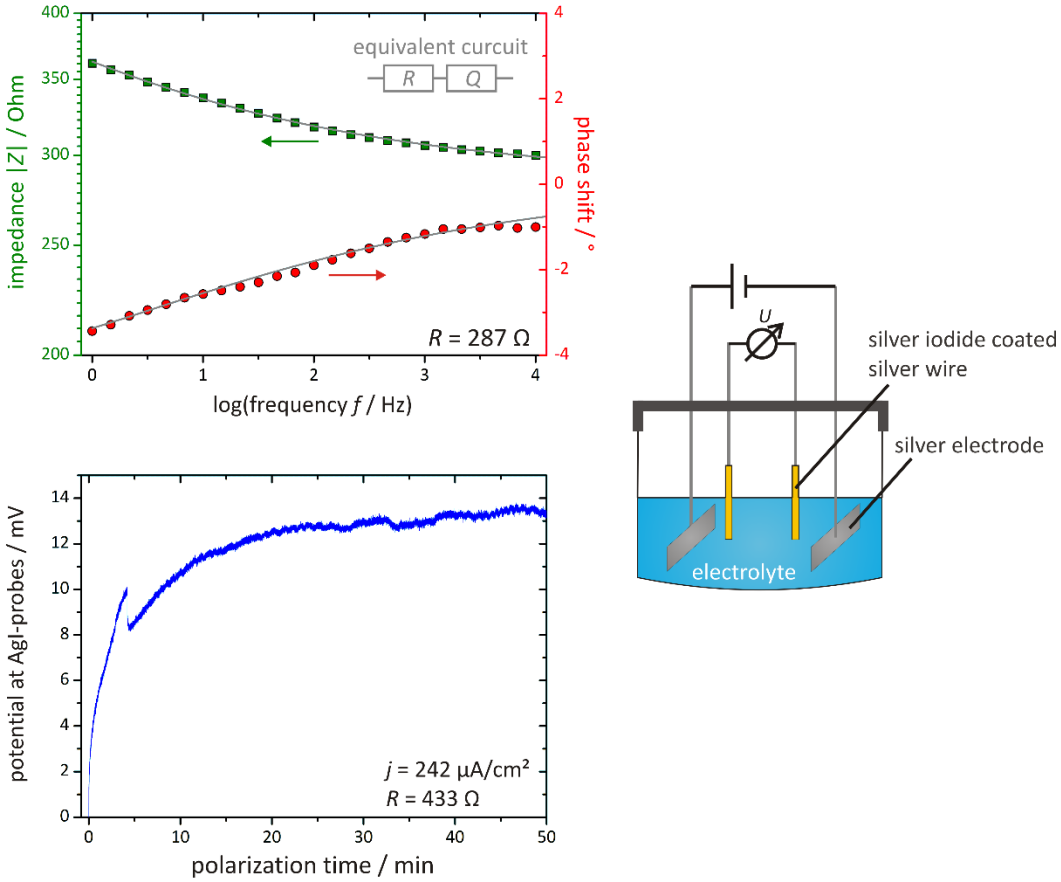

Figure 4.27: On the right side the cell set-up of the four-probe measurement with aqueous silver nitrate solution is presented. On the left side results from potentiostatic impedance spectroscopy (top left) and galvanostatic polarization with 242 µA/cm² (bottom left) are shown.

Obtaining a stable potential during galvanostatic polarization was difficult and required very small amounts of electrolyte and high temperature stability. Best results were obtained with the cell presented in the experimental section. Nevertheless the transference number was still overestimated corresponding to too low measured potential differences. Thus, the expected stationary concentration gradient could not be established during galvanostatic polarization. One possible explanation is that convection was still possible in the electrolyte. Furthermore, the silver iodide coating

may be dissolved in very small amounts in the electrolyte leading to convection due to density differences which destroy the concentration gradient established by the electric field. Although different cell set-ups were used convection could not be avoided in the cell. Thus, the transference number could not be measured reproducibly since absence of convection is an important prerequisite for a stable concentration gradient established by the electric field.

4.7 Model for ion mobility in IL electrolyte with silica

In accordance with literature the composite electrolytes showed poor performance in electrochemical/battery cells as cell tests were only possible with small current densities. So far the results on the influence of silica on lithium ion mobility are contradictory, since Saito et al. assumes an enhancement of lithium ion mobility [11, 25] and Nordström et al. believe that lithium ions are immobilized on the silica surface [26]. Saito et al. conclude from NMR results that silica induces a release of the anions from lithium complexes while Nordström et al. conclude from Raman results that lithium ions are adsorbed together with the IL ions on the silica surface. The present work shows that the electrochemical response of composite electrolytes in cyclic voltammetry with lithium iron phosphate as cathode and lithium as anode is similar to the electrochemical response of the neat IL electrolyte. Considering the strong increase in viscosity the electrochemical response should have been worse with respect to the neat IL electrolyte if the lithium ions were not influenced or were even trapped by the filler material. Thus, it is reasonable to assume that the lithium ion transference number is enhanced in the composite electrolytes in accordance with the results of Saito et al. In addition, the calculated equivalent conductivities, as determined from the Walden rule under the assumption that the ion coordination does not change in the composite electrolytes with respect to the neat IL electrolyte, were considerably smaller than the measured conductivities. Hence, the ion solvation is changed in the composite electrolytes and the mobility is improved, but a direct proof cannot be given, yet.

It is well accepted that interfaces are three dimensional in non-ideal systems [191]. If the physical properties of the interface region clearly differ from the ones of the two neighboring phases, this region should rather be understood as an interphase than an interface. It is shown in literature that ionic liquids form solid-like structures on silica surfaces which still remain good ion mobility [127] (cf. Chapter 2.2.1). Hence, the interface region has different properties than the bulk IL and may be considered as an interphase. To make sure that interphases affect bulk properties, a minimum amount of filler material is necessary for their cooperative interaction.

The solid-like structure in the interphase is formed by the IL ions, most probably. It remains unclear how the lithium ions are incorporated into the interphase. The lithium ion concentration and mobility may differ in the interphase and bulk electrolyte. Due to the small size of the lithium ions, they may have a higher mobility in the solid-like structure of the interphase. Moreover, the lithium ion concentration may be decreased in the bulk IL electrolyte resulting in higher conductivities since it is known that the conductivity of ionic liquids increases with decreasing concentration of conducting salt (cf. Figure 4.4). It is clear that the lithium ion conductivity is increased in IL composite electrolytes with silica as filler material with respect to the neat IL electrolyte, but no conclusion can be drawn whether the conductivity is enhanced in the interphase or bulk electrolyte.

Assuming that the enhanced lithium ion conductivity arises from increased lithium ion mobility in the interphase, an explanation can be given for the contradictory appearing results of Nordström et al. [26] and Saito et al. [11, 25]. Nordström et al. reported an enrichment of lithium ions at the silica surface, and Saito et al. showed that lithium ions are less coordinated in presence of silica particles. Combining their results with the observations in the present work, it may be concluded that lithium ions are present in the interphase showing a higher mobility than in the bulk electrolyte. Since the anions are incorporated into the solid-like structure of the interphase, the coordination of the lithium ions may be weaker in the interphase than in the bulk electrolyte resulting in higher mobilities. With rising temperature the order of the interphase decreases and the properties of the interface region and bulk electrolyte get closer. At higher temperatures the conductivities of composite electrolytes were stronger decreased with respect to the neat electrolyte (cf. Figure 4.7 and Figure 4.9). This can be explained by disappearance of the interphase with rising temperature. Then, the exclusion volume of the filler material becomes dominating. Hence, the improved lithium ion mobility has to arise from the interphase which has a higher lithium ion conductivity than the bulk IL electrolyte. Additionally, the lithium ion concentration of the bulk IL electrolyte may be decreased. It is known that lithium ion complexation increases with rising lithium salt concentration. Hence, if the lithium ion concentration is decreased in the bulk electrolyte, the lithium ion conductivity may be increased.

Figure 4.28 shows a proposal for the network established by the IL ions due to the solid-like ion arrangement in the interphase formed between silica and IL electrolyte which expands into the bulk electrolyte.

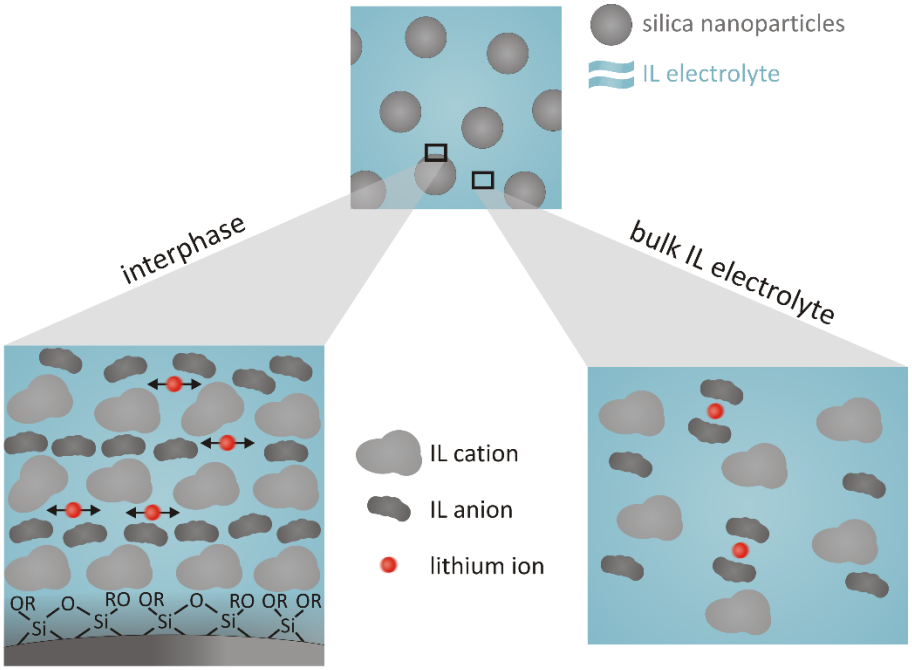

Figure 4.28: Model for the enhanced lithium ion mobility in composite electrolytes consisting of IL electrolyte and dispersed silica particles as filler materials. In comparison to the neat IL electrolyte where approximately 90 % of lithium ions are strongly coordinated by at least two anions, more free lithium ions exist in the composite electrolyte.

5 CONCLUSIONS AND OUTLOOK

In the present work the IL electrolyte 15 wt% lithium bis(trifluoromethylsulfon)imide (LiTFSI) in N-butyl-N-methylpyrrolidinium TFSI (BMP-TFSI) was investigated with different silica as filler materials. At least in theory, IL electrolytes offer advantageous properties, e.g. inherent safety due to high thermal and chemical stability. But yet they are not applied to lithium (ion) batteries since they comprise low lithium ion mobilities, resulting in slow discharge/charge kinetics during cell operation. Aim of the work was to investigate the influence of filler material with Lewis acidic surface on the electrolyte properties and to investigate whether lithium ion mobility can be enhanced by filler material. Recent literature shows inconsistent results by using different silica materials and different IL electrolytes. Hence, no unambiguous conclusions can be drawn. Even contradictory results were presented in literature (cf. Chapter 2.2.2). Thus, in the present work the filler material was varied systematically for the first time.

Surface-unmodified silica were investigated as unmilled and ball-milled materials resulting in different particle morphologies. The surfaces of the resulting nanoparticles were terminated mainly by silanol groups. Fumed silica nanoparticles were also used as their surface is mainly silanized. Since an interface effect was expected, mesoporous silica were also investigated due to their high surface areas. Moreover, the synthesized silica nanoparticles were surface-modified with methyl-, aminopropyl- and lithiumpropylsulfonate-groups. Ionic liquid modified silica, namely 1-methyl-3-propylimidazolium TFSI and N-propyl-N-methylpyrrolidinium TFSI, were also investigated as filler materials. With secondary electron microscopy it was shown that the different silica materials varied clearly in their morphologies. The neat IL electrolyte showed a total conductivity of 0.9 mS/cm which is well in line with literature data [31, 32]. By adding silica to the IL electrolyte the conductivity decreases except for the IL electrolyte with unmilled silica nanoparticles where conductivity hardly changed with varying amount of silica. Mass fractions of the filler material were varied between 2.5 wt% and 10 wt% in steps of 2.5 wt%. For the electrolyte with fumed silica a maximum silica fraction of 5 wt% was used since its gel-like consistency did not allow proper handling of the electrolyte with higher mass fractions

of silica. The conductivities were always between 0.5 mS/cm and 0.8 mS/cm except for the IL electrolytes containing the unmilled silica nanoparticles and 2.5 wt% imidazolium-functionalized silica nanoparticles, which showed conductivity values similar to the neat IL electrolyte. The conductivity decay was less pronounced for the surface-modified silica than for the unmodified silica. The former showed similar conductivity behaviors in the electrolyte as the IL electrolytes with ball-milled silica nanoparticles. The surface-modified and ball-milled silica have similar morphologies since surface-modification was carried out using the synthesized silica nanoparticles (cf. Chapter 3.1). Thus, it is assumed that the conductivity is mainly influenced by the morphologies of filler materials than by the chemical composition of filler surfaces since no obvious trend was observed for filler materials having similar morphologies with different surface modifications.

The viscosity of the neat IL electrolyte was determined as 0.3 Pa·s. Viscosities increased for all composite electrolytes but did not show any trend with morphologies or surfaces of filler materials. The IL electrolytes with 5 wt% fumed silica and 10 wt% mesoporous SBA-15 showed gel- and paste-like consistency with viscosity values of 20 kPa·s and 8 kPa·s, respectively. The composite electrolyte with 10 wt% imidazolium-functionalized silica nanoparticles had a viscosity of 10 kPa·s but appeared as liquid dispersion. Notably high viscosities in the range of kPa·s were achieved with fumed silica, unmilled silica nanoparticles, mesoporous SBA-15 as well as with silica nanoparticles containing positively polarized surfaces (aminopropyl-, imidazolium- and pyrrolidinium-functionalized silica nanoparticles). Viscosities of the other composite electrolytes were below 200 Pa·s. This trend is not reflected in the conductivity measurements since all conductivities were in the same range. Expected equivalent conductivities were derived from Walden's rule upon the assumption that ion solvation shells do not change in the composite electrolytes with respect to the neat IL electrolyte. The calculated values were compared with measured equivalent conductivities, with the latter being approximately two orders of magnitude higher. For composite electrolytes with 5 wt% ball-milled silica nanoparticles and with 5 wt% aminopropyl-, lithiumpropylsulfonate- and imidazolium-functionalized silica the difference of calculated and measured equivalent conductivities was less pronounced.

From the combination of mechanical and electrical properties, it is obvious that mobility of at least one ion species is increased since a surprisingly small conductivity decay is observed together with highly increased viscosities. As the chemical composition of the filler material surfaces did not influence electrolyte properties directly, it is concluded that varying silica morphologies form different networks in the IL electrolyte which have varying mobility mechanisms for at least one ion species.

The network was characterized by rheological oscillation experiments and showed a more rigid network with 10 wt% filler material than with 2.5 wt% filler material.

Very different shear moduli were achieved for the composite electrolytes. The neat IL electrolyte showed a shear modulus of 0.3 Pa. Electrolytes with 2.5 wt% silica showed shear moduli in the same range except the electrolytes with unmilled nanoparticles and fumed silica which reached shear moduli of 4 kPa and 10 kPa, respectively. The electrolytes with 10 wt% silica and 5 wt% fumed silica varied strongly in their shear moduli. The highest values were achieved by the electrolytes containing 10 wt% unmilled silica nanoparticles, fumed silica and mesoporous SBA-15 being 20 kPa, 22 kPa and 92 kPa, respectively. Exceptional behavior was shown by the IL electrolyte with 10 wt% lithiumpropylsulfonate-modified silica which had a shear modulus of 1 Pa. In summary, all composite electrolytes with 10 wt% silica except the nanoparticles with lithiumpropylsulfonate-modification were viscoelastic solids with stable networks. The mechanical properties were neither directly correlated to the morphology of the silica nor to the chemical composition of their surface.

Overall, the effect of filler material was most pronounced for electrolytes containing 10 wt% filler material. These composite electrolytes were also investigated by cyclic voltammetry in half cells with lithium iron phosphate as cathode material and lithium metal as anode. For the electrolyte containing fumed silica 5 wt% filler material was used due to its gel-like consistency which did not allow to disperse a higher mass fraction of silica. The measured voltammograms were compared with the voltammogram of the half cell with neat IL electrolyte. For the composite electrolytes with surface-unmodified unmilled and ball-milled silica nanoparticles a similar electrochemical response was achieved as for the neat IL electrolyte. The IL electrolytes with mesoporous KIT-6 and fumed silica showed also very similar results but with a poorer electrochemical response than the neat IL electrolyte since lower current densities were achieved. Lowest current densities resulted with the composite electrolyte containing mesoporous SBA-15. The experiments with IL electrolytes containing 10 wt% surface-modified silica nanoparticles showed similar results as the neat IL electrolyte. At very slow scan rate of 0.1 mV/s the electrolyte with lithiumpropylsulfonate-modified silica showed the worst electrochemical response being slightly decreased with respect to the neat IL electrolyte. The electrolytes with silica containing positively polarized surfaces (aminopropyl- and pyrrolidinium-modified silica nanoparticles) showed parasitic side reactions which occurred reversibly most likely with the iron phosphate of LFP since this reaction was also observed in cyclic voltammetry with steel and lithium as working and counter electrodes, respectively. Correlation of mechanical and electrical properties led to the conclusion that the mobility of at least one ion species is increased. Since the

electrochemical response in cyclic voltammetry experiments of the composite electrolytes did not decline considerably with respect to the neat IL electrolyte although viscosities of the electrolytes increased significantly, it is indirectly concluded that it is the lithium ion mobility which is increased.

As IL electrolytes are discussed for lithium (ion) batteries due to their inherent safety it was interesting how the silica influences the electrochemical stability. The neat IL electrolyte shows an electrochemical window of 4.3 V with the cathodic limit at 0.8 V and anodic limit at 5.1 V versus lithium with glassy carbon and platinum as working and counter electrodes, respectively. No clear trend could be identified for the influence of silica on the electrochemical stability. The cathodic limit was hardly influenced by the filler material and downgraded only for the electrolytes with 10 wt% mesoporous KIT-6 and 5 wt% fumed silica. A conspicuous improvement of cathodic stability was achieved with the electrolytes containing 2.5 wt% unmilled silica nanoparticles and 10 wt% lithiumpropylsulfonate-modified silica. The anodic limit was more influenced by the filler materials, mostly in the negative direction. The widest electrochemical window was attained for 10 wt% lithiumpropylsulfonate-modified silica containing IL electrolyte with an electrochemical window of 5.4 V. The narrowest electrochemical window was achieved with the electrolyte containing 5 wt% fumed silica being 4.1 V.

Overall, the best electrolyte properties were achieved with the composite electrolytes containing the unmilled silica nanoparticles since their conductivities did hardly change with respect to the neat IL electrolyte and the electrochemical response in the half cell with LFP was very similar to the one of the neat IL electrolyte, although they showed mainly viscoelastic properties with highly increased viscosities. The obtained results achieved in the present work are summarized in Figure 4.28. Although the results give indirect evidence on enhanced lithium ion mobility no direct prove can be yet presented. Thus, it is interesting to investigate the ion coordination in ionic liquid-based composite electrolytes microscopically to show directly how the lithium ion mobility is influenced.

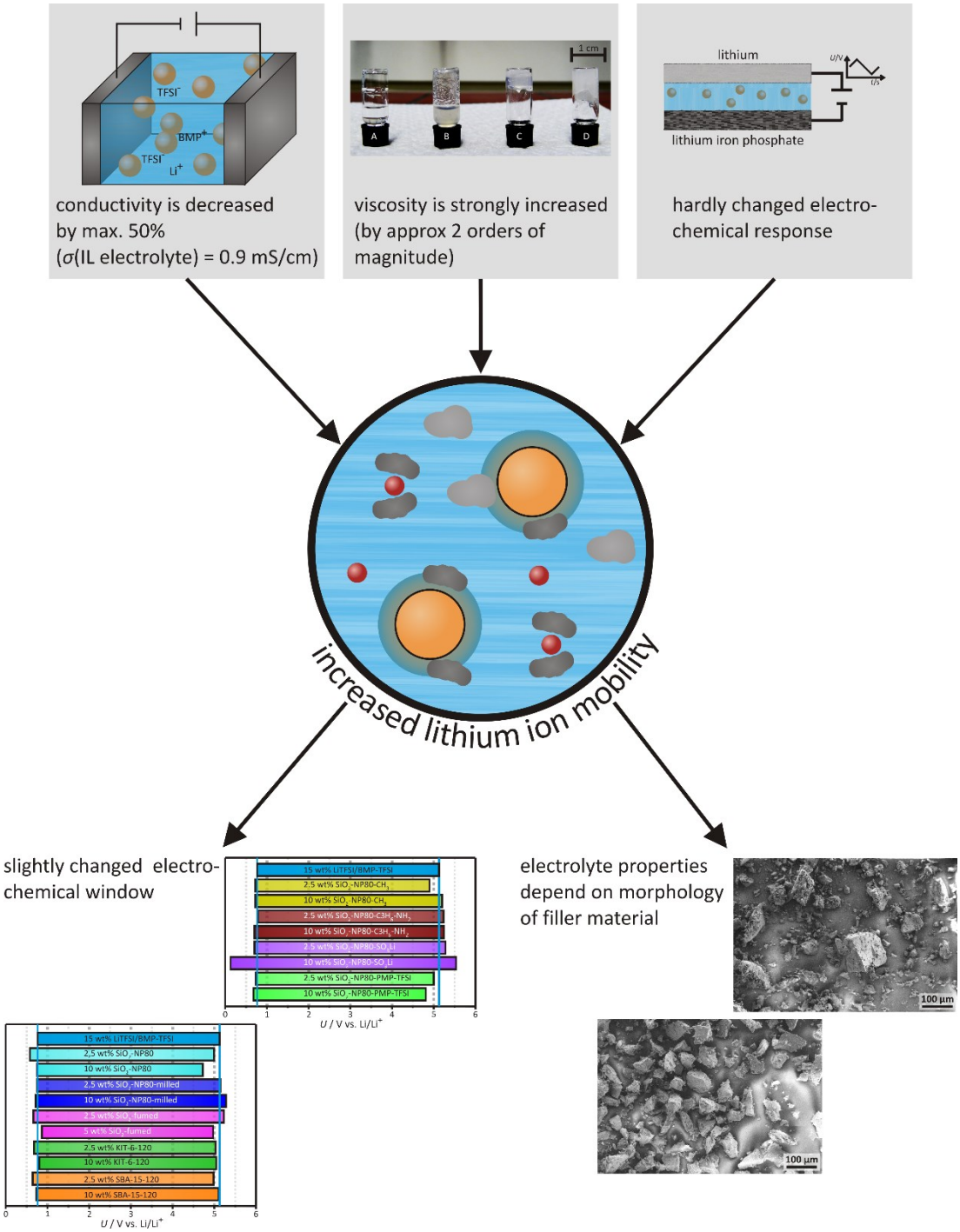

Figure 5.1: Summary of the results shown in the present work. Correlation of electrical and mechanical properties combined with comparison of cyclic voltammetry results showed enhanced lithium ion conductivity in ionic liquid-based composite electrolytes with silica as filler materials. No clear trend in the influence of filler material on electrochemical stability of electrolytes is found. Since the chemical composition of silica surface did not influence the electrolyte properties systematically, it is concluded that morphology of filler material is crucial for forming different networks which influence directly electrolyte properties.

For the investigation of the effect of filler materials on IL electrolytes from the microscopic point of view, one step back should be done and a simple model system should be developed. A smooth two-dimensional silica surface with a thin electrolyte

film may act as such a model system. Since the interphase may be small it is crucial to apply a planar silica surface. Then the interphase of the silica and IL electrolyte film might be investigated by angle resolved X-ray photoelectron spectroscopy [192, 193] or by small-angle neutron scattering [194, 195], for example. With surface-specific techniques it might be investigated which ions are involved in which manner in the solid-like structure. Then the IL electrolyte film thickness can be increased stepwise to study how the interphase evolves into the bulk electrolyte. Moreover, FT-IR and Raman spectroscopy can be carried out with this model system to investigate the ion coordination of lithium ions as a function of distance from the silica surface since the literature-known ion solvation of lithium ions in IL electrolytes were also derived from spectroscopic measurements [10–13, 43]. Nevertheless, the measurement of the lithium ion conductivity is crucial for a direct evidence on increased lithium ion mobility in ionic liquid-based composite electrolytes. Therefore, a stationary lithium ion concentration gradient during cell polarization has to be established. This is only possible if convection of the electrolyte can be avoided completely. Thus, a micro cell set-up is required with a very small electrolyte amount and very stable temperature control. Then, the four-probe measurement shown in the present work may be performed successfully. Moreover, it is interesting how the lithium ion mobility in the interphase looks like. For this purpose, an experiment measuring the lithium ion conductivity in a porous silica monolith is desirable.

A systematic investigation of different silica as filler materials in IL electrolyte is presented for the first time and their mechanical and electrical properties are correlated. In accordance to the work of Saito et al. [11, 25] it is shown that the lithium ion mobility is enhanced by adding filler material to the IL electrolyte. However, the resulting composite electrolytes still show poor electrochemical properties, especially a low lithium ion conductivity regarding the absolute value. Thus, the presented electrolytes are not applicable in lithium (ion) batteries due to their comparably slow kinetics. Nevertheless, it could be shown that the approach of heterogeneous doping which was shown in literature to improve the transport properties of solid, liquid and polymer electrolytes with different mechanisms [14–18, 58–78, 81, 83, 85, 86, 95–102] is also applicable to IL electrolytes. The effect of a second phase is clearly different from the ones reported so far for solid, liquid and polymer electrolytes. Although it remains unclear in which manner the mobilities are influenced microscopically by the filler material, it is proposed in the present work that interphases are formed on the particle surfaces with ordered arrangement of IL ions. Moreover, these interphases induce an order of ions reaching into the bulk electrolyte. Since it is known from literature that ionic liquids form solid-like structures on silica [117, 122–137], this explanation is the most evident. Furthermore, it is assumed that

the IL ions are mostly involved into the cross-linking of ions in the interphase. Therefore, the small lithium ions may have an improved mobility in the interphase. This would also explain the results of Nordström et al. [26] as they reported an adsorption of lithium ions on the silica surface. This adsorption might be the enrichment of lithium ions in the interphase. Moreover, lithium ion concentration may be different in the interphase and bulk electrolyte. A decreased concentration of lithium ions in the bulk electrolyte would explain improved lithium ion mobility since it is known that lithium complexation in ILs is weaker for small concentrations of conducting salt.

6 APPENDIX

For the sake of clarity, the results obtained with IL composite electrolytes using different mesoporous silica varying in pore size and surface composition are not presented in the main text but are shown in the appendix.

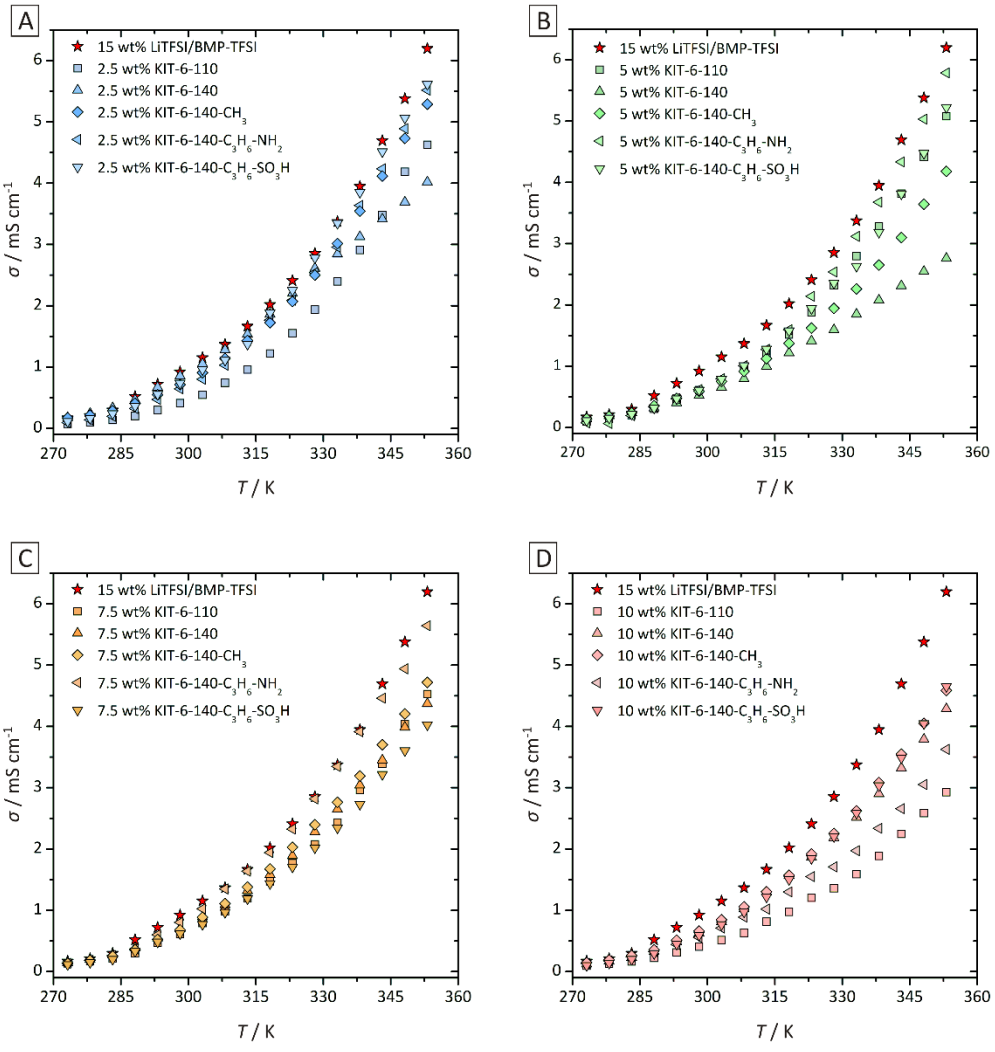

Figure 6.1: Temperature dependent conductivities σ of IL electrolytes containing mesoporous KIT-6 with two different pore sizes being 8 nm and 11 nm (KIT-6-110 and KIT-6-140, respectively) and of KIT-6 with different surface modifications, being methyl-, aminopropyl- and sulfonpropyl-groups. IL electrolytes with 2.5 wt%, 5 wt%, 7.5 wt% and 10 wt% filler material are shown in part A, B, C and D, respectively. For graphical reasons error bars are not shown but are depicted in Figure 6.2

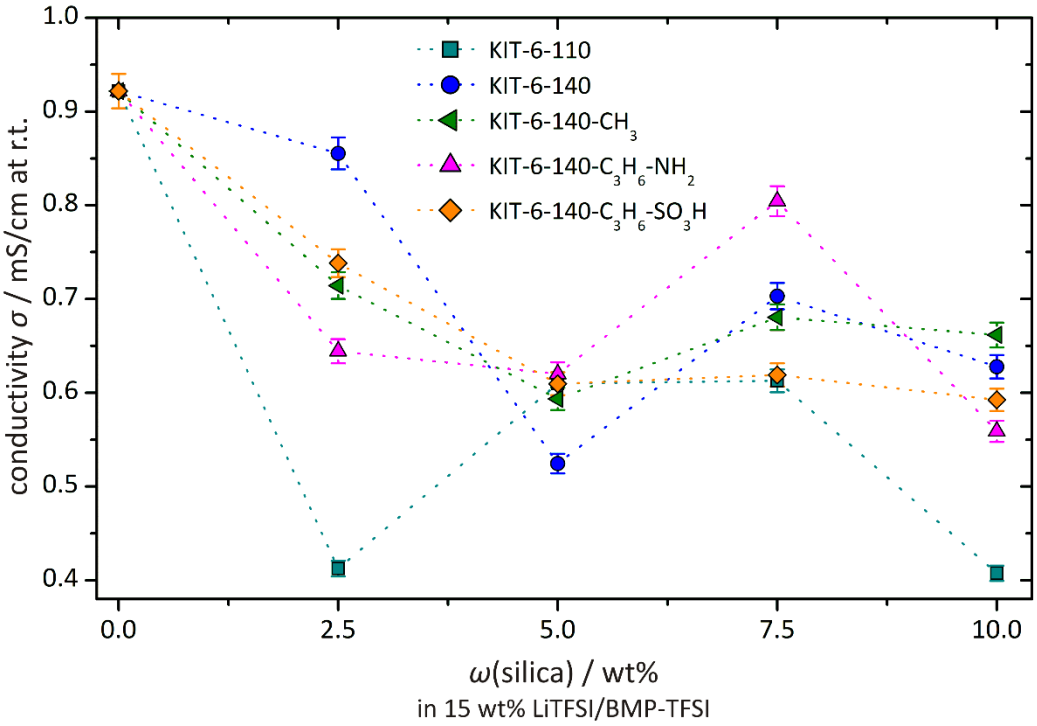

Figure 6.2: Room temperature conductivities σ of IL electrolytes containing mesoporous KIT-6 in dependence of the mass fraction of the silica. KIT-6 with different pore sizes being 8 nm and 11 nm for KIT-6-110 and KIT-6-140, respectively, were used and KIT-6 containing different surface modifications (methyl-, aminopropyl- and sulfonpropyl-groups).

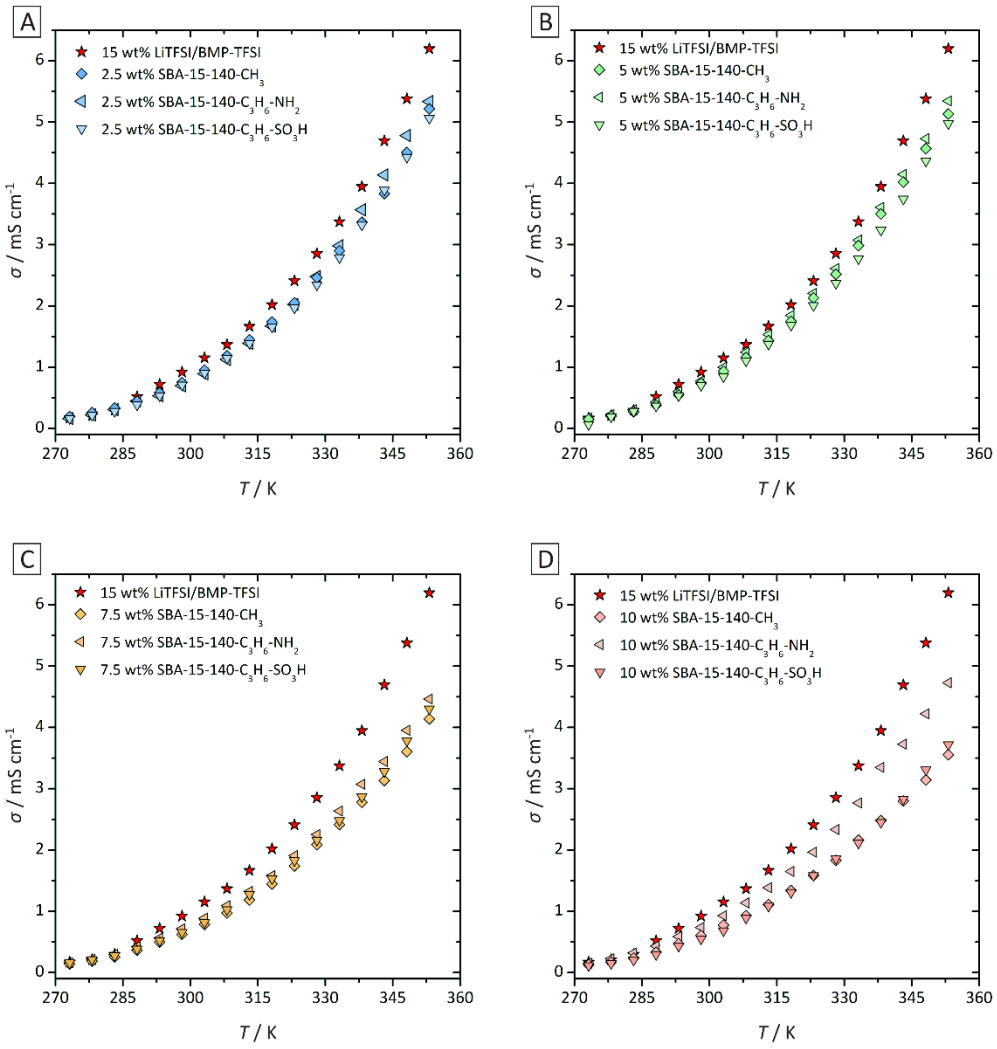

Figure 6.3: Temperature dependent conductivities σ of IL electrolytes containing mesoporous SBA-15 with different surface modification being methyl-, aminopropyl- and sulfonpropyl-groups. IL electrolytes with 2.5 wt%, 5 wt%, 7.5 wt% and 10 wt% SBA-15 are shown in part A, B, C and D, respectively. Error bars are not shown for graphical reasons but are presented in Figure 6.4.

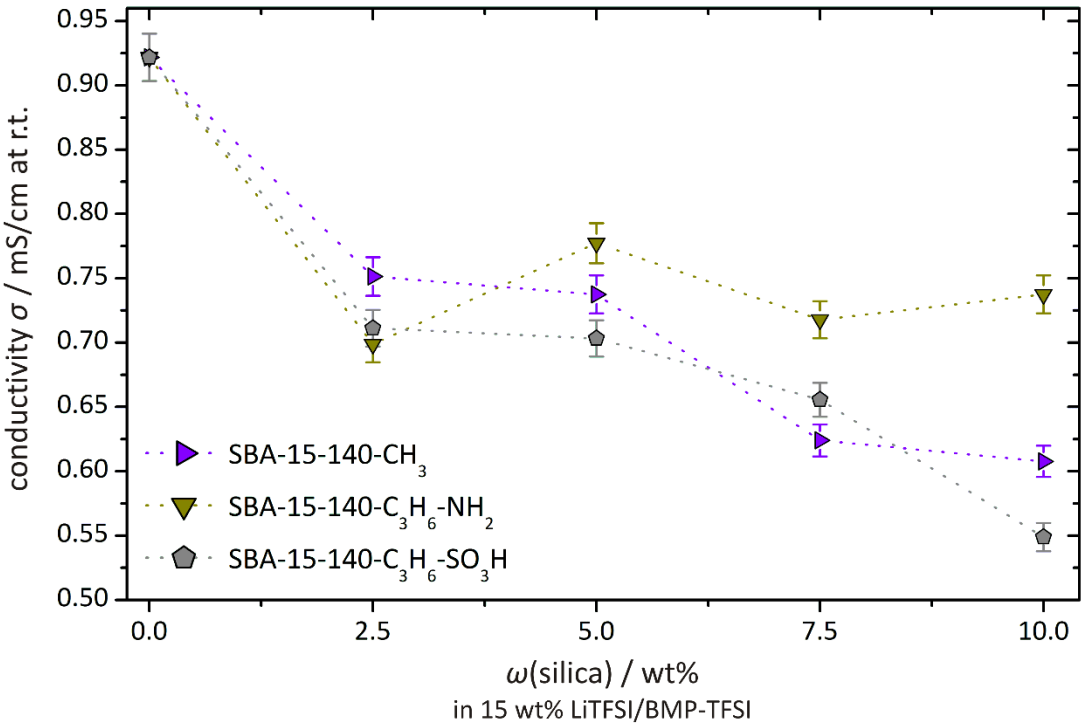

Figure 6.4: Room temperature conductivities σ of IL electrolytes containing SBA-15 with varying surface modifications being methyl-, aminopropyl- and sulfonpropyl-functionalizations.

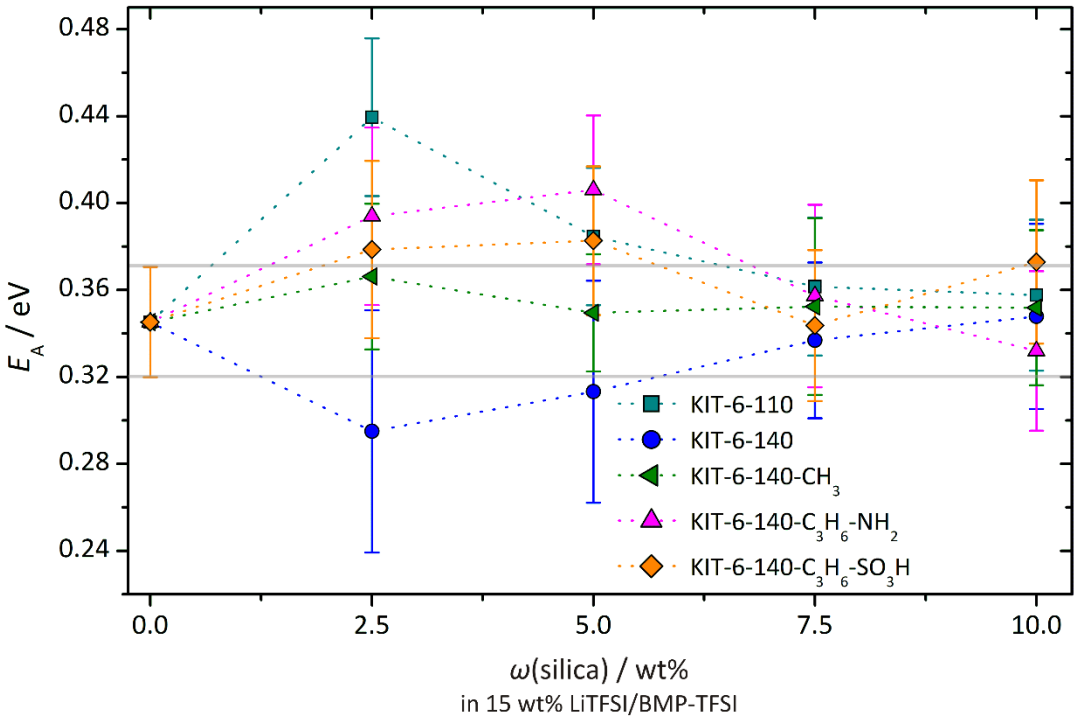

Figure 6.5: Activation energies E_A of IL electrolytes with different mesoporous KIT-6 silica. As silica KIT-6-110 and KIT-6-140 with varying pore sizes of 8 nm and 11 nm, respectively, were used and KIT-6 with different surface modifications being methyl-, aminopropyl- and sulfonpropyl-groups. Activation energies were determined by the Arrhenius equation (cf. equation (4.2)) for conductivities above 293 K.

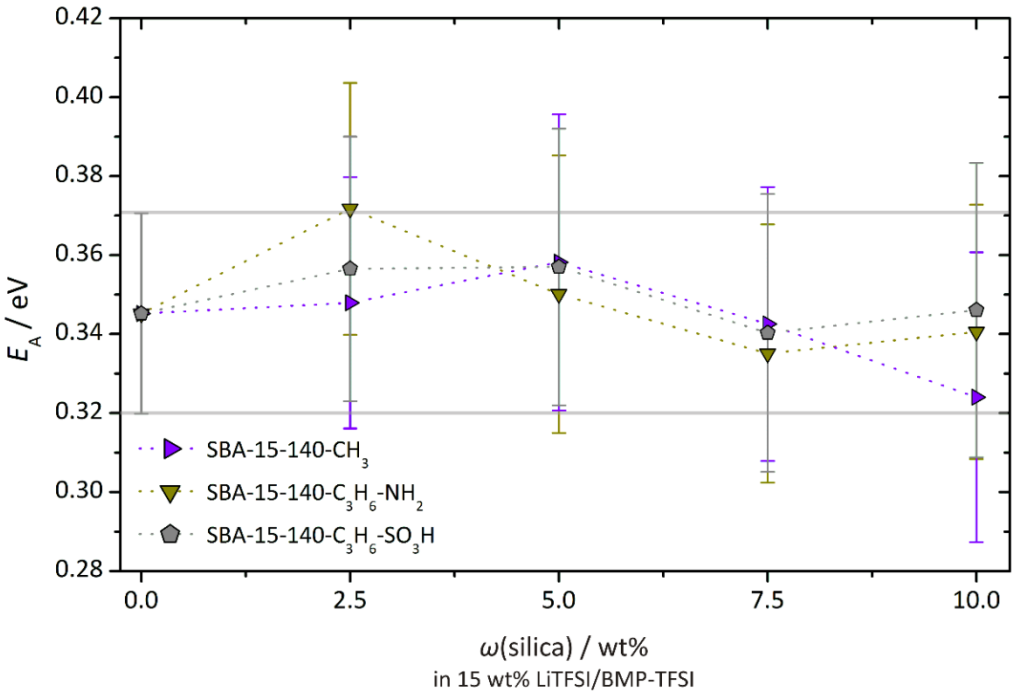

Figure 6.6: Activation energies of IL electrolytes with different mesoporous SBA-15 varying in the surface functionalization (methyl-, aminopropyl- and sulfonpropyl-groups). Activation energies were determined for conductivities above 293 K by Arrhenius equation (cf. equation (4.2)).

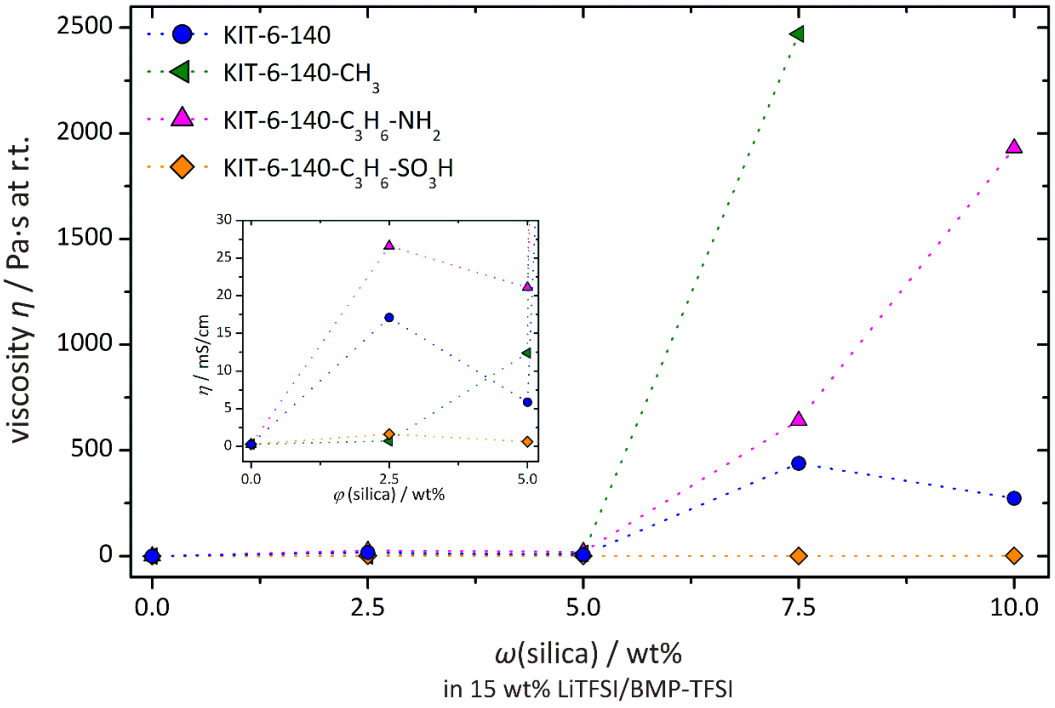

Figure 6.7: Room temperature viscosities η of IL electrolytes with mesoporous KIT-6 silica where the pore sizes were varied, being 8 nm and 11 nm for KIT-6-110 and KIT-6-140, respectively, and where surface functionalization was changed (methyl-, aminopropyl- and sulfonpropyl-groups). Since the error from the sample history is considerably higher than from the measurement and cannot be well estimated, error bars are not presented.

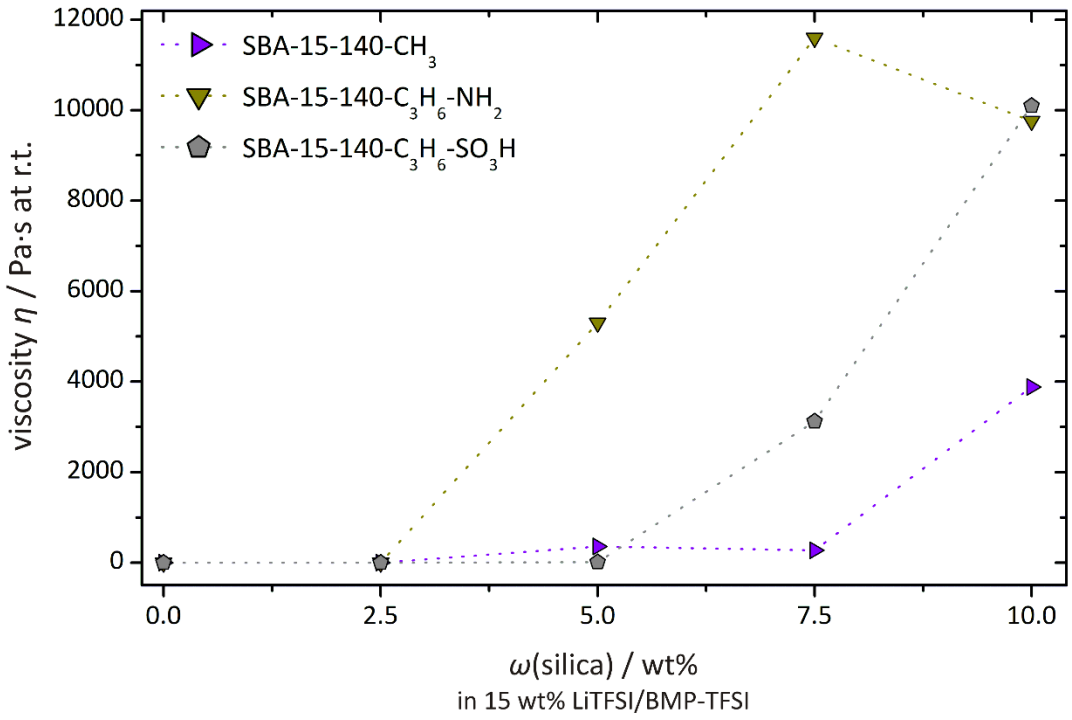

Figure 6.8: Room temperature viscosities η of IL electrolytes containing mesoporous SBA-15 varying in surface functionalization being methyl-, aminopropyl- and sulfonpropyl-groups. Error bars are not shown since the sample history causes a considerably higher error than the error resulting from the measurement.

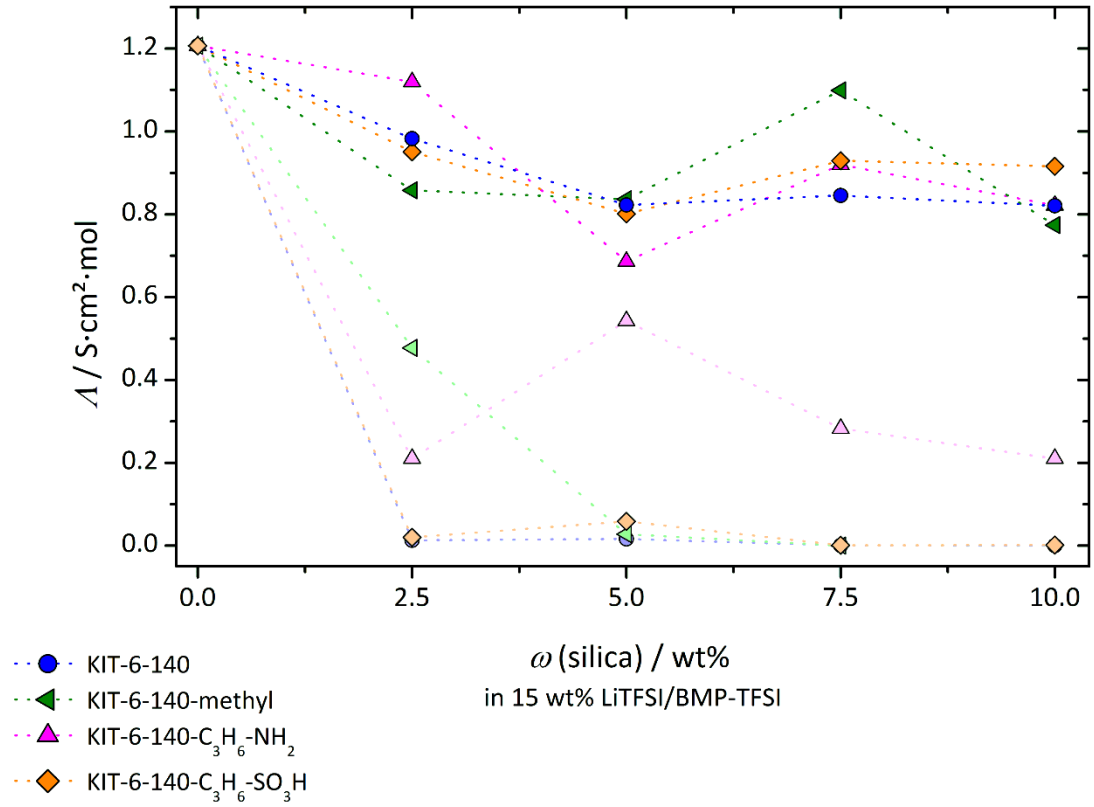

Figure 6.9: Equivalent conductivities Λ normalized to the concentration of LiTFSI in IL electrolytes containing different mesoporous KIT-6 silica. KIT-6-110 and KIT-6-140 with different pore sizes of 8 nm and 11 nm, respectively, were used and KIT-6 with varying surface modifications being methyl-, aminopropyl- and sulfonpropyl-groups. For determination of the conducting salt concentration a density of 2.2 g/mL was assumed for the silica, and the density of the IL electrolyte was determined with a pycnometer being 1.46 g/mL. In light colors the calculated equivalent conductivities are shown derived from the Walden rule with the assumption that the ion coordination properties of the IL in composite electrolytes did not change with respect to the neat IL electrolyte.

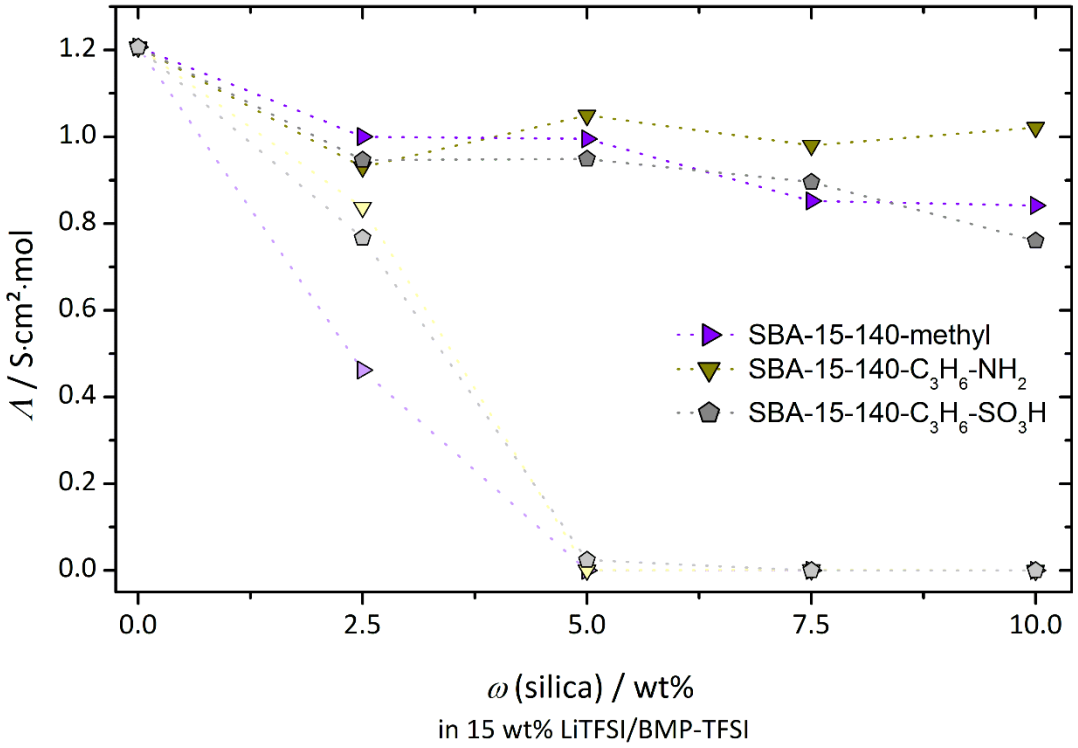

Figure 6.10: Equivalent conductivities Λ of IL electrolytes with different mesoporous SBA-15 varying in surface modification (methyl-, aminopropyl- and sulfonpropyl-groups). The equivalent conductivities were normalized to concetration of the conducting salt LiTFSI which was obtained assuming the silica density to be 2.2 g/mL. Electrolyte density was determined with a pycnometer. The calculated equivalent conductivities (light colors) were derived from the Walden rule assuming the ion coordination properties of the IL in composite electrolytes to be unchanged in comparison to the neat IL electrolyte.

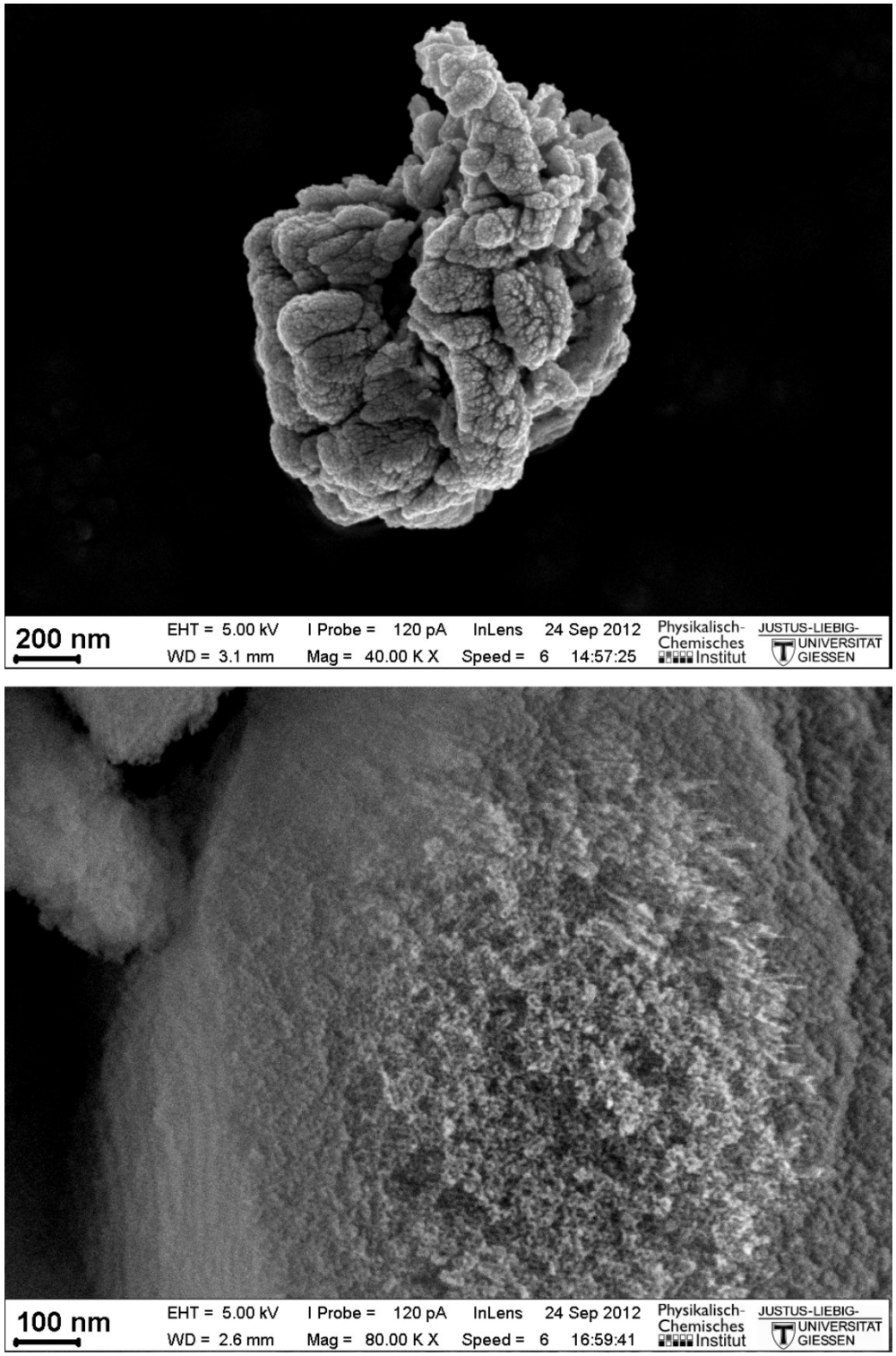

Figure 6.11: Secondary electron microscopy (SEM) images of KIT-6-110 (top) and KIT-6-140-$C_3H_6SO_3H$ (bottom). Due to their isolating properties the silica were sputtered with platinum prior to investigation by electron microscope.

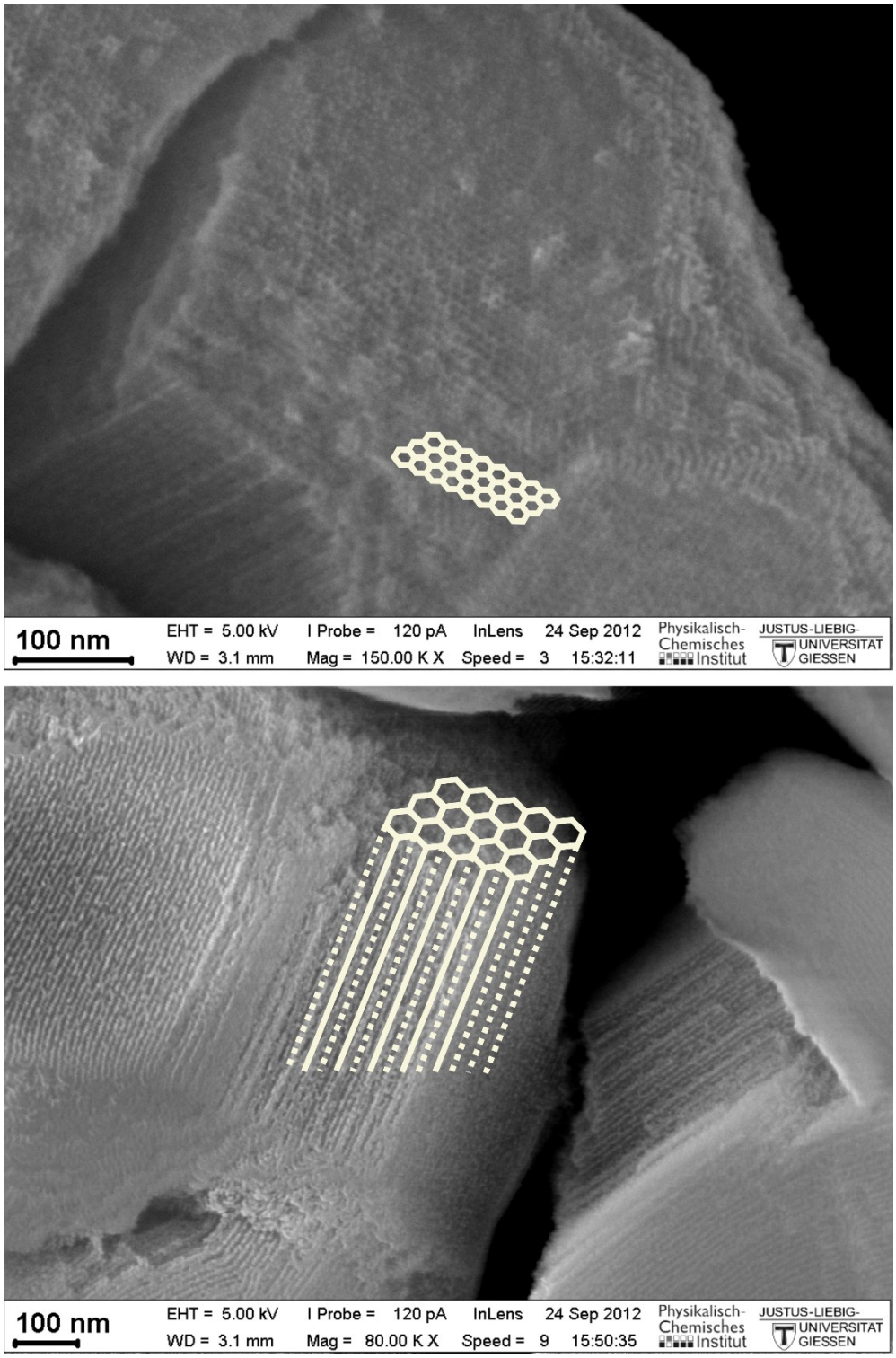

Figure 6.12: SEM images of SBA-15-120 after sputtering the silica with platinum.

Cyclic voltammetry with different composite electrolytes in half cells with lithium iron phosphate as cathode material was carried out with different scan rates. The results with scan rates of 0.1 mV/s and 0.4 mV/s are shown in Chapter 4.4. The results with other scan rates are presented here.

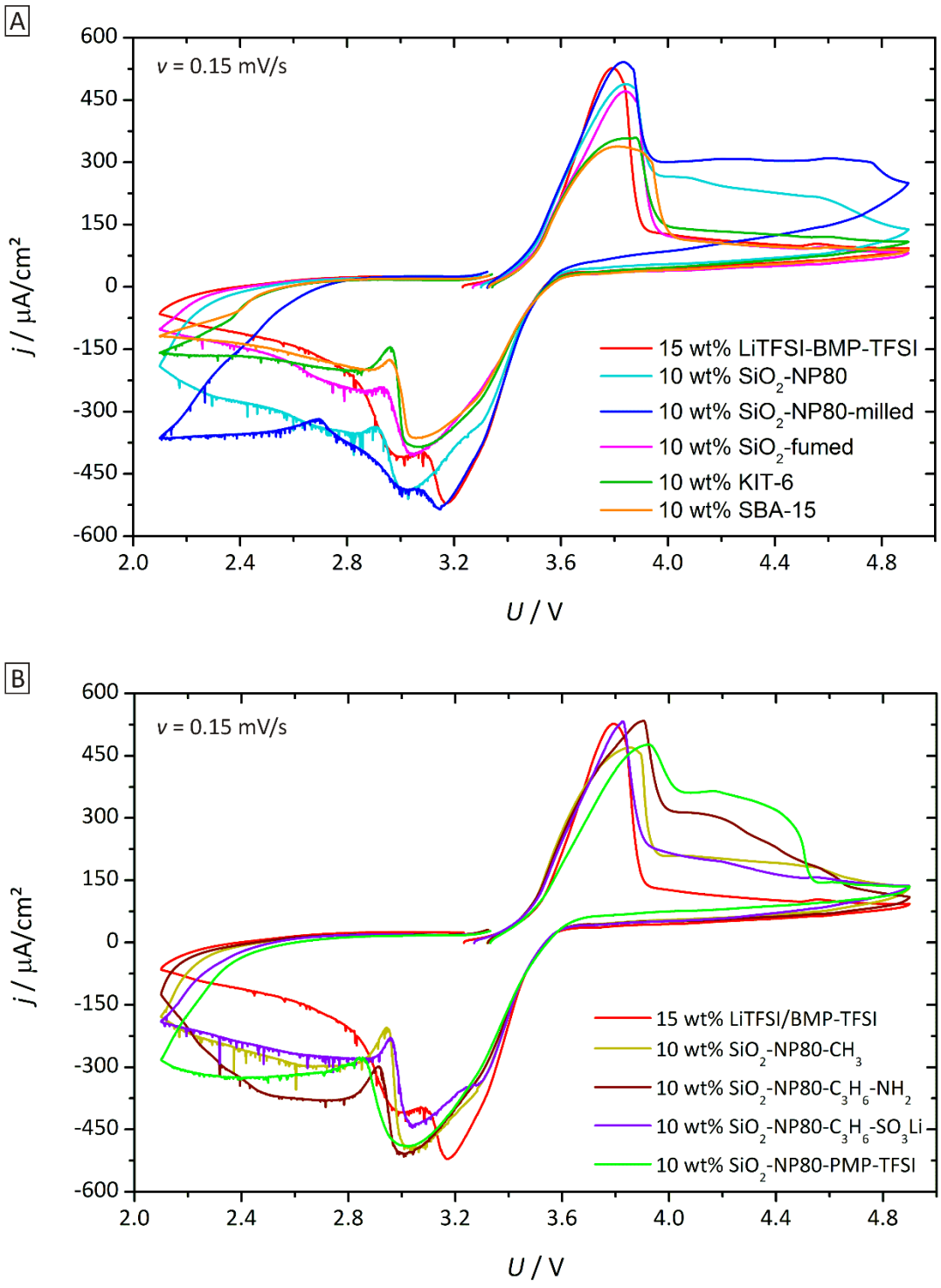

Figure 6.13: Cyclic voltammetry results obtained with a scan rate *v* of 0.15 mV/s for different ionic liquid-based composite electrolytes with lithium iron phosphate and lithium as electrode materials. In graph A results of IL electrolytes with different silica nanoparticles and the mesoporous silica KIT-6 and SBA-15 are presented. Graph B shows the results obtained with IL electrolytes containing silica nanoparticles with different surface modifications.

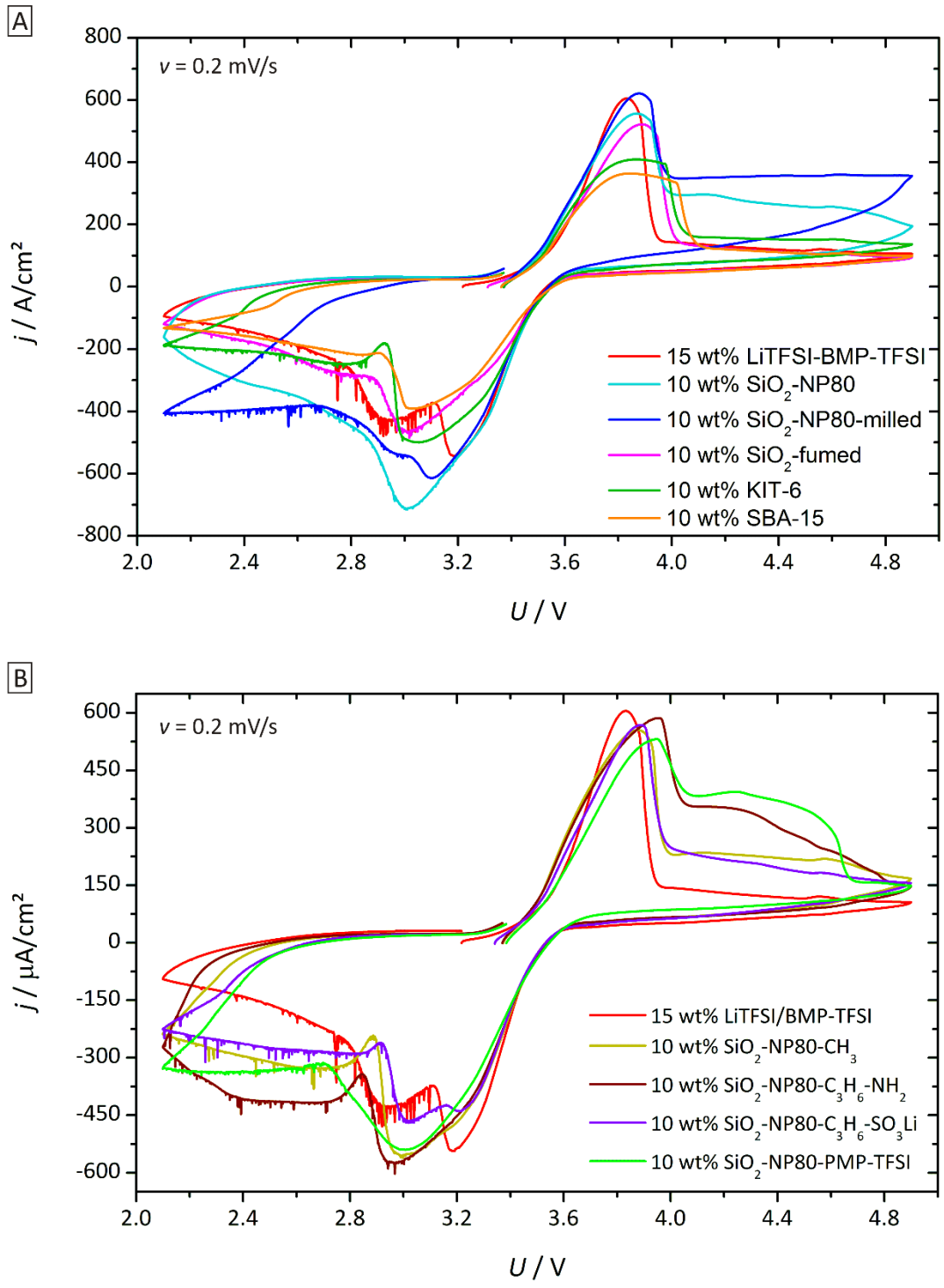

Figure 6.14: Cyclic voltammograms of different composite electrolytes obtained with lithium iron phosphate and lithium as electrodes. Scan rate *v* was 0.2 mV/s. Graph A shows results of IL electrolytes containing surface-unmodified silica nanoparticles as well as mesoporous silica, being KIT-6 and SBA-15. In Graph B results of IL electrolytes with silica nanoparticles varying in surface functionalization are presented.

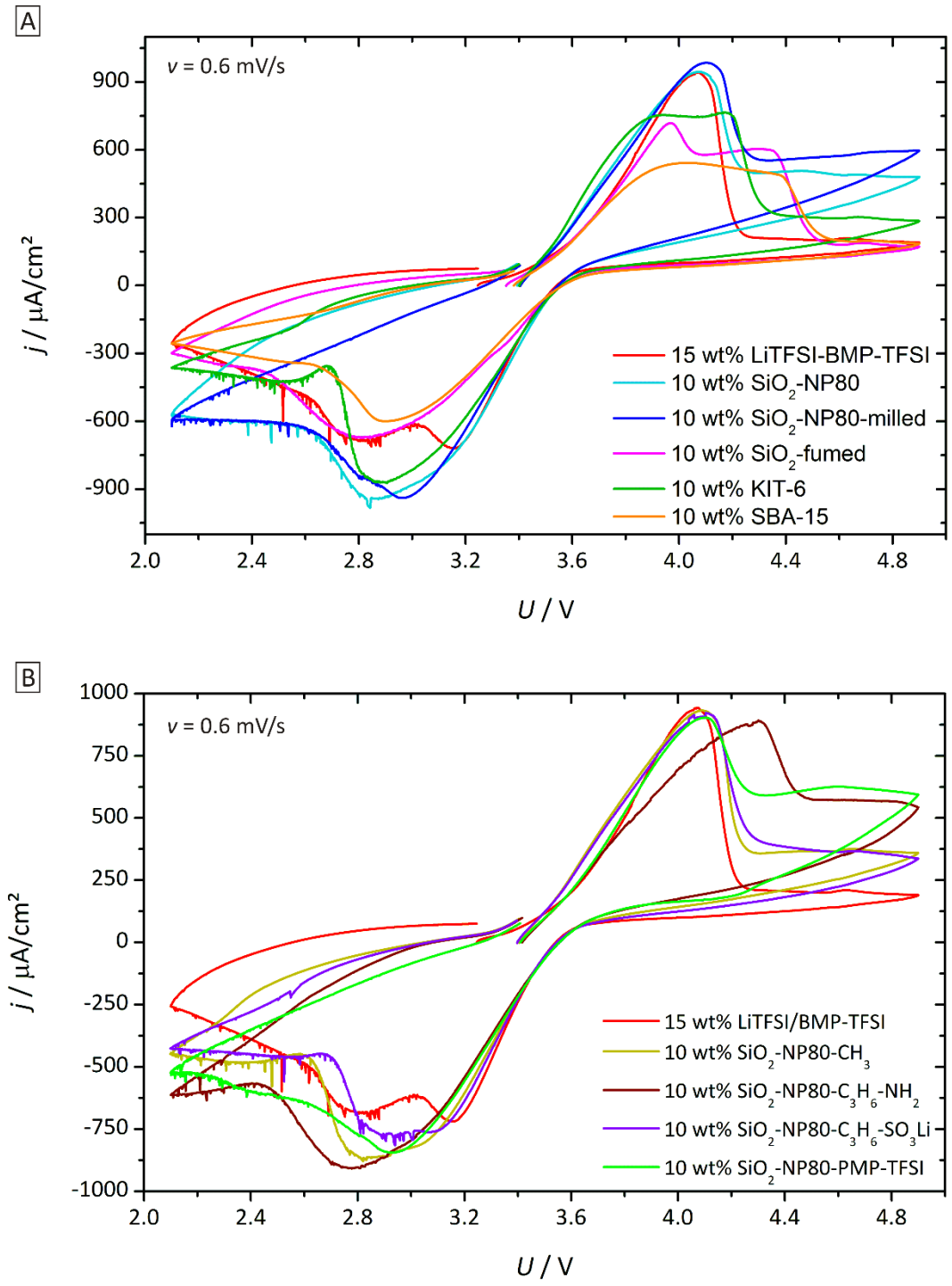

Figure 6.15: Results of cyclic voltammetry obtained with different IL-based composite electrolytes at a scan rate *v* of 0.6 mV/s. As electrodes lithium iron phosphate and lithium were used. In graph A results with IL electrolytes containing different silica nanoparticles and mesoporous KIT-6 and SBA-15 are shown. Graph B presents voltammograms of IL electrolytes with silica nanoparticles varying in surface modification.

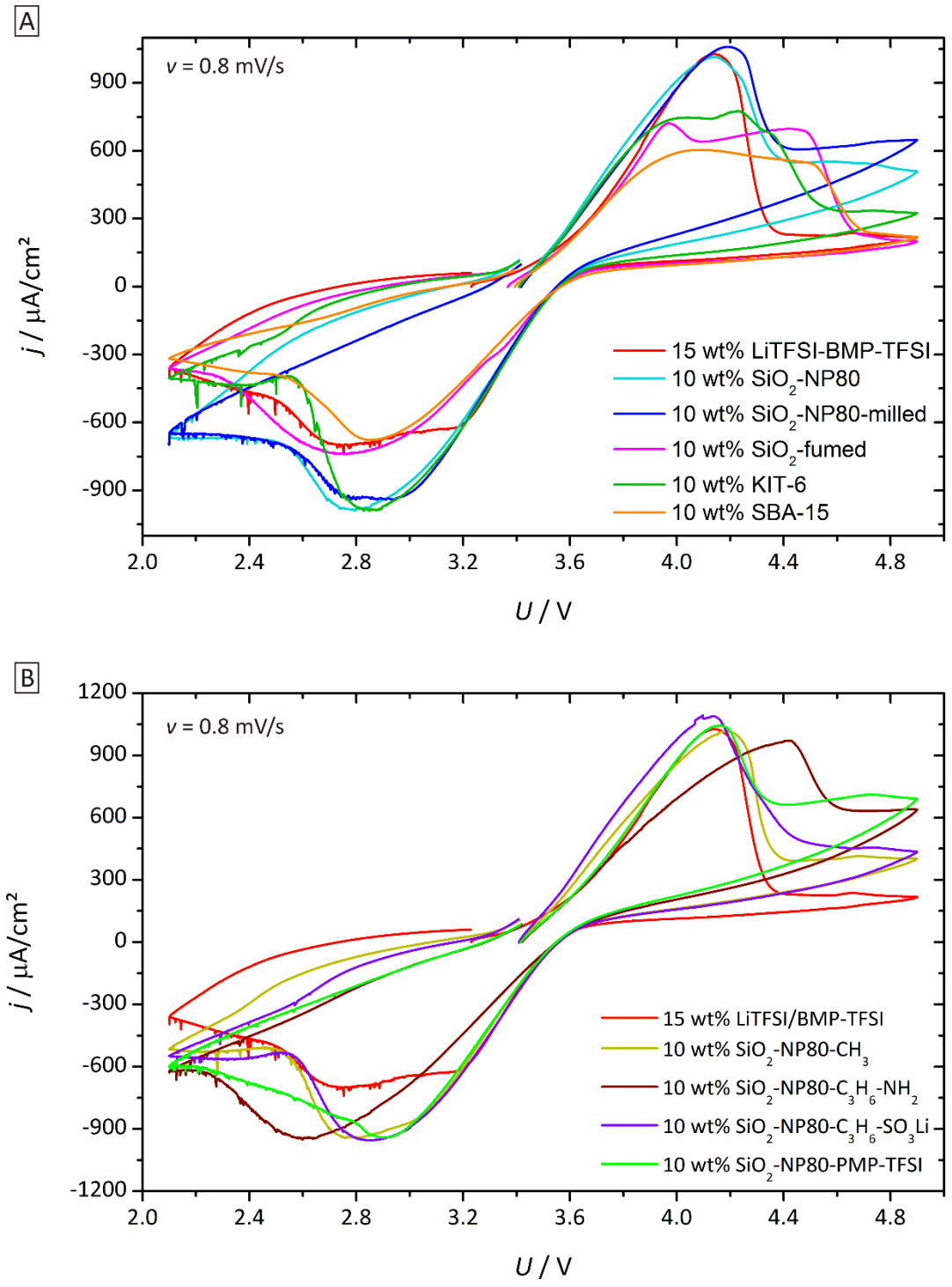

Figure 6.16: Cyclic voltammetry results obtained at a scan rate *v* of 0.8 mV/s with different IL composite electrolytes and lithium iron phosphate and lithium as electrodes. In graph A results of IL electrolytes with different silica nanoparticles and mesoporous silica are presented. Graph B shows results of IL electrolytes containing silica nanoparticles with different surface modifications.

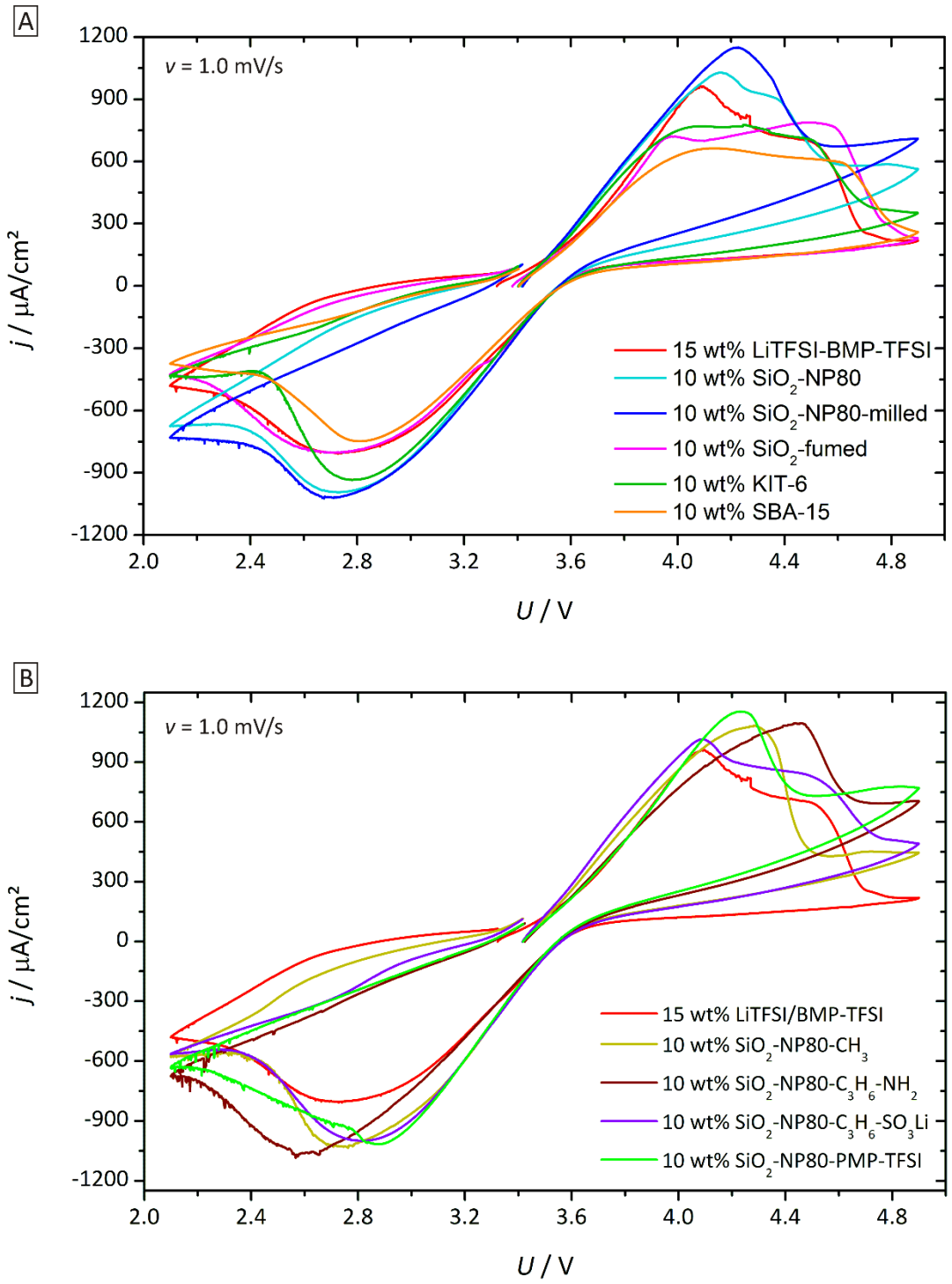

Figure 6.17: Cyclic voltammograms measured at a scan rate *v* of 1.0 mV/s of different IL composite electrolytes with lithium iron phosphate and lithium as electrodes. As filler materials different silica nanoparticles as well as mesoporous silica (shown in graph A) and silica nanoparticles with varying surface modifications (graph B) were used.

7 REFERENCES

[1] R. D. Rogers, K. R. Seddon, Ionic Liquids-Solvents of the Future? *Science* **2003**, *302 (5646)*, 792.

[2] M. Armand, F. Endres, D. R. MacFarlane, H. Ohno, B. Scrosati, Ionic-liquid materials for the electrochemical challenges of the future. *Nat. Mater.* **2009**, *8 (8)*, 621.

[3] K. R. Seddon, Ionic liquids: A taste of the future. *Nat. Mater.* **2003**, *2 (6)*, 363.

[4] B. Scrosati, J. Garche, Lithium batteries: Status, prospects and future. *J. Power Sources* **2010**, *195 (9)*, 2419.

[5] C. M. Hayner, X. Zhao, H. H. Kung, Materials for Rechargeable Lithium-Ion Batteries. *Annu. Rev. Chem. Biomol. Eng.* **2012**, *3 (1)*, 445.

[6] J.-M. Tarascon, M. Armand, Issues and challenges facing rechargeable lithium batteries. *Nature* **2001**, *414 (6861)*, 359.

[7] V. Thangadurai, S. Narayanan, D. Pinzaru, Garnet-type solid-state fast Li ion conductors for Li batteries: critical review. *Chem. Soc. Rev.* **2014**, *43 (13)*, 4714.

[8] Z. Li, J. Huang, B. Yann Liaw, V. Metzler, J. Zhang, A review of lithium deposition in lithium-ion and lithium metal secondary batteries. *J. Power Sources* **2014**, *254*, 168.

[9] K. Edström, T. Gustafsson, J. O. Thomas, The cathode–electrolyte interface in the Li-ion battery. *Electrochimica Acta* **2004**, *50 (2-3)*, 397.

[10] L. J. Hardwick, M. Holzapfel, A. Wokaun, P. Novák, Raman study of lithium coordination in EMI-TFSI additive systems as lithium-ion battery ionic liquid electrolytes. *J. Raman Spectrosc.* **2007**, *38 (1)*, 110.

[11] Y. Saito, T. Umecky, J. Niwa, T. Sakai, S. Maeda, Existing Condition and Migration Property of Ions in Lithium Electrolytes with Ionic Liquid Solvent. *J. Phys. Chem. B* **2007**, *111 (40)*, 11794.

[12] S. Duluard, J. Grondin, J.-L. Bruneel, I. Pianet, A. Grélard, G. Campet, M.-H. Delville et al., Lithium solvation and diffusion in the 1-butyl-3-methylimidazolium bis(trifluoromethanesulfonyl)imide ionic liquid. *J. Raman Spectrosc.* **2008**, *39 (5)*, 627.

[13] J.-C. Lassègues, J. Grondin, C. Aupetit, P. Johansson, Spectroscopic Identification of the Lithium Ion Transporting Species in LiTFSI-Doped Ionic Liquids. *J. Phys. Chem. A* **2009**, *113 (1)*, 305.

[14] J. Maier, Ionic Conduction in Space Charge Regions. *Prog. Solid St. Chem.* **1995**, *23 (3)*, 171.

[15] J. Maier, Nanoionics: ion transport and electrochemical storage in confined systems. *Nat. Mater.* **2005**, *4 (11)*, 805.

[16] C. Pfaffenhuber, M. Göbel, J. Popovic, J. Maier, Soggy-sand electrolytes: status and perspectives. *Phys. Chem. Chem. Phys.* **2013**, *15 (42)*, 18318.

[17] M. Kim, L. Lee, Y. Jung, S. Kim, Study on Ion Conductivity and Crystallinity of Composite Polymer Electrolytes Based on Poly(ethylene oxide)/Poly(acrylonitrile) Containing Nano-Sized Al_2O_3 Fillers. *J. Nanosci. Nanotech.* **2013**, *13 (12)*, 7865.

[18] J. Kim, D.-W. Park, S.-J. Park, S. Kim, Ion conducting properties of poly(ethylene oxide)-based electrolytes incorporating amorphous silica attached with imidazolium salts. *Res. Chem. Intermed.* **2013**, *39 (3)*, 1409.

[19] T. Echelmeyer, H. W. Meyer, L. van Wüllen, Novel Ternary Composite Electrolytes: Li Ion Conducting Ionic Liquids in Silica Glass. *Chem. Mater.* **2009**, *21 (11)*, 2280.

[20] J. Le Bideau, J.-B. Ducros, P. Soudan, D. Guyomard, Solid-State Electrode Materials with Ionic-Liquid Properties for Energy Storage: the Lithium Solid-State Ionic-Liquid Concept. *Adv. Funct. Mater.* **2011**, *21 (21)*, 4073.

[21] F. Wu, G. Tan, R. Chen, L. Li, J. Xiang, Y. Zheng, Novel Solid-State Li/$LiFePO_4$ Battery Configuration with a Ternary Nanocomposite Electrolyte for Practical Applications. *Adv. Mater.* **2011**, *23 (43)*, 5081.

[22] A. Unemoto, Y. Iwai, S. Mitani, S.-W. Baek, S. Ito, T. Tomai, J. Kawamura et al., Electrical conductivity and dynamics of quasi-solidified lithium-ion conducting ionic liquid at oxide particle surfaces. *Solid State Ionics* **2011**, *201 (1)*, 11.

[23] A. Unemoto, Y. Iwai, S. Mitani, S.-W. Baek, S. Ito, T. Tomai, J. Kawamura et al., Mass transport properties in quasi-solidified lithium-ion conducting ionic liquids at oxide particle surfaces. *Solid State Ionics* **2012**, *225*, 416.

[24] S. Ito, A. Unemoto, H. Ogawa, T. Tomai, I. Honma, Application of quasi-solid-state silica nanoparticles–ionic liquid composite electrolytes to all-solid-state lithium secondary battery. *J. Power Sources* **2012**, *208*, 271.

[25] T. Umecky, Y. Saito, Y. Okumura, S. Maeda, T. Sakai, Ionization Condition of Lithium Ionic Liquid Electrolytes under the Solvation Effect of Liquid and Solid Solvents. *J. Phys. Chem. B* **2008**, *112 (11)*, 3357.

[26] J. Nordström, L. Aguilera, A. Matic, Effect of Lithium Salt on the Stability of Dispersions of Fumed Silica in the Ionic Liquid $BMImBF_4$. *Langmuir* **2012**, *28 (9)*, 4080.

[27] J. Sun, P. Bayley, D. R. MacFarlane, M. Forsyth, Gel electrolytes based on lithium modified silica nano-particles. *Electrochimica Acta* **2007**, *52 (24)*, 7083.

[28] H. Ogawa, A. Unemoto, I. Honma, Quasi-Solid-State Lithium-Sulfur Battery Using Room Temperature Ionic Liquid-Li-salt-Fumed Silica Nanoparticle Composites as Electrolytes. *Electrochemistry* **2012**, *80 (10)*, 765.

[29] A. Unemoto, H. Ogawa, S. Ito, I. Honma, Electrical Conductivity, Self-Diffusivity and Electrolyte Performance of a Quasi-Solid-State Pseudo-Ternary System, Bis(trifluoromethanesulfonyl)amide-Based Room Temperature Ionic Liquid-Lithium Bis(trifluoromethanesulfonyl)amide-Fumed Silica Nanoparticles. *J. Electrochem. Soc.* **2013**, *160 (1)*, A138-A147.

[30] D. R. MacFarlane, M. Forsyth, P. C. Howlett, J. M. Pringle, J. Sun, G. Annat, W. Neil et al., Ionic Liquids in Electrochemical Devices and Processes: Managing Interfacial Electrochemistry. *Acc. Chem. Res.* **2007**, *40 (11)*, 1165.

[31] M. Galiński, A. Lewandowski, I. Stępniak, Ionic liquids as electrolytes. *Electrochimica Acta* **2006**, *51 (26)*, 5567.

[32] A. Lewandowski, A. Świderska-Mocek, Ionic liquids as electrolytes for Li-ion batteries—An overview of electrochemical studies. *J. Power Sources* **2009**, *194 (2)*, 601.

[33] A. Fernicola, B. Scrosati, H. Ohno, Potentialities of ionic liquids as new electrolyte media in advanced electrochemical devices. *Ionics* **2006**, *12 (2)*, 95.

[34] J.-S. Lee, J. Y. Bae, H. Lee, Quan Nguyen Dinh, H. S. Kim, H. Kim, Ionic Liquids as Electrolytes for Li Ion Batteries. *J. Ind. Eng. Chem.* **2004**, *10 (7)*, 1086.

[35] H. Matsumoto, H. Sakaebe, K. Tatsumi, M. Kikuta, E. Ishiko, M. Kono, Fast cycling of $Li/LiCoO_2$ cell with low-viscosity ionic liquids based on bis(fluorosulfonyl)imide $[FSI]^-$. *J. Power Sources* **2006**, *160 (2)*, 1308.

[36] S. Seki, Y. Kobayashi, H. Miyashiro, Y. Ohno, A. Usami, Y. Mita, N. Kihira et al., Lithium Secondary Batteries Using Modified-Imidazolium Room-Temperature Ionic Liquid. *J. Phys. Chem. B* **2006**, *110 (21)*, 10228.

[37] B. Garcia, S. Lavallée, G. Perron, C. Michot, M. Armand, Room temperature molten salts as lithium battery electrolyte. *Electrochimica Acta* **2004**, *49 (26)*, 4583.

[38] H. Nakagawa, S. Izuchi, K. Kuwana, Nukuda,, T., Y. Aihara, Liquid and Polymer Gel Electrolytes for Lithium Batteries Composed of Room-Temperature Molten Salt Doped by Lithium Salt. *J. Electrochem. Soc.* **2003**, *150 (6)*, A695-A700.

[39] H. Zheng, J. Qin, Y. Zhao, T. Abe, Z. Ogumi, Temperature dependence of the electrochemical behavior of $LiCoO_2$ in quaternary ammonium-based ionic liquid electrolyte. *Solid State Ionics* **2005**, *176 (29-30)*, 2219.

[40] J. Scheers, S. Fantini, P. Johansson, A review of electrolytes for lithium–sulphur batteries. *J. Power Sources* **2014**, *255*, 204.

[41] H. Sakaebe, H. Matsumoto, N-Methyl-N-propylpiperidinium bis(trifluoromethanesulfonyl)imide (PP13–TFSI) – novel electrolyte base for Li battery. *Electrochemistry Communications* **2003**, *5 (7)*, 594.

[42] K. Angenendt, P. Johansson, Ionic Liquid Based Lithium Battery Electrolytes: Charge Carriers and Interactions Derived by Density Functional Theory Calculations. *J. Phys. Chem. B* **2011**, *115 (24)*, 7808.

[43] Le, My Loan Phung, F. Alloin, P. Strobel, J.-C. Leprêtre, Pérez del Valle, Carlos, P. Judeinstein, Structure−Properties Relationships of Lithium Electrolytes Based on Ionic Liquid. *J. Phys. Chem. B* **2010**, *114 (2)*, 894.

[44] K. Fujii, H. Hamano, H. Doi, X. Song, S. Tsuzuki, K. Hayamizu, S. Seki et al., Unusual Li^+ Ion Solvation Structure in Bis(fluorosulfonyl)amide Based Ionic Liquid. *J. Phys. Chem. C* **2013**, 130913134838008.

[45] Y. Umebayashi, T. Mitsugi, S. Fukuda, T. Fujimori, K. Fujii, R. Kanzaki, M. Takeuchi et al., Lithium Ion Solvation in Room-Temperature Ionic Liquids Involving Bis(trifluoromethanesulfonyl) Imide Anion Studied by Raman Spectroscopy and DFT Calculations. *J. Phys. Chem. B* **2007**, *111 (45)*, 13028.

[46] Y. Umebayashi, S. Mori, K. Fujii, S. Tsuzuki, S. Seki, K. Hayamizu, S.-I. Ishiguro, Raman Spectroscopic Studies and Ab Initio Calculations on Conformational Isomerism of 1-Butyl-3-methylimidazolium Bis-(trifluoromethanesulfonyl)amide Solvated to a Lithium Ion in Ionic Liquids: Effects of the Second Solvation Sphere of the Lithium Ion. *J. Phys. Chem. B* **2010**, *114 (19)*, 6513.

[47] Y. Umebayashi, H. Hamano, S. Seki, B. Minofar, K. Fujii, K. Hayamizu, S. Tsuzuki et al., Liquid Structure of and Li^+ Ion Solvation in Bis(trifluoromethanesulfonyl)amide Based Ionic Liquids Composed of 1-Ethyl-3-methylimidazolium and N -Methyl- N -propylpyrrolidinium Cations. *J. Phys. Chem. B* **2011**, *115 (42)*, 12179.

[48] T. Frömling, M. Kunze, M. Schönhoff, J. Sundermeyer, B. Roling, Enhanced Lithium Transference Numbers in Ionic Liquid Electrolytes. *J. Phys. Chem. B* **2008**, *112 (41)*, 12985.

[49] M. Balaish, A. Kraytsberg, Y. Ein-Eli, A critical review on lithium–air battery electrolytes. *Phys. Chem. Chem. Phys.* **2014**, *16 (7)*, 2801.

[50] P. Wasserscheid, W. Keim, Ionic Liquids-New "Solutions" for Transition Metal Catalysis. *Angew. Chem. Int. Ed.* **2000**, *39 (21)*, 3772.

[51] K. R. Seddon, Ionic Liquids for Clean Technology. *J. Chem. Tech. Biotechnol.* **1997**, *68 (4)*, 351.

[52] F. G. Edwards, J. E. Enderby, R. A. Howe, D. I. Page, The structure of molten sodium chloride. *J. Phys. Chem. C: Solid State Phys.* **1975**, *8*, 3483.

[53] R. L. McGreevy, M. A. Howe, The structure of molten LiCl. *J. Phys.: Condens. Matter* **1989**, *1*, 9957.

[54] A. P. Abbott, Application of Hole Theory to the Viscosity of Ionic and Molecular Liquids. *ChemPhysChem* **2004**, *5 (8)*, 1242.

[55] R. Fürth, On the theory of the liquid state - I. The statistical treatment of the thermodynamics of liquids by the theory of holes. *Mathematical Proceedings of the Cambridge Philosophical Society* **1941**, *37 (3)*, 252.

[56] R. Fürth, On the theory of the liquid state - III. The hole theory of the viscous flow of liquids. *Mathematical Proceedings of the Cambridge Philosophical Society* **1941**, *37 (3)*, 281.

[57] A. P. Abbott, Model for the Conductivity of Ionic Liquids Based on an Infinite Dilution of Holes. *ChemPhysChem* **2005**, *6 (12)*, 2502.

[58] C. C. Liang, Conduction Characteristics of the Lithium Iodide-Aluminium Oxide Solid Electrolytes. *J. Electrochem. Soc.* **1973**, *120 (10)*, 1289.

[59] J. Maier, Defect Chemistry and Conductivity Effects in Heterogeneous Solid Electrolytes. *J. Electrochem. Soc.* **1987**, *134 (6)*, 1524.

[60] S. Jiang, J. B. Wagner, A Theoretical Model for Composite Electrolytes-II. Percolation Model for Ionic Conductivity Enhancement. *J. Phys. Chem. Solids* **1995**, *56 (8)*, 1113.

[61] J. Maier, Defect chemistry and ion transport in nanostructured materials Part II. Aspects of nanoionics. *Solid State Ionics* **2003**, *157 (1-4)*, 327.

[62] H. E. Roman, A continuum percolation model for dispersed ionic conductors. *J. Phys.: Condens. Matter* **2**, *1990 (17)*, 3909.

[63] A. Bunde, W. Dieterich, Percolation in Composites. *Journal of Electroceramics* **2000**, *5 (2)*, 81.

[64] T. Jow, J. B. Wagner, The Effect of Dispersed Alumina Particles on the Electrical Conductivity of Cuprous Chloride. *J. Electrochem. Soc.* **1979**, *126 (11)*, 1963.

[65] A. M. Stoneham, Wade, Evelyn, Kilner, J. A., A Model for the Fast Ionic Diffusion in Alumina-Doped LiI. *Mat. Res. Bull.* **1979**, *14 (5)*, 661.

[66] K. Shahi, J. B. Wagner, Ionic Conductivity and Thermoelectric Power of Pure and Al_2O_3-Dispersed AgI. *J. Electrochem. Soc.* **1981**, *128 (1)*, 6.

[67] J. Maier, Space Charge Regions in Solid Two-Phase Systems and their Conduction Contribution-I. Conductance Enhancement in the System Ionic Conductor-'Inert' Phase and Application on $AgCl:Al_2O_3$ and $AgCl:SiO_2$. *J. Phys. Chem. Solids* **1985**, *46 (3)*, 309.

[68] R. Akila, K. T. Jacob, Combined Homo-Hetero Doping for Enhancement of Ionic Conductivity. *Solid State Ionics* **1987**, *25 (2-3)*, 217.

[69] H. Eduardo Roman and M. Yussouff, Particle-size effect on the conductivity of dispersed ionic conductors. *Phys. Rev. B* **1987**, *36 (13)*, 7285.

[70] F. W. Poulsen, N. H. Andersen, B. Kindl, J. Schoomann, Properties of LiI - Alumina Composite Electrolytes. *Solid State Ionics* **1983**, *9-10*, 119.

[71] A. J. Bhattacharyya, M. Dollé, J. Maier, Improved Li-Battery Electrolytes by Heterogeneous Doping of Nonaqueous Li-Salt Solutions. *Electrochemical and Solid-State Letters* **2004**, *7 (11)*, A432.

[72] A. J. Bhattacharyya, J. Maier, Second Phase Effects on the Conductivity of Non-Aqueous Salt Solutions: “Soggy Sand Electrolytes”. *Adv. Mater.* **2004**, *16 (910)*, 811.

[73] A. J. Bhattacharyya, J. Maier, R. Bock, F. Lange, New class of soft matter electrolytes obtained via heterogeneous doping: Percolation effects in “soggy sand” electrolytes. *Solid State Ionics* **2006**, *177 (26-32)*, 2565.

[74] S. K. Das, A. J. Bhattacharyya, Oxide Particle Surface Chemistry and Ion Transport in “Soggy Sand” Electrolytes. *J. Phys. Chem. C* **2009**, *113 (16)*, 6699.

[75] S. K. Das, A. J. Bhattacharyya, Influence of Oxide Particle Network Morphology on Ion Solvation and Transport in “Soggy Sand” Electrolytes. *J. Phys. Chem. B* **2010**, *114 (20)*, 6830.

[76] S. K. Das, S. S. Mandal, A. J. Bhattacharyya, Ionic conductivity, mechanical strength and Li-ion battery performance of mono-functional and bi-functional (“Janus”) “soggy sand” electrolytes. *Energy Environ. Sci.* **2011**, *4 (4)*, 1391.

[77] A. J. Bhattacharyya, Ion Transport in Liquid Salt Solutions with Oxide Dispersions: “Soggy Sand” Electrolytes. *J. Phys. Chem. Lett.* **2012**, *3 (6)*, 744.

[78] N. Kaskhedikar, Y. Karatas, G. Cui, J. Maier, H.-D. Wiemhöfer, Nanocomposites based on borate esters as improved lithium-ion electrolytes. *J. Mater. Chem.* **2011**, *21 (32)*, 11838.

[79] K. Sann. Oral communication.

[80] K. Sann, J. Roggenbuck, N. Krawczyk, H. Buschmann, B. Luerßen, M. Fröba, J. Janek, Conductivity of liquid lithium electrolytes with dispersed mesoporous silica particles. *Electrochimica Acta* **2012**, *60*, 1.

[81] C. Pfaffenhuber, S. Sörgel, K. Weichert, M. Bele, T. Mundinger, M. Göbel, J. Maier, In Situ Recording of Particle Network Formation in Liquids by Ion Conductivity Measurements. *J. Am. Chem. Soc.* **2011**, *133 (37)*, 14514.

[82] K. Sann. PhD Thesis, Gießen **in preparation**.

[83] C. Pfaffenhuber, J. Maier, Quantitative estimate of the conductivity of a soggy sand electrolyte: example of ($LiClO_4$, THF):SiO_2. *Phys. Chem. Chem. Phys.* **2013**, *15 (6)*, 2050.

[84] C. Pfaffenhuber, F. Hoffmann, M. Fröba, J. Popovic, J. Maier, Soggy-sand effects in liquid composite electrolytes with mesoporous materials as fillers. *J. Mater. Chem. A* **2013**, *1 (40)*, 12560.

[85] A. Jarosik, S. Hore, N. Kaskhedikar, C. Pfaffenhuber, J. Maier, Heterogeneously doped polyethylene glycol as nano-composite soft matter electrolyte. *Electrochimica Acta* **2011**, *56 (24)*, 8115.

[86] A. Jarosik, U. Traub, J. Maier, A. Bunde, Ion conducting particle networks in liquids: modeling of network percolation and stability. *Phys. Chem. Chem. Phys.* **2011**, *13 (7)*, 2663.

[87] J. L. Schaefer, S. S. Moganty, D. A. Yanga, L. A. Archer, Nanoporous hybrid electrolytes. *J. Mater. Chem.* **2011**, *21 (27)*, 10094.

[88] Y. Lu, S. K. Das, S. S. Moganty, L. A. Archer, Ionic Liquid-Nanoparticle Hybrid Electrolytes and their Application in Secondary Lithium-Metal Batteries. *Adv. Mater.* **2012**, *24 (32)*, 4430.

[89] Y. Lu, S. S. Moganty, J. L. Schaefer, L. A. Archer, Ionic liquid-nanoparticle hybrid electrolytes. *J. Mater. Chem.* **2012**, *22 (9)*, 4066.

[90] J. L. Schaefer, D. A. Yanga, L. A. Archer, High Lithium Transference Number Electrolytes via Creation of 3-Dimensional, Charged, Nanoporous Networks from Dense Functionalized Nanoparticle Composites. *Chem. Mater.* **2013**, *25 (6)*, 834.

[91] S. Xu, Y. Lu, H. Wang, H. D. Abruña, L. A. Archer, A rechargeable Na–CO 2 /O 2 battery enabled by stable nanoparticle hybrid electrolytes. *J. Mater. Chem. A* **2014**.

[92] Y. Lu, K. Korf, Y. Kambe, Z. Tu, L. A. Archer, Ionic-Liquid-Nanoparticle Hybrid Electrolytes: Applications in Lithium Metal Batteries. *Angew. Chem. Int. Ed.* **2014**, *53 (2)*, 488.

[93] M. D. Tikekar, L. A. Archer, D. L. Koch, Stability Analysis of Electrodeposition across a Structured Electrolyte with Immobilized Anions. *Journal of the Electrochemical Society* **2014**, *161 (6)*, A847.

[94] K. S. Korf, Y. Lu, Y. Kambe, L. A. Archer, Piperidinium tethered nanoparticle-hybrid electrolyte for lithium metal batteries. *J. Mater. Chem. A* **2014**, *2 (30)*, 11866.

[95] S. Kim, S.-J. Park, Preparation and electrochemical behaviors of polymeric composite electrolytes containing mesoporous silicate fillers. *Electrochimica Acta* **2007**, *52 (11)*, 3477.

[96] L. Lee, I.-J. Kim, S. Yang, S. Kim, Filler Effect of Ionic Liquid Attached Titanium Oxide on Conducting Property of Poly(ethylene oxide)/Poly(methyl methacrylate) Composite Electrolytes. *J. Nanosci. Nanotechnol.* **2014**, *14 (10)*, 8010.

[97] N. Angulakshmi, D. J. Yoo, K. S. Nahm, C. Gerbaldi, A. M. Stephan, $MgAl_2SiO_6$-incorporated poly(ethylene oxide)-based electrolytes for all-solid-state lithium batteries. *Ionics* **2014**, *20 (2)*, 151.

[98] L. Lee, S.-J. Park, S. Kim, Effect of nano-sized barium titanate addition on PEO/PVDF blend-based composite polymer electrolytes. *Solid State Ionics* **2013**, *234*, 19.

[99] S.-J. Park, A.-R. Han, J.-S. Shin, S. Kim, Influence of crystallinity on ion conductivity of PEO-based solid electrolytes for lithium batteries. *Macromol. Res.* **2010**, *18 (4)*, 336.

[100] Y. Liu, J. Y. Lee, L. Hong, Morphology, crystallinity, and electrochemical properties ofin situ formed poly(ethylene oxide)/TiO2 nanocomposite polymer electrolytes. *J. Appl. Polym. Sci.* **2003**, *89 (10)*, 2815.

[101] B. Scrosati, F. Croce, L. Persi, Impedance Spectroscopy Study of PEO-Based Nanocomposite Polymer Electrolytes. *J. Electrochem. Soc.* **2000**, *147 (5)*, 1718.

[102] R. A. Vaia, S. Vasudevan, W. Krawiec, L. G. Scanlon, E. P. Giannelis, New polymer electrolyte nanocomposites: Melt intercalation of poly(ethylene oxide) in mica-type silicates. *Adv. Mater.* **1995**, *7 (2)*, 154.

[103] F. Croce, G. B. Appetecchi, L. Persi, B. Scrosati, Nanocomposite polymer electrolytes for lithium batteries. *Nature* **1998**, *394 (6692)*, 456.

[104] W. Wieczorek, Z. Florjanczyk, J. R. Stevens, Composite polyether based solid electrolytes. *Electrochimica Acta* **1995**, *40 (13-14)*, 2251.

[105] H. Kasemägi, Aabloo, A., Klintenberg, M. K., J. O. Thomas, Molecular dynamics simulation of the effect of nanoparticle fillers on ion motion in a polymer host. *Solid State Ionics* **2004**, *168 (3-4)*, 249.

[106] Y.-Z. Su, Y.-C. Fu, Y.-M. Wei, J.-W. Yan, B.-W. Mao, The Electrode/Ionic Liquid Interface: Electric Double Layer and Metal Electrodeposition. *Chem. Eur. J. of Chem. Phys.* **2010**, *11 (13)*, 2764.

[107] H.-P. Steinrück, Recent developments in the study of ionic liquid interfaces using X-ray photoelectron spectroscopy and potential future directions. *Phys. Chem. Chem. Phys.* **2012**, *14 (15)*, 5010.

[108] S. Perkin, Ionic liquids in confined geometries. *Phys. Chem. Chem. Phys.* **2012**, *14 (15)*, 5052.

[109] M. Drüschler, N. Borisenko, J. Wallauer, C. Winter, B. Huber, F. Endres, B. Roling, New insights into the interface between a single-crystalline metal electrode and an extremely pure ionic liquid: slow interfacial processes and the influence of temperature on interfacial dynamics. *Phys. Chem. Chem. Phys.* **2012**, *14 (15)*, 5090.

[110] M. V. Fedorov, A. A. Kornyshev, Ionic Liquids at Electrified Interfaces. *Chem. Rev.* **2014**, *114 (5)*, 2978.

[111] S. Baldelli, Interfacial Structure of Room-Temperature Ionic Liquids at the Solid–Liquid Interface as Probed by Sum Frequency Generation Spectroscopy. *J. Phys. Chem. Lett.* **2013**, *4 (2)*, 244.

[112] S. Baldelli, Surface Structure at the Ionic Liquid−Electrified Metal Interface. *Acc. Chem. Res.* **2008**, *41 (3)*, 421.

[113] T. Carstens, R. Hayes, Abedin, Sherif Zein El, B. Corr, G. B. Webber, N. Borisenko, R. Atkin et al., In situ STM, AFM and DTS study of the interface 1-hexyl-3-methylimidazolium tris(pentafluoroethyl)trifluorophosphate/Au(111). *Electrochimica Acta* **2012**, *82*, 48.

[114] R. Atkin, N. Borisenko, M. Drüschler, El Abedin, Sherif Zein, F. Endres, R. Hayes, B. Huber et al., An in situ STM/AFM and impedance spectroscopy study of the extremely pure 1-butyl-1-methylpyrrolidinium tris(pentafluoroethyl)trifluorophosphate/Au(111) interface: potential dependent solvation layers and the herringbone reconstruction. *Phys. Chem. Chem. Phys.* **2011**, *13 (15)*, 6849.

[115] R. Hayes, N. Borisenko, M. K. Tam, P. C. Howlett, F. Endres, R. Atkin, Double Layer Structure of Ionic Liquids at the Au(111) Electrode Interface: An Atomic Force Microscopy Investigation. *J. Phys. Chem. C* **2011**, *115 (14)*, 6855.

[116] T. Cremer, M. Stark, A. Deyko, H.-P. Steinrück, F. Maier, Liquid/Solid Interface of Ultrathin Ionic Liquid Films: $[C_1C_1Im][Tf_2N]$ and $[C_8C_1Im][Tf_2N]$ on Au(111). *Langmuir* **2011**, *27 (7)*, 3662.

[117] R. Hayes, G. G. Warr, R. Atkin, At the interface: solvation and designing ionic liquids. *Phys. Chem. Chem. Phys.* **2010**, *12 (8)*, 1709.

[118] M. Mezger, H. Schröder, H. Reichert, S. Schramm, J. S. Okasinski, S. Schröder, V. Honkimäki et al., Molecular Layering of Fluorinated Ionic Liquids at a Charged Sapphire (0001) Surface. *Science* **2008**, *322 (5900)*, 424.

[119] B. Roling, M. Drüschler, B. Huber, Slow and fast capacitive process taking place at the ionic liquid/electrode interface. *Faraday Discuss.* **2011**, *154*, 303.

[120] Y.-Z. Su, Y.-C. Fu, J.-W. Yan, Z.-B. Chen, B.-W. Mao, Double Layer of Au(100)/Ionic Liquid Interface and Its Stability in Imidazolium-Based Ionic Liquids. *Angew. Chem.* **2009**, *121 (28)*, 5250.

[121] A. M. Smith, Lovelock, Kevin R. J., N. N. Gosvami, P. Licence, A. Dolan, T. Welton, S. Perkin, Monolayer to Bilayer Structural Transition in Confined Pyrrolidinium-Based Ionic Liquids. *J. Phys. Chem. Lett.* **2013**, *4 (3)*, 378.

[122] R. Atkin, G. G. Warr, Structure in Confined Room-Temperature Ionic Liquids. *J. Phys. Chem. C* **2007**, *111 (13)*, 5162.

[123] M. R. Castillo, J. M. Fraile, J. A. Mayoral, Structure and Dynamics of 1-Butyl-3-methylimidazolium Hexafluorophosphate Phases on Silica and Laponite Clay: From Liquid to Solid Behavior. *Langmuir* **2012**, *28 (31)*, 11364.

[124] C. Sievers, O. Jimenez, T. E. Müller, S. Steuernagel, J. A. Lercher, Formation of Solvent Cages around Organometallic Complexes in Thin Films of Supported Ionic Liquid. *J. Am. Chem. Soc.* **2006**, *128 (43)*, 13990.

[125] J. Le Bideau, P. Gaveau, S. Bellayer, M.-A. Néouze, A. Vioux, Effect of confinement on ionic liquids dynamics in monolithic silica ionogels: 1H NMR study. *Phys. Chem. Chem. Phys.* **2007**, *9 (40)*, 5419.

[126] S. Shimano, H. Zhou, I. Honma, Preparation of Nanohybrid Solid-State Electrolytes with Liquidlike Mobilities by Solidifying Ionic Liquids with Silica Particles. *Chem. Mater.* **2007**, *19 (22)*, 5216.

[127] K. Ueno, M. Kasuya, M. Watanabe, M. Mizukami, K. Kurihara, Resonance shear measurement of nanoconfined ionic liquids. *Phys. Chem. Chem. Phys.* **2010**, *12 (16)*, 4066.

[128] R. Göbel, P. Hesemann, J. Weber, E. Möller, A. Friedrich, S. Beuermann, A. Taubert, Surprisingly high, bulk liquid-like mobility of silica-confined ionic liquids. *Phys. Chem. Chem. Phys.* **2009**, *11 (19)*, 3653.

[129] S. Bovio, A. Podestà, C. Lenardi, P. Milani, Evidence of Extended Solidlike Layering in [Bmim][NTf_2] Ionic Liquid Thin Films at Room-Temperature. *J. Phys. Chem. B* **2009**, *113 (19)*, 6600.

[130] C. Iacob, J. R. Sangoro, P. Papadopoulos, T. Schubert, S. Naumov, R. Valiullin, J. Kärger et al., Charge transport and diffusion of ionic liquids in nanoporous silica membranes. *Phys. Chem. Chem. Phys.* **2010**, *12 (41)*, 13798.

[131] M. P. Singh, R. K. Singh, S. Chandra, Studies on Imidazolium-Based Ionic Liquids Having a Large Anion Confined in a Nanoporous Silica Gel Matrix. *J. Phys. Chem. B* **2011**, *115 (23)*, 7505.

[132] J. Le Bideau, L. Viau, A. Vioux, Ionogels, ionic liquid based hybrid materials. *Chem. Soc. Rev.* **2011**, *40 (2)*, 907.

[133] B. D. Fitchett, J. C. Conboy, Structure of the Room-Temperature Ionic Liquid/SiO_2 Interface Studied by Sum-Frequency Vibrational Spectroscopy. *J. Phys. Chem. B* **2004**, *108 (52)*, 20255.

[134] J. B. Rollins, B. D. Fitchett, J. C. Conboy, Structure and Orientation of the Imidazolium Cation at the Room-Temperature Ionic Liquid/SiO_2 Interface Measured by Sum-Frequency Vibrational Spectroscopy. *J. Phys. Chem. B* **2007**, *111 (18)*, 4990.

[135] R. Göbel, A. Friedrich, A. Taubert, Tuning the phase behavior of ionic liquids in organically functionalized silica ionogels. *Dalton Trans.* **2010**, *39 (2)*, 603.

[136] M.-A. Néouze, J. Le Bideau, A. Vioux, Versatile heat resistant solid electrolytes with performances of liquid electrolytes. *Progress in Solid State Chemistry* **2005**, *33 (2-4)*, 217.

[137] M.-A. Néouze, J. Le Bideau, P. Gaveau, S. Bellayer, A. Vioux, Ionogels, New Materials Arising from the Confinement of Ionic Liquids within Silica-Derived Networks. *Chem. Mater.* **2006**, *18 (17)*, 3931.

[138] J. C. Maxwell, *A treatise on electricity and magnetism vol. 2*, Clarendon Press, Oxford **1873**.

[139] R. Lemlich, A Theory for the Limiting Conductivity of Polyhedral Foam at Low Density. *J. Colloid Interface Sci.* **1978**, *64 (1)*, 107.

[140] K. Feitosa, S. Marze, A. Saint-Jalmes, D. J. Durian, Electrical conductivity of dispersions: from dry foams to dilute suspensions. *J. Phys.: Condens. Matter* **2005**, *17 (41)*, 6301.

[141] B. Scrosati, Power sources for portable electronics and hybrid cars: lithium batteries and fuel cells. *Chem. Record* **2005**, *5 (5)*, 286.

[142] S. Zugmann, M. Fleischmann, M. Amereller, R. M. Gschwind, H. D. Wiemhöfer, H. J. Gores, Measurement of transference numbers for lithium ion electrolytes via four different methods, a comparative study. *Electrochimica Acta* **2011**, *56 (11)*, 3926.

[143] H. Buschmann, J. Dölle, S. Berendts, A. Kuhn, P. Bottke, M. Wilkening, P. Heitjans et al., Structure and dynamics of the fast lithium ion conductor "$Li_7La_3Zr_2O_{12}$". *Phys. Chem. Chem. Phys.* **2011**, *13 (43)*, 19378.

[144] J. Reinacher, S. Berendts, J. Janek, Preparation and electrical properties of garnet-type $Li_6BaLa_2Ta_2O_{12}$ lithium solid electrolyte thin films prepared by pulsed laser deposition. *Solid State Ionics* **2014**, *258*, 1.

[145] D. A. MacInnes, M. Dole, The transference numbers of potassium chloride. New determinations by the Hittorf method and a comparison with results obtained by the moving boundary method. *J. Am. Chem. Soc.* **1931**, *53 (4)*, 1357.

[146] L. G. Longsworth, Transference numbers of aqueous solutions of potassium chloride, sodium chloride, lithium chloride and hydrochloric acid at 25° by the moving boundary method. *J. Am. Chem. Soc.* **1932**, *54 (7)*, 2741.

[147] H. S. Harned, E. C. Dreby, Properties of Electrolytes in Mixtures of Water and Organic Solvents. IV. Transference Numbers of Hydrochloric Acid in Water and Dioxane-Water Mixtures from 0 to 50°. *J. Am. Chem. Soc.* **1939**, *61 (11)*, 3113.

[148] M. Bester-Rogac, R. Neueder, J. Barthel, Conductivity of Sodium Chloride in Water + 1,4-Dioxane Mixtures at Temperatures from 5 to 35°C I. Dilute Solutions. *Journal of Solution Chemistry* **1999**, *28 (9)*, 1071.

[149] P. G. Bruce, C. A. Vincent, Steady state current flow in solid binary electrolyte cells. *J. Electroanal. Chem.* **1987**, *225 (1-2)*, 1.

[150] V. Mauro, A. Daprano, F. Croce, M. Salomon, Direct determination of transference numbers of LiClO solutions in propylene carbonate and acetonitrile. *J. Power Sources* **2005**, *141 (1)*, 167.

[151] Y. Ma, M. Doyle, T. F. Fuller, M. M. Doeff, De Jonghe, Lutgard C., J. Newman, The Measurement of a Complete Set of Transport Properties for a Concentrated Solid Polymer Electrolyte Solution. *J. Electrochem. Soc.* **1995**, *142 (6)*, 1859.

[152] Y. M. Lee, J. E. Seo, N.-S. Choi, J.-K. Park, Influence of tris(pentafluorophenyl) borane as an anion receptor on ionic conductivity of $LiClO_4$-based electrolyte for lithium batteries. *Electrochimica Acta* **2005**, *50 (14)*, 2843.

[153] A. Narita, W. Shibayama, K. Sakamoto, T. Mizumo, N. Matsumi, H. Ohno, Lithium ion conduction in an organoborate zwitterion-LiTFSI mixture. *Chem. Commun.* **2006** *(18)*, 1926.

[154] A. Fernicola, F. Croce, B. Scrosati, M. Watanabe, H. Ohno, LiTFSI-BEPyTFSI as an improved ionic liquid electrolyte for rechargeable lithium batteries. *J. Power Sources* **2007**, *174 (1)*, 342.

[155] L. F. Li, H. S. Lee, H. Li, X. Q. Yang, K. W. Nam, W. S. Yoon, J. McBreen et al., New electrolytes for lithium ion batteries using LiF salt and boron based anion receptors. *J. Power Sources* **2008**, *184 (2)*, 517.

[156] H. F. Xiang, B. Yin, H. Wang, H. W. Lin, X. W. Ge, S. Xie, C. H. Chen, Improving electrochemical properties of room temperature ionic liquid (RTIL) based electrolyte for Li-ion batteries. *Electrochimica Acta* **2010**, *55 (18)*, 5204.

[157] K. Perzyna, R. Borkowska, J. Syzdek, A. Zalewska, W. Wieczorek, The effect of additive of Lewis acid type on lithium–gel electrolyte characteristics. *Electrochimica Acta* **2011**, *57*, 58.

[158] S. Zugmann, D. Moosbauer, M. Amereller, C. Schreiner, F. Wudy, R. Schmitz, R. Schmitz et al., Electrochemical characterization of electrolytes for lithium-ion batteries based on lithium difluoromono(oxalato)borate. *J. Power Sources* **2011**, *196 (3)*, 1417.

[159] Y. An, P. Zuo, X. Cheng, L. Liao, G. Yin, Preparation and Properties of Ionic-Liquid Mixed Solutions as a Safety Electrolyte for Lithium Ion Batteries. *Int. J. Electrochem. Sci.* **2011**, *6 (7)*, 2398.

[160] E. Zygadło-Monikowska, Z. Florjańczyk, P. Kubisa, T. Biedroń, W. Sadurski, A. Puczyłowska, N. Langwald et al., Lithium electrolytes based on modified imidazolium ionic liquids. *Int. J. Hydrogen Energy* **2014**, *39 (6)*, 2943.

[161] S. A. Krachkovskiy, A. D. Pauric, I. C. Halalay, G. R. Goward, Slice-Selective NMR Diffusion Measurements: A Robust and Reliable Tool for In Situ Characterization of Ion-Transport Properties in Lithium-Ion Battery Electrolytes. *J. Phys. Chem. Lett.* **2013**, *4 (22)*, 3940.

[162] T.-Y. Wu, L. Hao, C.-W. Kuo, Y.-C. Lin, S.-G. Su, P.-L. Kuo, I.-W. Sun, Ionic Conductivity and Diffusion in Lithium Tetrafluoroborate Ionic Liquid. *Int. J. Electrochem. Sci.* **2012**, *7 (3)*, 2047.

[163] T.-Y. Wu, L. Hao, P.-R. Chen, J.-W. Liao, Ionic Conductivity and Transporting Properties in LiTFSI-Doped Bis(trifluoromethanesulfonyl)imide-Based Ionic Liquid Electrolyte. *Int. J. Electrochem. Sci.* **2013**, *8 (2)*, 2606.

[164] K. Hayamizu, Y. Aihara, H. Nakagawa, T. Nukuda, W. S. Price, Ionic Conduction and Ion Diffusion in Binary Room-Temperature Ionic Liquids Composed of [emim][BF_4] and $LiBF_4$. *J. Phys. Chem. B* **2004**, *108 (50)*, 19527.

[165] R. Hartl, M. Fleischmann, R. M. Gschwind, M. Winter, H. J. Gores, A Liquid Inorganic Electrolyte Showing an Usually High Lithium Ion Transference Number: A Concentrated Solution of $LiAlCl_4$ in Sulfur Dioxide. *Energies* **2013**, *6*, 4448.

[166] I. Nicotera, C. Oliviero, W. A. Henderson, G. B. Appetecchi, S. Passerini, NMR Investigation of Ionic Liquid−LiX Mixtures: Pyrrolidinium Cations and TFSI - Anions. *J. Phys. Chem. B* **2005**, *109 (48)*, 22814.

[167] T. G. Mezger, *The rheology handbook: For users of rotational and oscillatory rheometers,* 2nd edn., Vincentz Network, Hannover **2006**.

[168] G. G. Stokes, Report on the recent researches in Hydrodynamics. *British Association Report* **1846**, 1.

[169] G. G. Stokes, On some cases of fluid motion. *Cambridge Philosophical Society Transactions* **1849**, *8*, 105.

[170] G. G. Stokes, On the theories of the internal friction of fluids in motion and of the equilibrium and motion of elastic solids. *Cambridge Philosophical Society Transactions* **1849**, *8*, 287.

[171] G. G. Stokes, On the effect of the internal friction of fluids on the motion of pendulums. *Cambridge Philosophical Society Transactions* **1851**, *9*, 8.

[172] I. Newton, *Philosophiae Naturalis Principia Mathematica*, London **1687**.

[173] R. Hooke, *De potentia restitutiva*, London **1678**.

[174] F. Kleitz, S. Hei Choi, R. Ryoo, Cubic Ia3d large mesoporous silica: synthesis and replication to platinum nanowires, carbon nanorods and carbon nanotubes. *Chem. Commun.* **2003** *(17)*, 2136.

[175] D. Zhao, J. Feng, Q. Huo, N. Melosh, G. H. Fredrickson, B. F. Chmelka, G. D. Stucky, Triblock Copolymer Syntheses of Mesoporous Silica with Periodic 50 to 300 Angstrom Pores. *Science* **1998**, *279 (5350)*, 548.

[176] W. Stöber, A. Fink, E. Bohn, Controlled growth of monodisperse silica spheres in the micron size range. *J. Colloid Interface Sci.* **1968**, *26 (1)*, 62.

[177] J. C. Moreira, Y. Gushikem, Preconcentration of metal ions on silica gel modified with 3(1-imidazolyl)propyl groups. *Analytica Chimica Acta* **1985**, *176*, 263.

[178] A. M. Lazarin, Y. Gushikem, de Castro, Sandra C., Cellulose aluminium oxide coated with organofunctional groups containing nitrogen donor atoms. *J. Mater. Chem.* **2000**, *10 (11)*, 2526.

[179] S. Brenna, T. Posset, J. Furrer, J. Blümel, ^{14}N NMR and Two-Dimensional Suspension ^{1}H and ^{13}C HRMAS NMR Spectroscopy of Ionic Liquids Immobilized on Silica. *Chem. Eur. J.* **2006**, *12 (10)*, 2880.

[180] G. Liu, M. Hou, J. Song, Z. Zhang, T. Wu, B. Han, Ni2+-containing ionic liquid immobilized on silica: Effective catalyst for styrene oxidation with H2O2 at solvent-free condition. *J. Mol. Catal. A: Chem.* **2010**, *316 (1-2)*, 90.

[181] Izgorodina, E. I., M. Forsyth, D. R. MacFarlane, Towards a Better Understanding of 'Delocalized Charge' in Ionic Liquid Anions. *Aust. J. Chem.* **2007**, *60 (1)*, 15.

[182] K. Ueno, A. Inaba, M. Kondoh, M. Watanabe, Colloidal Stability of Bare and Polymer-Grafted Silica Nanoparticles in Ionic Liquids. *Langmuir* **2008**, *24 (10)*, 5253.

[183] K. Ueno, S. Imaizumi, K. Hata, M. Watanabe, Colloidal Interaction in Ionic Liquids: Effects of Ionic Structures and Surface Chemistry on Rheology of Silica Colloidal Dispersions. *Langmuir* **2009**, *25 (2)*, 825.

[184] K. Ueno, M. Watanabe, From Colloidal Stability in Ionic Liquids to Advanced Soft Materials Using Unique Media. *Langmuir* **2011**, *27 (15)*, 9105.

[185] K. Ueno, K. Hata, T. Katakabe, M. Kondoh, M. Watanabe, Nanocomposite Ion Gels Based on Silica Nanoparticles and an Ionic Liquid: Ionic Transport, Viscoelastic Properties, and Microstructure. *J. Phys. Chem. B* **2008**, *112 (30)*, 9013.

[186] N. Krawczyk, *Electrochemical Characterization of Lithium Electrolytes Based on Ionic Liquids*. Master Thesis, Gießen **2010**.

[187] S. Tsuzuki, Factors Controlling the Diffusion of Ions in Ionic Liquids. *ChemPhysChem* **2012**, *13 (7)*, 1664.

[188] W. Xu, E. I. Cooper, C. A. Angell, Ionic Liquids: Ion Mobilities, Glass Temperatures, and Fragilities. *J. Phys. Chem. B* **2003**, *107 (25)*, 6170.

[189] C. Schreiner, S. Zugmann, R. Hartl, H. J. Gores, Fractional Walden Rule for Ionic Liquids: Examples from Recent Measurements and a Critique of the So-Called Ideal KCl Line for the Walden Plot. *J. Chem. Eng. Data* **2010**, *55 (5)*, 1784.

[190] M. J. Pikal, D. G. Miller, Determination and comparison of Hittorf and cell transference numbers for aqueous silver nitrate solutions at 25°C. *J. Phys. Chem.* **1970**, *74 (6)*, 1337.

[191] E. A. Guggenheim, The thermodynamics of interfaces in systems of several components. *Trans. Faraday Soc.* **1940**, *35*, 397.

[192] M. E. Carbone, R. Ciriello, A. Guerrieri, A. M. Salvi, XPS investigation on the chemical structure of a very thin, insulating, film synthesized on platinum by electropolymerization of o-aminophenol (oAP) in aqueous solution at neutral pH. *Surf. Interface Anal.* **2014** *(ECASIA 2013 special issue)*.

[193] M. Kleine-Boymann, M. Rohnke, A. Henss, K. Peppler, J. Sann, J. Janek, Discrimination between biologically relevant calcium phosphate phases by surface-analytical techniques. *Appl. Surf. Sci.* **2014**, *309*, 27.

[194] W. A. Hamilton, L. Porcar, L. J. Magid, Using neutron reflectometry and reflection geometry “near-surface” SANS to investigate surfactant micelle organization at a solid–solution interface. *Physica B* **2005**, *357 (1-2)*, 88.

[195] B. Cattoz, de Vos, Wiebe M., T. Cosgrove, M. Crossman, M.-S. Appavou, S. W. Prescott, Complexation of polymeric stabilisers in solution and at the silica nanoparticle interface. *Colloids Surf., A* **2014**, *449*, 57.

8 LIST OF FIGURES

9 ABBREVIATIONS

AFM	atomic force microscopy
Au	gold
BDMI	1-butyl-2,3-dimethylimidazolium
BF_4	tetrafluoroborate
BMI	1-butyl-3-methylimidazolium
BMP	N-butyl-N-methylpyrrolidinium
c	concentration
CV	cyclic voltammetry
D	diffusion coefficient
DEME	N,N-diethyl-N-methyl-N-(2-methoxyethyl)ammonium
DLS	differential light scattering
DSC	differential scanning calorimetry
EDX	energy-dispersive X-ray spectroscopy
EMI	1-ethyl-3-methylimidazolium
et al.	et alii
FAP	tris(pentafluroethyl)trifluorophosphate
FSI	bis(fluorosulfon)imide
FTIR	Fourier transform infrared
G	shear modulus
HMI	1-hexyl-3-methylimidazolium

IL	ionic liquid
IR	infrared
j	current density
KIT-6	mesoporous silica with cubic pore structure
LFP	lithium iron phosphate
$LiClO_4$	lithium perchlorate
$LiPF_6$	lithium hexafluorophosphate
LiTf	lithium triflate
LiTFSI	lithium bis(trifluoromethylsulfon)imide
M	molar
MMI	1,3-dimethylimidazolium
NMR	nuclear magnetic resonance spectroscopy
PEIS	potentiostatic electrochemical impedance spectroscopy
PFG-NMR	pulsed field gradient – NMR
PMI	1-methyl-3-propylimidazoilum
PMP	N-methyl-N-propylpyrrolidinium
PMPip	N-methyl-N-propylpiperidinium
ppm	parts per million
PTFE	polytetrafluoroethylene
PVDF	polyvinylidene fluorid
Q	constant phase element
S (mS)	siemens or millisiemens (unit of electric conductance)
SBA-15	mesoporous silica with hexagonal pore structure
SEM	secondary electron microscopy
SiO_2-fumed	fumed silica particles
SiO_2-NP80	silica nanoparticles with primary particle size of 80 nm
SiO_2-NP80-C_3H_6-NH_2	silica nanoparticles surface-modified with aminopropyl
SiO_2-NP80-C_3H_6-SO_3Li	silica nanoparticles surface-modified with lithiumpropylsulfonate

SiO_2-NP80-CH_3	silica nanoparticles surface-modified with methyl
SiO_2-NP80-milled	ball-milled silica nanoparticles
SiO_2-NP80-PMI-TFSI	silica nanoparticles surface-modified with PMI-TFSI
SiO_2-NP80-PMP-TFSI	silica nanoparticles surface-modified with PMP-TFSI
STM	scanning tunneling microscopy
TEM	transmission electron microscopy
TFSI	bis(trifluoromethylsulfon)imide
THF	tetrahydrofuran
XRD	X-ray diffraction
ε	volume fraction of electrolyte
η	viscosity
Λ	equivalent conductivity
ρ	density
σ	conductivity
ω	mass fraction of filler material
Ω	ohm (unit of electric resistance)